CURING OF COMPOSITES: AN INTEGRATED MULTISCALE PROCESS DESCRIPTION TOWARD TAILORED STRUCTURES AND PROPERTIES

PROF. RANGA PITCHUMANI
Department of *Mechanical Engineering* and *Institute of Materials Science*
University of Connecticut
191 Auditorium Road, Unit 3139
Storrs, CT 06269-3139
Email: *r.pitchumani@uconn.edu* • Tel: (860) 486-2090 • Fax: (860) 486-5088

AFOSR GRANT NUMBER: F49620-01-1-0521
AFOSR PROGRAM MANAGER: Dr. Charles Lee

Final Report
September 1, 2001 to November 30, 2004

DISTRIBUTION STATEMENT A
Approved for Public Release
Distribution Unlimited

OVERALL PROGRAM OBJECTIVES:

The overall goal of the investigation was to develop a fundamental physical modeling of the complex thermal and mass transport mechanisms at the various scales (from the *laminate* to the *microstructural* and *phase* levels) that govern the interphase formation during cure. In particular, the goal of the University of Connecticut MEANS effort was to develop a comprehensive multiscale description of the cure process by addressing processing-related issues at the *phase, microstructural,* and *laminate* scales. The integrated modeling tool was aimed at predicting the constituent phases and their properties, as function of the process parameters; these, in turn, were to be used in the mechanics models for property prediction of composite structures. The multiscale modeling was aimed at providing the critical information on ***processing-interphase-property*** relationships necessary for viable modeling, analysis, design, and accelerated insertion of high performance composite materials in various aerospace applications. Detailed theoretical and experimental investigations were carried out. The research was synergistic with the activities of AFRL's Structural Materials Branch (Materials and Manufacturing Directorate) on mechanics modeling as well as a companion MEANS effort at Pennsylvania State University on microstructural modeling.

To this end, the specific **S&T Objectives** are to:

- Develop fundamental models for the micro/nanoscale (phase and micromechanical level) transport processes contributing to interphase formation, and to quantify the parameters involved in the physical description.
- Couple the micro/nanoscale process description with the macroscale (laminate level) thermochemical cure models

20050519 091

REPORT DOCUMENTATION PAGE

AFRL-SR-AR-TR-05-

0191

The public reporting burden for this collection of information is estimated to average 1 hour per response, includi... gathering and maintaining the data needed, and completing and reviewing the collection of information. Send comm... of information, including suggestions for reducing the burden, to Department of Defense, Washington Headc... (0704-0188), 1215 Jefferson Davis Highway, Suite 1204, Arlington, VA 22202-4302. Respondents should be av... subject to any penalty for failing to comply with a collection of information if it does not display a currently valid OMI...
PLEASE DO NOT RETURN YOUR FORM TO THE ABOVE ADDRESS.

1. REPORT DATE *(DD-MM-YYYY)*	2. REPORT TYPE	3. DATES COVERED *(From - To)*
	Final Report	1 Sep 2001 - 30 Nov 2004

4. TITLE AND SUBTITLE
Curing of Composites: An Integrated Multiscale Process Description Toward Tailored Structures and Properties

5a. CONTRACT NUMBER

5b. GRANT NUMBER
F49620-01-1-0521

5c. PROGRAM ELEMENT NUMBER

5d. PROJECT NUMBER

5e. TASK NUMBER

5f. WORK UNIT NUMBER

6. AUTHOR(S)
Professor Ranga Pitchumani

7. PERFORMING ORGANIZATION NAME(S) AND ADDRESS(ES)
Department of Mechanical Engineering & Institute of Materials Science
University of Connecticut
191 Auditorium Road, Unit 3139
Storrs CT 06269-3139 NL

8. PERFORMING ORGANIZATION REPORT NUMBER

9. SPONSORING/MONITORING AGENCY NAME(S) AND ADDRESS(ES)
USAF/AFRL
AFOSR
875 North Randolph Street
Arlington VA 22203

10. SPONSOR/MONITOR'S ACRONYM(S)
AFOSR

11. SPONSOR/MONITOR'S REPORT NUMBER(S)

12. DISTRIBUTION/AVAILABILITY STATEMENT
Distribution Statement A. Approved for public release; distribution is unlimited.

13. SUPPLEMENTARY NOTES

14. ABSTRACT
During the cure of thermosetting polymer composites, the presence of reinforcing fibers significantly alters the resin composition in the vicinity of the fiber surface via several microscale processes, forming an interphase region with different chemical and physical properties form the bulk resin. The interphase composition is an important parameter that determines the micromechanical properties of the composite. Interphase development during processing is a result of the mass-transport processes of adsorption, desorption, and diffusion near the fiber surface, which are accompanied by simultaneous cure reactions between the resin components. Due to complexities of the molecular-level mechanisms near the fiber surface, few studies have been carried out on the prediction of the interphase evolution as function of the process parameters. To address this void, a kinetics model was developed in this study to describe the coupled mass-transfer and reaction processes leading to interphase formation. The parameters of the model were determined for an aluminum fiber/diglycidyl ether of bisphenol-A/bis(p-aminocyclohexyl) methane resin system from available experimental data in the literature. Parametric studies are presented to show the effects of different governing mechanisms on the formation of the interphase region for a general

15. SUBJECT TERMS

16. SECURITY CLASSIFICATION OF:			17. LIMITATION OF ABSTRACT	18. NUMBER OF PAGES	19a. NAME OF RESPONSIBLE PERSON
a. REPORT	b. ABSTRACT	c. THIS PAGE			19b. TELEPHONE NUMBER *(Include area code)*
U	U	U	UU	91	

- Determine using the integrated description, the interphase structure and composition as function of the materials and process parameters
- Develop through systematic tests and existing information in the literature, detailed mapping of the interphase structure and composition, to thermal, mechanical, and thermomechanical properties
- Develop models to establish interphase-property relationships.
- Integrate Processing-Interphase and Interphase-Property relationships, and conduct studies on predicting the interphase structure, composition, and overall composite properties and performance as a function of the cure cycle and material parameters
- Using the integrated description to develop guidelines for cure cycle selection for processing composites with tailored phase structures and properties

SUMMARY OF S&T COMPLETED:

- Physical models have been developed to describe the kinetics of the adsorption, desorption, diffusion, and reaction phenomena at the micro/nanoscales, leading to interphase formation. Numerical solution of the governing equations has been implemented for simulation of the interphase formation as function of the processing temperature, fiber surface, and resin/catalyst system parameters. Parametric studies have been conducted to elicit the effects of the various parameters on the interphase evolution with time.
- Micromechanical modeling of the effects of the interphase property variation on the elastic modulus and stress concentration factors has been completed toward establishing *interphase-property* relationships.
- The phase and micromechanical level description of the interphase formation phenomena have been coupled with a macroscale thermochemical description to obtain a comprehensive processing-interphase-property mapping.
- Systematic studies were conducted during the year to study the influence of the cure cycles on the interphase formation and, in turn, the composite properties; The results provide for selection of optimal cure temperature and time based on properties desired in the final composite.
- The activities also focused on determination of the model parameters. Approaches for the estimation of the model parameters, based on direct measurements of the nanoscale interphase composition as well as based on measured property variations near a fiber surface using micro-interferometry and nano-indentation tests, were developed. Additional experiments are being carried out for a comprehensive evaluation of all the model parameters. AFM images such as the one shown alongside are being used to determine the interphase thickness, which together with nanoindentation test measurements, are used to extract the model parameters.

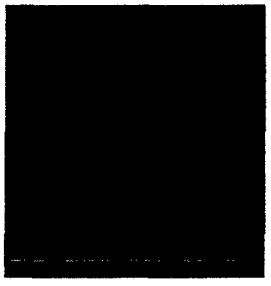

- Details of the completed tasks are provided in selected publications attached to this report.

PUBLICATIONS (COPIES OF SELECTED PUBLICATIONS ARE ENCLOSED):

1. **F. Yang and R. Pitchumani, "Studies on Fiber/Matrix Interphase Development in Thermosetting Matrix Composites," in *Proceedings of the 12th International Heat Transfer Conference*, Vol. 3, pp. 153-158, 2002.**
2. **F. Yang and R. Pitchumani, "A Kinetics Model for Interphase Formation in Thermosetting-Matrix Composites," *Journal of Applied Polymer Science*, 89(12), pp. 3220-3236, 2003.**
3. R.J. Johnson and R. Pitchumani, "Enhancement of Resin Flow in VARTM Using Induction Heating," *Composites Science and Technology*, 63, pp. 2201-2215, 2003.
4. **F. Yang and R. Pitchumani, "Effects of Process and Material Parameters on the Interphase, and the Relationship to Mechanical Properties of Thermosetting Matrix Composites," *International Conference on Composite Materials* (ICCM), San Diego, 2003.**
5. **F. Yang and R. Pitchumani, "Processing-Interphase Relationships for the Curing of Thermosetting-matrix Composites," *SAMPE Technical Conference*, Dayton OH, October 2003.**
6. **F. Yang and R. Pitchumani, "Effects of Interphase Formation on the Modulus and Strength of Fiber-reinforced Thermosetting-matrix Composites," *Composites Science and Technology*, 64(10-11), pp. 1437-1452, 2004.**
7. X. Guan and R. Pitchumani, "Modeling of Spherulitic Crystallization in Thermoplastic Tow-Placement Process: Heat Transfer Analysis," *Composites Science and Technology*, 64(9), pp. 1123-1134, 2004.
8. X. Guan and R. Pitchumani, "Modeling of Spherulitic Crystallization in Thermoplastic Tow-Placement Process: Spherulitic Microstructure Evolution," *Composites Science and Technology*, 64(9), pp. 1363-1374, 2004.
9. X. Guan and R. Pitchumani, "A Micromechanical Model for the Elastic Properties of Semicrystalline Thermoplastic Polymers," *Polymer Engineering and Science*, 44(3), pp. 433-451, 2004.
10. **F. Yang and R. Pitchumani, "Characterization of the Interphase Formation Kinetics in Thermosetting-Matrix Composites," *SAMPE 2004*, Long Beach, CA, May 16-20, 2004.**
11. R.J Johnson and R. Pitchumani, "Simulation of Active Flow Control based on Localized Preform Heating in a VARTM Process," *Composites A: Applied Science and Manufacturing*, In Revision, 2004.
12. R.J. Johnson and R. Pitchumani, "Active Flow Control in a VARTM Process Using Localized Induction Heating," *FPCM7: Seventh International Conference on Flow Processes in Composite Materials*, S.G. Advani, ed., pp. 247-252, 2004.
13. **F. Yang and R. Pitchumani, "Processing-Interphase-Property Relationships in Fiber-reinforced Thermosetting-matrix Composites," *Polymer Composites*, 26(2), pp. 193-208, 2005.**
14. F. Yang and R. Pitchumani, "An Analytical Solution for Thermal Transport in Deep X-ray Lithography," *Journal of Micromechanics and Microengineering*, 15(3), pp. 474-484, 2005.

A Kinetics Model for Interphase Formation in Thermosetting Matrix Composites

F. Yang, R. Pitchumani

Composites Processing Laboratory, Department of Mechanical Engineering, University of Connecticut, Storrs, Connecticut 06269-3139

Received 19 July 2002; accepted 15 November 2002

ABSTRACT: During the cure of thermosetting polymer composites, the presence of reinforcing fibers significantly alters the resin composition in the vicinity of the fiber surface via several microscale processes, forming an interphase region with different chemical and physical properties from the bulk resin. The interphase composition is an important parameter that determines the micromechanical properties of the composite. Interphase development during processing is a result of the mass-transport processes of adsorption, desorption, and diffusion near the fiber surface, which are accompanied by simultaneous cure reactions between the resin components. Due to complexities of the molecular-level mechanisms near the fiber surface, few studies have been carried out on the prediction of the interphase evolution as function of the process parameters. To address this void, a kinetics model was developed in this study to describe the coupled mass-transfer and reaction processes leading to interphase formation. The parameters of the model were determined for an aluminum fiber/diglycidyl ether of bisphenol-A/bis(*p*-aminocyclohexyl)methane resin system from available experimental data in the literature. Parametric studies are presented to show the effects of different governing mechanisms on the formation of the interphase region for a general fiber–resin system. The interphase structure obtained from the model may be used as input data for the prediction of the overall composite properties.
© 2003 Wiley Periodicals, Inc. J Appl Polym Sci 89: 3220–3236, 2003

Key words: adsorption; composites; curing of polymers; interfaces; kinetics (polym.)

INTRODUCTION

Fabrication of thermosetting matrix composites is based on a critical step of cure, which involves applying a predefined temperature cycle to a fiber–resin matrix mixture. The elevated temperatures initiate a crosslinking cure reaction among the species in the matrix. The presence of fibers has been found to significantly influence the cure reaction, resulting in the formation of a third phase, known as the *interphase*, which possesses properties distinct from those of the bulk fiber and the matrix. The interphase resides in a region between the original constituents of the composite with a size of a few to a few thousand nanometers.[1–4] Although the region has a submicroscopic scale, it essentially forms a significant portion of the matrix in the composite.[1] Also, the performance of the composite is determined by the ability of the matrix to transfer load to the reinforcing fiber and is thus controlled by the interphase region. The structure and properties of the interphase are the dominant factors governing the overall composite properties and performance.

Prediction of the overall composite properties in the presence of the interphase region involves the following steps:[1]

- First, the manufacturing parameters must be linked with the interphase structures. For example, given a cure temperature and pressure cycle, the chemical composition of the interphase should be determined. In this step, physical and chemical mechanisms must be identified and modeled to predict the interphase structure.
- In the second step, the known interphase structure is related to the interphase material properties such as glass-transition temperature (T_g), flexural modulus, or thermal expansion coefficient. This step is primarily based on the experimental correlation of the interphase chemical composition to the measured interphase material properties.
- The last step is to link the interphase material properties to overall composite properties such as the strength, fracture, and environmental resistance.

A majority of the studies in the literature focus on the experimental determination of the influence of

Correspondence to: R. Pitchumani (r.pitchumani@uconn.edu).
Contract grant sponsor: National Science Foundation; contract grant number: CTS-9912093.
Contract grant sponsor: Air Force Office of Scientific Research; contract grant number: F496200110521.

Journal of Applied Polymer Science, Vol. 89, 3220–3236 (2003)
© 2003 Wiley Periodicals, Inc.

interphase layers on the behavior of composite materials,[2–5] that is, steps 2 and 3. Surface treatment and sizing parameters are widely varied to tailor the structure of the interphase region and to examine the effects of different interphases on the mechanical behavior of the composite materials. Several studies have been conducted in this regard with experimental approaches or numerical calculations such as finite element methods.[4,6,7] The studies so far have provided insights into the qualitative description of the interphase regions and their influence on the composite properties for typical material systems used in practice.

The first step, that is, the prediction of the interphase structure as a function of the process parameters, forms the basis of the other two steps. However, due to complexities of the molecular-level mechanisms that occur in the vicinity of the fibers during the process, few investigations have been conducted in this area. The overhead comes from the fact that a dozen physical and chemical mechanisms contribute simultaneously to the formation of the interphase region, and only few of these mechanisms can be rigorously described in mathematical models. Garton et al.[8] showed that the carbon surfaces influenced the crosslinking reaction in an anhydride–epoxy system by adsorbing the tertiary amine catalyst and forming amine-rich interphase regions near the carbon surfaces. Similarly, Sellitti et al.[9] used Fourier transform IR attenuated total reflection spectroscopy to characterize the interphase phenomena in an epoxy–anhydride–catalyst system and showed that the surface species introduced on graphitized carbon fibers could promote or inhibit the crosslinking process by the preferential adsorption of the catalyst. Other possible interphase mechanisms were proposed by Drzal,[4] including: the skin area of the fiber might have morphological deviation from the bulk fiber; the surface proximity of the fiber changes the structure of the resin in the interphase; surface treatments give rise to chemically and structurally different regions near the fiber surface; exposure to air before composite processing results in the adsorption of impurities that are desorbed at elevated temperatures; and the presence of a thin monomer coating on the surface of the fiber.

To our knowledge, the first work on modeling interphase formation in thermosetting composites was presented by Palmese.[1] The model predicts the interphase composition under thermodynamic equilibrium conditions of an epoxy–amine resin mixture near a fiber surface. The Gibbs phase rule was used to set up the equilibrium state, accounting for the enthalpy interaction between fiber surface and resin components, and the calculation of Gibbs free energy was based on a Flory–Huggins type lattice structure. The model does not take the chemical reactions into account, and furthermore, because of the assumption of thermodynamic equilibrium, it cannot predict the interphase evolution with time during processing. Hrivnak[10] extended Palmese's model to a reacting system by using renewal theory models to construct the assembly Gibbs free energy and the associated chemical potential.

Adsorption from a mixture of polymer chains and solvent molecules near a surface was presented by Scheutjens and Fleer[11] with a statistical approach. The partition function for the mixture was evaluated with a quasicrystalline lattice model, which in turn, gave the number of chains in each conformation in equilibrium. The focus of the work was on polymer adsorption, whereas the interphase formation in thermosetting materials is based on monomer transport.

The objective of this study was to develop a kinetics model for the prediction of the interphase growth with time during thermosetting composite processing, which would account for the simultaneous cure reaction. The model describes the mass transfer of the monomer components in the composite system before the formation of the polymer macromolecules. Clearly, our intention was not to study all of the previously-mentioned mechanisms contributing to interphase development. Rather, our focus was on the mechanism of preferential adsorption of the resin components. The model development and analysis presented here were based on the rationale that for a given specific surface treatment and coating process, among others, the formation of the interphase is governed by manufacturing-process-dependent mechanisms, principally those of preferential adsorption. A systematic study of the adsorption mechanism will provide information on how the interphase evolves during the manufacturing processes and, in turn, point out ways to design cure cycles to optimally tailor the interphase.

Experimental studies[12–14] have shown that the adsorption of an epoxy system can form an interphase layer 100–500 nm in thickness, which indicates that adsorption effects penetrate beyond one molecular layer. In this study, a multilayer coupled adsorption–desorption–diffusion–reaction model was developed to predict the interphase composition evolution for a thermosetting system. The formulation was based on the principle of mass conservation applied to a domain consisting of discrete molecular layers. The model was correlated to experimental data reported in the literature to determine the parameters of the model. Parametric studies are presented to illustrate the effects of the various dimensionless parameters on the interphase development.

INTERPHASE FORMATION MODEL

The cure of thermosetting resin systems is characterized by the reaction between prepolymer (or mono-

mer) molecules and a curing agent to form a crosslinked network that cannot flow on vitrification. The reinforcing fibers alter the cure characteristics by selective adsorption of resin components, which changes the concentration of the reacting species in the vicinity of the fiber surfaces. The goal of this study was to predict the concentration profiles of the constituent species near the fiber surface by consideration of the processes that occur in the cure reaction. An inorganic fiber/epoxy–amine thermosetting system is considered in the following discussion; however, all of the derivations and results are applicable to a general two-component thermosetting system.

The geometry considered is the half-infinite space contacting an infinitely large flat fiber surface, which may be justified by the fact that the interphase thickness is much smaller in comparison to the fiber diameter. The fiber is considered to have an epoxy sizing layer applied to its surface. The sized fiber is exposed to an epoxy–amine resin mixture, and the epoxy and amine species begin reacting with each other at $t = 0^+$. Accompanying the chemical reaction, epoxy molecules diffuse away from the sizing layer adjacent to the fiber. In a reverse movement, the amine molecules diffuse into the sizing layer due to the relatively higher amine concentration in the bulk resin region. The diffusion process has a tendency to eliminate the concentration gradients. In addition, the "force field" of the fiber surfaces causes the epoxy and amine molecules to migrate in the direction towards the surfaces, a process referred to as adsorption. Also the adsorbed molecules may be desorbed to the bulk resin in a desorption process. Unlike the diffusion process, the net effect of the adsorption and desorption processes is the build up of concentration gradients. All the processes mentioned above take place simultaneously, resulting in a continuously evolving concentration profile that is "frozen" in space upon gelation of the thermosetting system.

The adsorption phenomenon at the equilibrium state near solid surfaces was described by Brunauer, Emmett, and Teller (referred to as the BET theory).[15,16] In this development, the concepts in BET theory were extended to the transient processes in the interphase evolution. Following the approach of the BET theory, the domain surrounding the fiber surface was divided into molecular layers where one molecule of epoxy or amine could occupy only one of these layers. Due to the interaction between resin molecules and the fiber surface, as well as those among resin molecules themselves, epoxy and amine molecules can move from layer to layer. Adsorption is a process where molecules bind in one or more layers onto a solid surface through chemical or physical forces. The molecules that bind to the surface are called the adsorbate[16] and are referred to be in the "adsorbed" state. Other molecules that are unbound to the surface are considered to be in the "bulk" state. The solid surface can adsorb molecules from a bulk state into an adsorbed state, and conversely, molecules in the adsorbed state may be desorbed into the bulk state. Molecules in the adsorbed state are treated to be fixed in the space and are not permitted to diffuse, whereas molecules in the bulk state may diffuse within the resin mixture.

Figure 1 shows the molecular layers in the model domain, where the adsorption layers contain molecules in the adsorbed state, whereas the bulk layers hold molecules in the bulk state. Although the adsorption and bulk layers are drawn separately to illustrate the mass exchange between the adsorbed and bulk states, the corresponding layers essentially occupy the same space; that is, the ith adsorption layer and the ith bulk layer overlap. The multiple adsorption layers are formed as follows: at $t = 0$, there are no molecules in the adsorbed layers because the adsorption process has not begun, and all of the resin molecules are in the bulk state. At the beginning of the process, $t = 0^+$, some bulk-state molecules in the first or second molecular layers are adsorbed into the first layer of the adsorbed state and occupy the adsorption sites on the bare fiber surface. Note that the molecules beyond the second layer cannot be adsorbed directly into the first layer because of the fact that they are out of contact with the first layer. In the next time step, three mass movements could happen: (1) some of the molecules adsorbed in the first layer could be desorbed into the bulk in the first and second layers, (2) the molecules in the bulk state in the first and second layers could be continuously adsorbed into the first layer at the remaining adsorption sites on the fiber surface, and (3) the molecules in the bulk state in the first, second, and third layers could be adsorbed on top of the molecules in the first adsorption layer, forming a second adsorption layer. Similar processes continue and result in a multilayer adsorbed state, as shown in Figure 1.

Because the molecules in the adsorbed state are not free to diffuse, the diffusion process is only driven by the concentration gradient in the bulk state. Chemical reactions between epoxy (E) and amine (A) happen simultaneously during the adsorption, desorption, and diffusion processes. The reaction equation may be written as

$$n_1\mathrm{E} + n_2\mathrm{A} \rightarrow \mathrm{P} \tag{1}$$

where P denotes the product and n_1 and n_2 are the molar numbers of the reactants needed to produce 1 mol of product.

The governing equations for the mechanisms discussed so far may be derived with the principle of mass conservation for a control volume (CV); namely, the rate of increase of mass in the CV (storage) equals the difference between the rate of mass flow into the CV and the total depletion of mass from the CV aris-

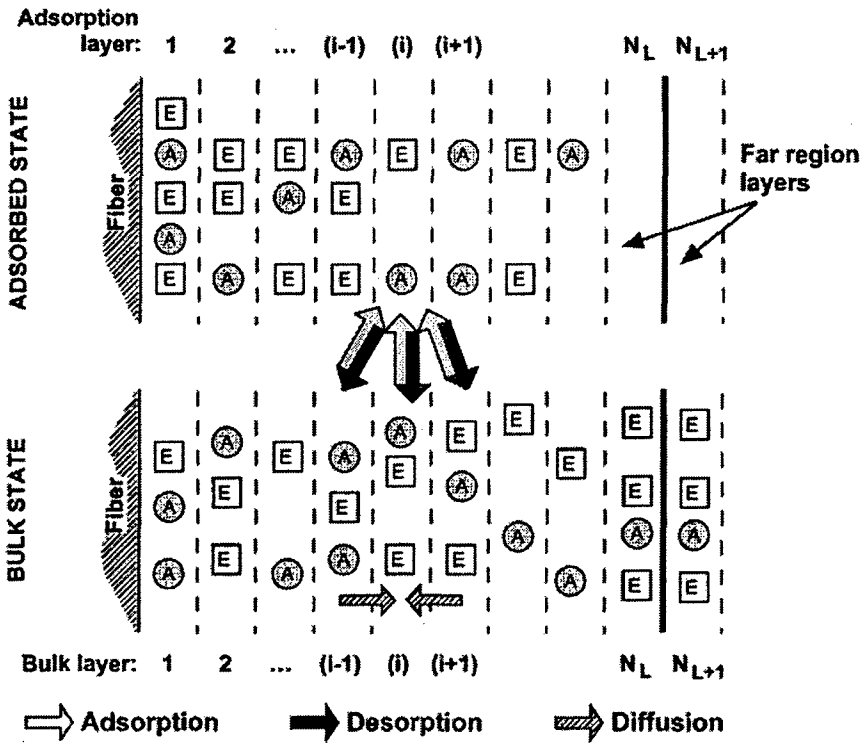

Figure 1 Schematic of the adsorption, desorption, and diffusion processes in an epoxy-amine system.

ing from mass outflow and mass consumption due to chemical reactions. With any ith adsorption layer in Figure 1 referred to as a CV, the principle of mass conservation for the epoxy molecule yields

$$\underbrace{\frac{dN_{E,i}}{dt}}_{\text{Storage}} = \underbrace{R_{a,E}(i-1,i) + R_{a,E}(i,i) + R_{a,E}(i+1,i)}_{\text{Adsorption, } \Re_{a,E}(i)}$$

$$\underbrace{- R_{d,E}(i-1,i) - R_{d,E}(i,i) - R_{d,E}(i+1,i)}_{\text{Desorption, } \Re_{d,E}(i)}$$

$$\underbrace{- \Re_{r,E}(i)}_{\text{Depletion (reaction)}} \qquad (2)$$

where $dN_{E,i}/dt$ is the rate of change of the total number of epoxy molecules in the ith adsorption layer, and the subscripts E and i denote the epoxy and ith layer, respectively. Epoxy molecules in the bulk state in the $(i-1)$th, ith, and $(i+1)$th layers may be adsorbed into the ith molecular layer, denoted by the rate terms $R_{a,E}(i-1,i)$, $R_{a,E}(i,i)$, and $R_{a,E}(i+1,i)$, respectively; in a reverse process, the adsorbed epoxy molecules in the ith layer can be desorbed into the bulk in the $(i-1)$th, ith, and $(i+1)$th layers, and their respective rates are denoted as $R_{d,E}(i-1,i)$, $R_{d,E}(i,i)$, and $R_{d,E}(i+1,i)$. Further, the depletion of epoxy in the ith adsorption layer through chemical reaction is represented by the rate term $\Re_{r,E}(i)$.

The determination of the rate terms of adsorption, desorption, and reaction are illustrated in the following discussion. The adsorption of epoxy molecules from the $(i-1)$th layer of the bulk state to ith layer of the adsorbed state is given as

$$R_{a,E}(i-1,i) = k_{a,E}(N_{i-1} - N_i) \times \exp\left(-\frac{E_{a,E}}{RT}\right)\frac{N_{E\infty,i-1}}{N_{\infty,i-1} + N_{\infty,i} + N_{\infty,i+1}} \qquad (3)$$

where the parameter $k_{a,E}$ is the frequency factor in the adsorption rate of epoxy molecules and N_i is the total number of epoxy and amine molecules adsorbed in the ith layer, that is, $N_i = N_{E,i} + N_{A,i}$. Because a molecule adsorbed into the ith layer must adjoin an adsorbed epoxy or amine molecule in the $(i-1)$th layer, the term $N_{i-1} - N_i$ yields the number of available sites in the $(i-1)$th layer that are open for adsorption. For $i = 1$, the term $N_0 - N_1$ denotes the available sites in the first adsorption layer, where N_0 is the number of adsorption sites on the bare fiber surface. The activation energy of adsorption for the epoxy molecules is denoted as $E_{a,E}$, which defines the energy barrier to be crossed for an epoxy molecule to be adsorbed, and R and T in Eq. (3) are the Universal gas constant and the temperature, respectively. The pa-

rameters $N_{E\infty,i}$ and $N_{A\infty,i}$ are the number of epoxy and amine molecules in the bulk state in the ith molecular layer, and $N_{\infty,i} = N_{E\infty,i} + N_{A\infty,i}$. Because the epoxy molecules adsorbed into the ith layer come from the $(i - 1)$th, ith, and $(i + 1)$th layers, the fraction $(N_{E\infty,i-1}/N_{\infty,i-1} + N_{\infty,i} + N_{\infty,i+1})$ in eq. (3) denotes the probability that a site can capture an epoxy molecule from the $(i - 1)$th layer of the bulk state. It is intuitively expected that the parameter $k_{a,E}$ should vary from layer to layer, corresponding to a progressively decreasing adsorption force field away from the fiber surface. However, because the variation of $k_{a,E}$ is not readily obtained from existing theoretical or experimental means, the adsorption rate, $k_{a,E}$, and all other adsorption/desorption rates are assumed to be independent of location, as in the BET theory. This assumption will be relaxed in the future development of the model.

Other rate terms can be defined in a similar way, and are summarized next:

$$R_{a,E}(i, i) = k_{a,E}(N_{i-1} - N_i) \times exp\left(-\frac{E_{a,E}}{RT}\right)\frac{N_{E\infty,i}}{N_{\infty,i-1} + N_{\infty,i} + N_{\infty,i+1}} \quad (4)$$

$$R_{a,E}(i + 1, i) = k_{a,E}(N_{i-1} - N_i) \times exp\left(-\frac{E_{a,E}}{RT}\right)\frac{N_{E\infty,i+1}}{N_{\infty,i-1} + N_{\infty,i} + N_{\infty,i+1}} \quad (5)$$

$$R_{d,E}(i - 1, i) = R_{d,E}(i, i) = R_{d,E}(i + 1, i) = \frac{1}{3}k_{d,E}(N_i - N_{i+1})\exp\left(-\frac{E_{d,E}}{RT}\right)\frac{N_{E,i}}{N_i} \quad (6)$$

$$\Re_{r,E}(i) = n_1 k_r N_{E,i} \quad (7)$$

where $R_{d,E}(i - 1, i)$ is the rate term of the desorption of epoxy molecules from the ith absorption layer to the $(i - 1)$th bulk layer, $R_{d,E}(i, i)$ is the rate term of the desorption of epoxy molecules from the ith absorption layer to the ith bulk layer, and $R_{d,E}(i + 1, i)$ is the rate term of the desorption of epoxy molecules from the ith absorption layer to the $(i + 1)$th bulk layer. The fraction $\frac{1}{3}$ in the desorption terms arises from the assumption that the probabilities of desorption from the ith adsorbed layer to each of the three neighborhood bulk layers are identical. The parameter $k_{d,E}$ is the frequency factor in the desorption rate of epoxy molecules. Because a molecule in the adsorbed layer i can be desorbed into the bulk state only if the molecule has no molecule adjoining it in the $(i + 1)$th adsorbed layer, the term $N_i - N_{i+1}$ yields the number of molecules in the ith adsorbed layer that may be desorbed into the bulk state. The activation energy of desorption $(E_{d,E})$ for the epoxy molecules defines the energy barrier to be crossed for an epoxy molecule to be desorbed. The fraction $N_{E,i}/N_i$ arises from the fact that among all of the molecules desorbed from the ith adsorbed layer, the probability of finding an epoxy molecule is its molar fraction in the adsorbed layer. The depletion term, $\Re_{r,E}(i)$ in eq. (2), is determined by the crosslinking chemical reaction between epoxy and amine, where k_r is the reaction rate.

A similar mass conservation analysis may be applied to the amine molecules in the adsorbed state and to the product molecules, yielding the following equations for these species:

$$\underbrace{\frac{dN_{A,i}}{dt}}_{\text{Storage}} = \underbrace{R_{a,A}(i - 1, i) + R_{a,A}(i, i) + R_{a,A}(i + 1, i)}_{\text{Adsorption, } \Re_{a,A}(i)} - \underbrace{R_{d,A}(i - 1, i) - R_{d,A}(i, i) - R_{d,A}(i + 1, i)}_{\text{Desorption, } \Re_{d,A}(i)} - \underbrace{\Re_{r,A}(i)}_{\text{Depletion (reaction)}} \quad (8)$$

$$\frac{dN_{P,i}}{dt} = k_r N_{E,i} \quad (9)$$

where the rate terms are defined similarly to those in eqs. (3)–(7) by changing the subscript E (epoxy) to A (amine), and $\Re_{r,A}(i)$ is the rate term representing the depletion of amine in the ith absorption layer through chemical reaction. The right hand side of eq. (9) has only the reaction term because the product molecules are assumed to have no mobility and will stay in their space of formation. Also, $N_{P,i}$ is the number of product segments in the ith layer due to the reaction in the adsorbed state.

Equations (2), (8), and (9) pertain to the mass transfer rates of the molecules in the adsorbed state. The adsorbed state exchanges mass with the bulk state, in which the molecules undergo diffusion in addition to the adsorption, desorption, and reaction processes. Considering the rate of change of the number of epoxy molecules in the bulk state in the ith layer, that is, $dN_{E\infty,i}/dt$, the following four types of contributions were identified: (1) diffusion of epoxy molecules in the bulk state from the $(i + 1)$th and $(i - 1)$th layers to ith layer, which increases $N_{E\infty,i}$; (2) desorption of epoxy molecules in the adsorbed state in the $(i - 1)$th, ith, and $(i + 1)$th layers to the ith layer of the bulk state, which increases $N_{E\infty,i}$; (3) epoxy molecules in the bulk state in the ith layer being adsorbed to the $(i - 1)$th, ith, and $(i + 1)$th layers of the adsorbed state, which reduces

$N_{E\infty,i}$; and (4) chemical reaction in the bulk in ith layer, which depletes $N_{E\infty,i}$. We then obtained

$$\frac{dN_{E\infty,i}}{dt} = D_{EA}\left(\frac{N_{E\infty,i-1} + N_{E\infty,i+1} - 2N_{E\infty,i}}{\Delta L^2}\right) + R_{d,E}(i, i-1) + R_{d,E}(i, i) + R_{d,E}(i, i+1) - R_{a,E}(i, i-1) - R_{a,E}(i, i) - R_{a,E}(i, i+1) - n_1 k_r N_{E\infty,i} \quad (10)$$

where D_{EA} is the mutual diffusion coefficient in the binary epoxy–amine mixture and ΔL corresponds to the physical size of a molecular layer. All the rate terms were defined previously [eqs. (3)–(6)]. Similarly, we obtained the rate equations for $N_{A\infty,i}$ and $N_{P\infty,i}$ as

$$\frac{dN_{A\infty,i}}{dt} = D_{EA}\left(\frac{N_{A\infty,i-1} + N_{A\infty,i+1} - 2N_{A\infty,i}}{\Delta L^2}\right) + R_{d,A}(i, i-1) + R_{d,A}(i, i) + R_{d,A}(i, i+1) - R_{a,A}(i, i-1) - R_{a,A}(i, i) - R_{a,A}(i, i+1) - n_2 k_r N_{E\infty,i} \quad (11)$$

$$\frac{dN_{P\infty,i}}{dt} = k_r N_{E\infty,i} \quad (12)$$

where $N_{P\infty,i}$ is the number of product segments in the ith layer due to the reaction in the bulk state.

The rate equations for species in the bulk state must be solved simultaneously with those corresponding to the adsorbed state. The diffusivity (D_{EA}) and k_r are functions of the extent of cure. The diffusivity is described by free-volume theory as[17]

$$D_{EA} = D_0 \exp(-E_D/RT)\exp[-b_D/(f_g + \alpha_f[T - T_g(\xi)])] \quad (13)$$

where D_0, f_g, and α_f are constants; E_D is the activation energy; and b_D is an empirical constant. $T_g(\xi)$ defines the available free volume and degree of rotational restriction, which in turn, are functions of the reaction extent, $\xi = N_E(t)/N_{E0}$, defined as the ratio of the total concentration of epoxy at a time instant to that at time zero (initial concentration). The parameters D_0, b_D, f_g, α_f, and E_D in the model depend on the type of thermosetting system and can be determined by the approach described by Sanford.[17] The DiBenedetto equation relates T_g to the extent of cure as[17]

$$\frac{T_g(\xi) - T_g^0}{T_g^0} = \frac{(E_x/E_m - F_x/F_m)(1-\xi)}{1 - (1 - F_x/F_m)(1-\xi)} \quad (14)$$

where the constants T_g^0, E_x/E_m, and F_x/F_m can be obtained through experimental data of T_g versus ξ. k_r is controlled by the retarded diffusion process at later stages of the cure and is given as

$$k_r = \frac{k_{r0}\exp(-E_a/RT)}{1 + \frac{\delta_0}{D_{EA}}\exp(-E_a/RT)} \quad (15)$$

where k_{r0} is the Arrhenius pre-exponential constant, δ_0 is the coordination sphere reaction parameter, and E_a is the reaction rate activation energy.[17]

The unknowns in eqs. (2)–(12) are the number of molecules, $N_{E,i}$, $N_{A,i}$, $N_{P,i}$, $N_{E\infty,i}$, $N_{A\infty,i}$, and $N_{P\infty,i}$. When i goes from 1 (corresponding to the layer adjacent to the fiber surface) to N_L (corresponding to a far region layer), we have six more unknown variables than equations because the equations for N_Lth layer involve the number of molecules in the (N_L + 1)th layer. We assumed that the influence of the fiber surface cannot propagate to an infinite distance, which yielded two conditions for the far region: (1) the numbers of molecules in the adsorbed state are zero, and (2) the numbers of molecules in the bulk state are constants. The far region conditions provide six additional equations:

$$[\text{Adsorbed state}]\ N_{E,N_L+1} = 0; \quad N_{A,N_L+1} = 0; \quad N_{P,N_L+1} = 0$$
$$[\text{Bulk state}]\ N_{E\infty,N_L} = N_{E\infty,N_L+1}; \quad N_{A\infty,N_L} = N_{A\infty,N_L+1}; \quad N_{P\infty,N_L} = N_{P\infty,N_L+1} \quad (16)$$

Equations (2) and (8)–(12), where $i = 1, 2, \ldots, N_L$, and the far region conditions constitute a complete ordinary differential equation system for the $6N_L$ unknowns. For a thermosetting system with a fiber sizing thickness of N_S molecular layers, the initial conditions of the ODE system are (1) the numbers of molecules for each species in the adsorbed state and the number of product in the bulk state are zero; (2) within the epoxy sizing layer, the number of the epoxy is a constant, $N_{E,1}$, whereas the number of the amine is zero; and (3) beyond the sizing layer, the numbers of epoxy and amine species are constants, $N_{E,0}$ and $N_{A,0}$, respectively. The mathematical expressions for the initial conditions may be written as:

$$N_{E,i} = N_{A,i} = N_{P,i} = N_{P\infty,i} = 0 \quad (i = 1, 2, \ldots, N_L)$$
$$N_{E\infty,i} = N_{E,1}; \quad N_{A\infty,i} = 0 \quad (i = 1, 2, \ldots, N_S)$$
$$N_{E\infty,i} = N_{E,0}; \quad N_{A\infty,i} = N_{A,0} \quad (i = N_S + 1, \ldots, N_L) \quad (17)$$

The initial conditions for the species in the adsorbed state require that the resin mixture is separated from

TABLE I
Properties of the DGEBA/PACM20 Resin Components[14]

Resin component	M (g/mol)	ρ (kg/m^3)
DGEBA	382.4	1170
PACM20	198.3	960

the fiber surface before $t \leq 0$, which corresponds to the manufacturing processes of the thermosetting prepregs or processes such as resin transfer molding. For composite materials processing that utilizes prepregs, the initial conditions may be changed to the concentration profiles within the prepreg materials.

Equations (2) and (8)–(12) were solved with a fourth-order Runge–Kutta method.[18] Corresponding to the numerical range of the dimensionless groups introduced later in this article, a dimensionless time step of 0.001 yielded converged results. The numerical computations were carried out until the system reached its gelation point, which was defined as the point where the total number of the epoxy molecules reduced to 40% of its original value.

RESULTS AND DISCUSSION

The model developed in the previous section was used to calculate the molar concentration of the resin components as a function of molecular layers under isothermal conditions, $T = T_0$, where T_0 is the constant temperature at which the process takes place. The model was correlated to the concentration profile measured experimentally by Arayasantiparb et al.[14] to determine the parameters of the model. The experimental study measured the composition of an epoxy–aluminum interphase with spatially resolved electron energy-loss spectroscopy (EELS) in a scanning transmission electron microscope. The material system consisted of an aliphatic bis(*p*-aminocyclohexyl)methane (PACM20) curing agent, an aromatic diglycidyl ether of bisphenol-A (DGEBA) epoxy resin, and a single aluminum fiber with a diameter of 125 μm. The properties of the resin components as reported in ref. 14 are given in Table I. Energy-loss spectra were collected for the DGEBA/PACM20 system at different locations of the sample and were used to determine the local volume fraction of PACM20. More discussion on the experimental measurement can be found in ref. 14.

Because the experimental data was presented in the form of PACM20 (in a binary mixture of DGEBA and PACM20) volume fraction as a function of distance from the aluminum fiber surface, the molar numbers and molecular layer used in the model needed to be transformed to the corresponding quantities. The physical dimensions of the molecular layers in the system could be estimated as the size of resin molecules. The calculations assumed the molecules to be spheres and a uniform molecular weight distribution equal to the average molecular weight. The assumptions could be relaxed if we accounted for a monomer molecular weight and shape distribution to arrive at better estimates of the sizes. The molecular volume v_m was found as $v_m = (M/\rho N_a)$, where M, ρ, and N_a are the molecular weight, density, and Avogadro's number, respectively. The size of each molecular layer was estimated as $[6v_m/\pi]^{1/3}$ and was evaluated to be 1.00 nm from the size of the DGEBA molecules. The size of PACM20 molecules was 0.87 nm, which was similar to that of DGEBA. Furthermore, the molar concentrations of each species could be transformed to volume fractions through the expression $n = (V\rho/M)$, where n is the molar number of a species and V is the volume. The volume fraction of PACM20 (Φ_A) may be related to its molar fraction (X_A) as

$$\Phi_A = \frac{X_A M_A/\rho_A}{X_A M_A/\rho_A + (1 - X_A)M_E/\rho_E}$$

where the subscripts, E and A, denote the DGEBA and PACM20, respectively.

The goal of the correlation study was primarily to examine the ability of the model to reflect the physical trends in the data. At this stage, a systematic approach to directly determine all the parameters of the model is not available and may be a subject of future work. An optimization program implementing the simulated annealing method[19] was used to minimize the objective function that defines the sum of the squares of the difference between the model prediction of the composition profile and the experimental data from Arayasantiparb et al.[14] The objective function is governed by eight independent variables, namely, the diffusion parameters, $D_0\exp(-E_D/RT)/\Delta L^2$ and b_D; the reaction parameter, $k_{r0}\exp(-E_a/RT)$; the relative number of adsorption sites on the fiber surface, N_0/N_{E0}; and the adsorption and desorption rate parameters, $k_{a,E}\exp(-E_{a,E}/RT)$, $k_{d,E}\exp(-E_{d,E}/RT)$, $k_{a,A}\exp(-E_{a,A}/RT)$, and $k_{d,A}\exp(-E_{d,A}/RT)$ where $k_{a,A}$ is the absorption rate of amine molecules, $E_{a,A}$ is the adsorption activation energy of amine molecules, $k_{d,A}$ is the desorption rate of amine molecules, and $E_{d,A}$ is the desorption activation energy of amine molecules. The method of simulated annealing draws analogy from thermodynamics, specifically the way that liquids freeze and crystallize or that metals cool and anneal. At high temperatures, molecules move freely with respect to one another. If the cooling is carried out slowly, the atoms often line themselves up probabilistically and form a pure, ordered crystalline structure, which represents a minimum energy state. Analogously, the optimization objective function is treated as an energy, and for an assumed cooling schedule, called the annealing schedule, the design configurations undergo a series of

TABLE II
Model Parameters Reported in the Literature for the DGEBA/PACM20 System[17]

Parameter	Value	Parameter	Value
E_x/E_m	0.337	F_x/F_m	0.194
T_g^0 (K)	254	f_g	0.025
α_f (K^{-1})	5.0×10^{-4} ($T > T_g$); 5.0×10^{-5} ($T < T_g$	δ_0 (cm^2/s)	0.220

probabilistic rearrangements, eventually leading to the minimum energy solution. More detail is available in the literature on the optimization technique.[19]

The parameters of the model available in the literature[17] are given in Table II, and the values of the parameters obtained from the correlation are tabulated in Table III. The following observations are illustrated in Table III: (1) the adsorption rate of DGEBA, $k_{a,E}\exp(-E_{a,E}/RT)$, was three orders of magnitude smaller than its desorption rate, $k_{d,E}\exp(-E_{d,E}/RT)$, indicating that the aluminum surface did not have affinity with the DGEBA molecules; (2) the adsorption rate of PACM20, $k_{a,A}\exp(-E_{a,A}/RT)$, was two orders of magnitude larger than its desorption rate, $k_{d,A}\exp(-E_{d,A}/RT)$, denoting a preferential adsorption on the PACM20 species as reported by Arayasantiparb et al.; (3) the value of reaction rate, $k_{r0}\exp(-E_a/RT)$, was similar to that reported by Sanford,[17] and (4) the value of diffusivity determined by the parameters $D_0\exp(-E_D/RT)/\Delta L^2$ and b_D was roughly an order of magnitude larger than that reported by Sanford, and (5) the number of adsorption sites on the aluminum surface (N_0) was about 65% of the initial number of DGEBA molecules in the bulk (N_{E0}). In most cases, the fitting results were consistent with the data in the literature.

Figure 2(a) shows the correlation results in terms of the PACM20 volume fraction as a function of distance from the aluminum wire surface. The dashed line denotes the experimental data, and the solid line corresponds to model prediction. The prediction closely followed the data over the entire range. The concentration of PACM20 in terms of percentage volume was a large value, 80%, at the aluminum surface, indicating a preferential adsorption on the species, and decreased sharply away from the fiber surface. In the region between 100 and 1500 nm, experimental measurements were not reported, and Arayasantiparb et al.[14] stated that the concentration was a constant bulk value of 25%. As shown in Figure 2(a), the model predicted a decrease in the concentration to 22% before the recovery of the bulk concentration at 25%. The model prediction pointed to the fact that the mass aggregation in the region 0–100 nm had to be compensated by the mass deficit beyond the region. However, the deficit may be too small to have been discerned in the experimental measurement technique. Figure 2(b) shows a close-up view of Figure 2(a) in the region 0–100 nm. The error bars of the experimental data as provided in ref. 14 are included for comparison. Overall, Figure 2 demonstrates the ability of the model to represent the physical trends. As pointed out previously, the parameters of the model should be

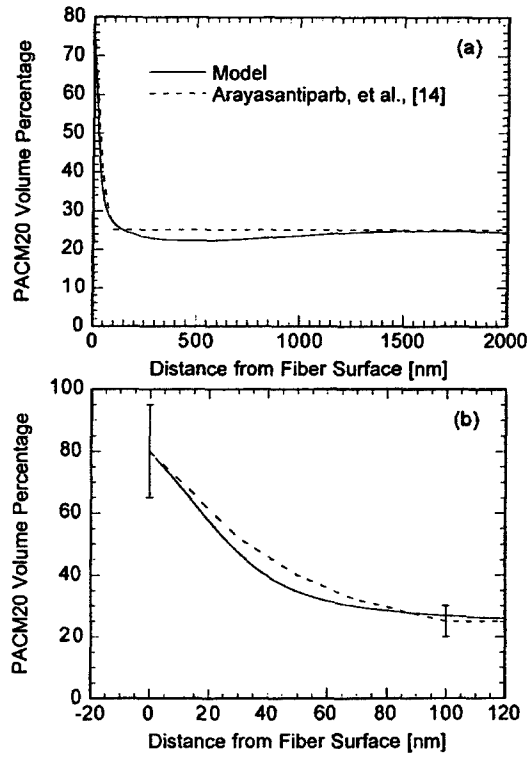

Figure 2 Comparison of the interphase composition profile predicted by the model and available experimental data[14] for an aluminum fiber/DGEBA-PACM20 system, over (a) a relative large region from the fiber surface, and (b) the interphase region.

TABLE III
Model Parameters Determined by the Correlation to Experimental Data

Parameter	Value	Parameter	Value
$D_0\exp(-E_D/RT)/\Delta L^2$ (1/s)	6.05×10^4	b_D	5.48×10^{-2}
$k_{r0}\exp(-E_a/RT)$ (1/s)	1.08×10^{-4}	N_0/N_{E0}	0.65
$k_{aE}\exp(-E_{aE}/RT)$ (1/s)	2.04×10^{-5}	$k_{dE}\exp(-E_{dE}/RT)$ (1/s)	1.58×10^{-2}
$k_{aA}\exp(-E_{aA}/RT)$ (1/s)	0.85	$k_{dA}\exp(-E_{dA}/RT)$ (1/s)	1.03×10^{-2}

determined through direct experimental or theoretical methods in a future work.

With the correlation results of the interphase formation model as basis, parametric studies were conducted to illustrate the effects of different parameters on the interphase composition and thickness of an epoxy/amine system. Dimensionless forms of eqs. (2)–(12) were used to identify relevant nondimensional groups that governed the process. By introducing a dimensionless time (t') as $k_{a,E}e^{-(E_{a,E}/RT_0)}t$ and dividing all the number of molecules (e.g., $N_{E,i}$, $N_{A,i}$, N_0) by the initial number of epoxy molecules in the far region layers (N_{E0}; e.g., $N'_{E,i} = N_{E,i}/N_{E0}$), we identified the principal dimensionless groups as follows: (1) epoxy desorption ratio, $\beta_E = (k_{d,E}/k_{a,E})e^{-(E_{d,E}-E_{a,E})/RT_0}$; (2) amine desorption ratio, $\beta_A = (k_{d,A}/k_{a,E})e^{-(E_{d,A}-E_{a,E})/RT_0}$; (3) amine adsorption ratio, $\alpha_A = (k_{a,A}/k_{a,E})e^{-(E_{a,A}-E_{a,E})/RT_0}$; (4) adsorption Damköhler number, $\gamma = (k_r/k_{a,E})e^{(E_{a,E}/RT_0)}$; and (5) diffusion ratio, $\phi_{EA} = (D_{EA}/\Delta L^2 k_{a,E})e^{(E_{a,E}/RT_0)}$. In the parametric study, the number of molecular layers in the model domain was kept fixed at $N_L = 100$, and the physical dimension of a molecular layer was chosen to be 1.00 nm, that is, the value for the DGEBA/PACM20 system.

Figures 3–5 present the evolution of the concentration profiles with time for three selected scenarios to illustrate the influence of each mechanism considered in the model. Although the total concentrations are the most relevant to the composite material properties, the results of the adsorbed and bulk fractions are presented as well to better elucidate the trends in the total concentration development. Figure 3(a–f) shows the distributions of the number of epoxy and amine molecules from the fiber surface (layer 1) to the far region (layer 100) at different nondimensional times during the process. Figure 3(a,b) presents the concentration profiles for the molecules in the adsorbed state, Figure 3(c,d) corresponds to bulk state concentration profiles, and Figure 3(e,f) shows the total concentrations of epoxy and amine, $N'_{E,\text{tot}}$ and $N'_{A,\text{tot}}$, respectively. The results correspond to the parameter combination of $N_S = 0$ (i.e., without a sizing layer), $\gamma = 0$, $\beta_E = 0.5$, $\alpha_A + 1.5$, $\beta_A = 0.5$, $N'_{E0} = N'_{A0} = 1$, $N'_{E,1} = 2$, $N'_0 = 1$ [$N'_0 = (N_0/N_{E0})$], and $\phi_{EA} = 60.0$. γ was set to zero to examine the effects of the adsorption and desorption processes in the absence of chemical reactions. The desorption ratios β_E and β_A were relatively small, which indicated that the resin molecules were easily adsorbed onto the fiber surface.

In the adsorbed state profiles, Figure 3(a,b), the number of molecules for both of the species increased due to adsorption onto the surface, resulting in a high concentration region near the fiber surface. The concentration profiles propagated from a small region near the fiber surface at $t' = 0.2$ to the far region at the final time $t' = 102.0$, which was identified as a strong adsorption effect. The number of epoxy molecules near the fiber surface was smaller than that of the amine molecules because of the larger amine adsorption rate ($\alpha_A = 1.5$). The adsorption/desorption processes caused the deficit of species in the bulk state near the fiber surface, as shown in Figure 3(c,d) from $t' = 0.2$ to $t' = 25.0$. However, the diffusion process compensated for the deficit at the final time, $t' = 102.0$, when the concentration gradients in the bulk state approached zero. The total concentration profiles of each species [Fig. 3(e,f)] showed minima at $t' = 10.0$ and $t' = 25.0$, which could be explained by the coupled influence of the adsorption/desorption and the diffusion processes as discussed.

The interphase thickness is a critical factor influencing the overall composite performance and properties, as noted in the literature.[3,7] For example, Rydin et al.[3] reported that a thin ductile interphase increased the interlaminar toughness through crack blunting, enhanced frictional sliding, and greater part deflections prior to fracture. However, a further increase in the thickness was shown to facilitate debonding and delamination because the strong adhesion between fiber and matrix was replaced by weak dipole–dipole interactions between the interphase and the matrix. In another study, Liu et al.[7] found that when the modulus of the interphase was greater than that of the matrix, an increase in the interphase thickness (δ) led to an increase in the overall composite modulus.

Interphase thickness may be defined in a similar way as the boundary layer thickness in fluid mechanics, such as the number of layers from the fiber surface beyond which the epoxy concentration is within 1% of the epoxy concentration in the far region layers [Fig. 3(e)]. A similar thickness, δ_A, may be defined on the basis of the amine concentration profile. With the thickness based on the epoxy concentration profile denoted as δ_E, an overall δ was determined in this study as the larger of the two values obtained from the epoxy and amine profiles, that is, $\delta = \max(\delta_E, \delta_A)$. As shown in Figure 3(e,f), the interphase was thin at an early time ($t' = 0.2$) and grew as the process progressed ($t' = 102.0$); the profiles at $t' = 102.0$ are the equilibrium profiles representing the balance among the adsorption, desorption, and diffusion processes. For the combination of parameters in Figure 3, because of the absence of the reaction and the relatively small desorption, the influence of the fiber surface propagated all the way to the far region layer, leading to a very thick or no distinct interphase formation at the final time.

Figure 4(a–f) presents the concentration profile evolution, following the presentation format in Figure 3(a–f), for the parameter combination of $\beta_E = 1.5$, $\alpha_A = 0.5$, and $\beta_A = 2.0$; all other parameters retained the values as in Figure 3. Figure 4(a,b) shows that the concentration profiles in the adsorbed state grew from $t' = 0.2$ to $t' = 10.0$ and remained invariant afterward.

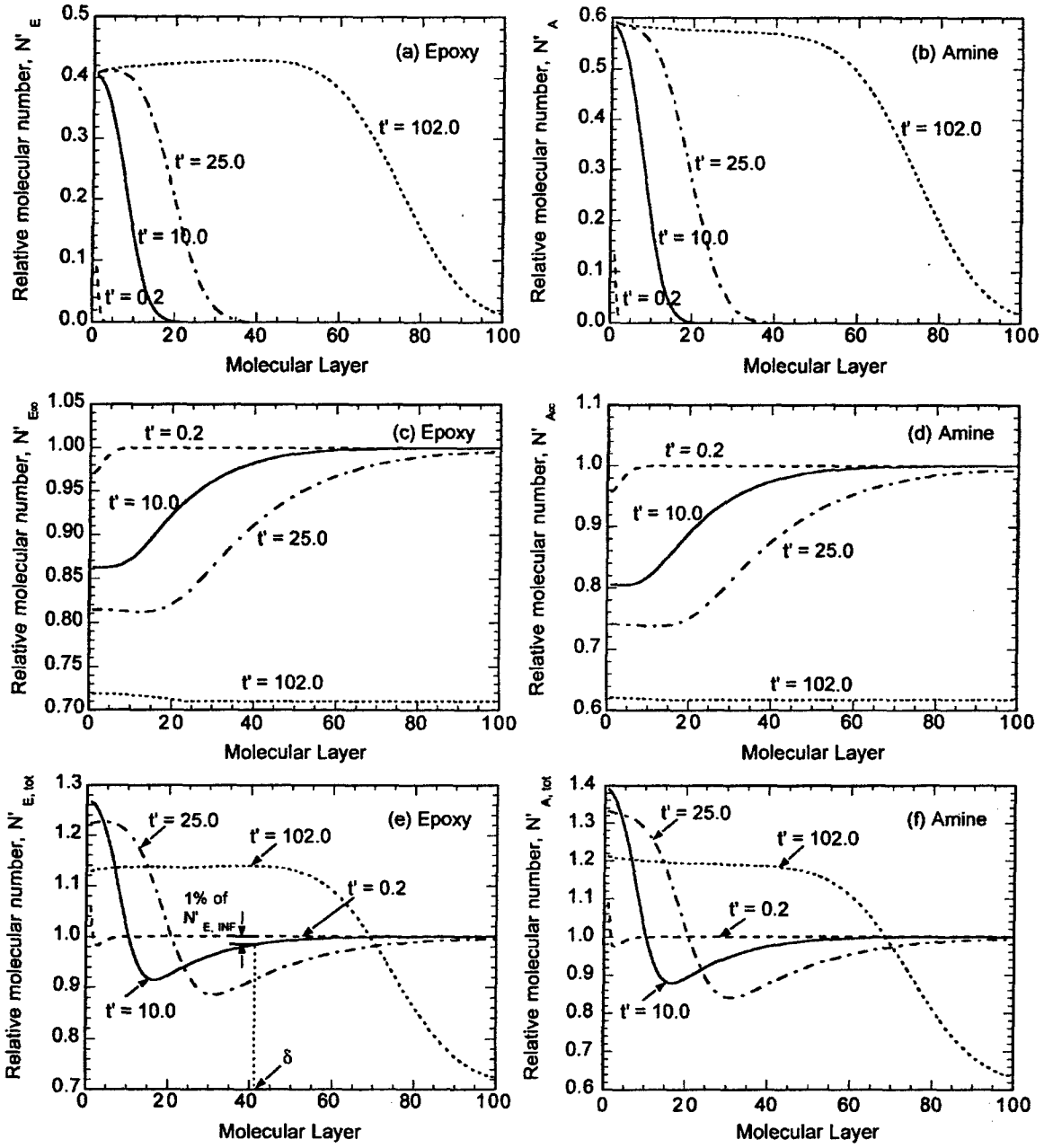

Figure 3 Interphase concentration profiles in terms of the relative number of (a) epoxy molecules in the adsorbed state, and (b) amine molecules in the adsorbed state; (c) epoxy molecules in the bulk state, and (d) amine molecules in the bulk state; (e) total epoxy molecules in both states, and (f) total amine molecules in both states, as a function of the molecular layer at four different times during the isothermal cure process. The parameter combination corresponds to a unsized system with strong adsorption effect and zero reaction rate.

An equilibrium state was thus reached, where the desorption and adsorption processes balanced each other and the influence of the fiber surface only propagated to a few molecular layers. The concentration profiles in the bulk state [Fig. 4(c,d)] predicted large concentration gradients at time $t' = 0.2$; at $t' > 0.2$, because to the diffusion process, the gradients decreased and reached zero at $t' = 82.0$. At $t' = 10.0$ and $t' = 25.0$, the regions with nonzero gradients in the bulk state were wider than the corresponding regions in the adsorbed state. Consequently, the total concentration profiles [Fig. 4(e,f)] showed that the interphase thickness first increased from $t' = 0.2$ to $t' = 25.0$, mostly due to the contributions from the bulk state,

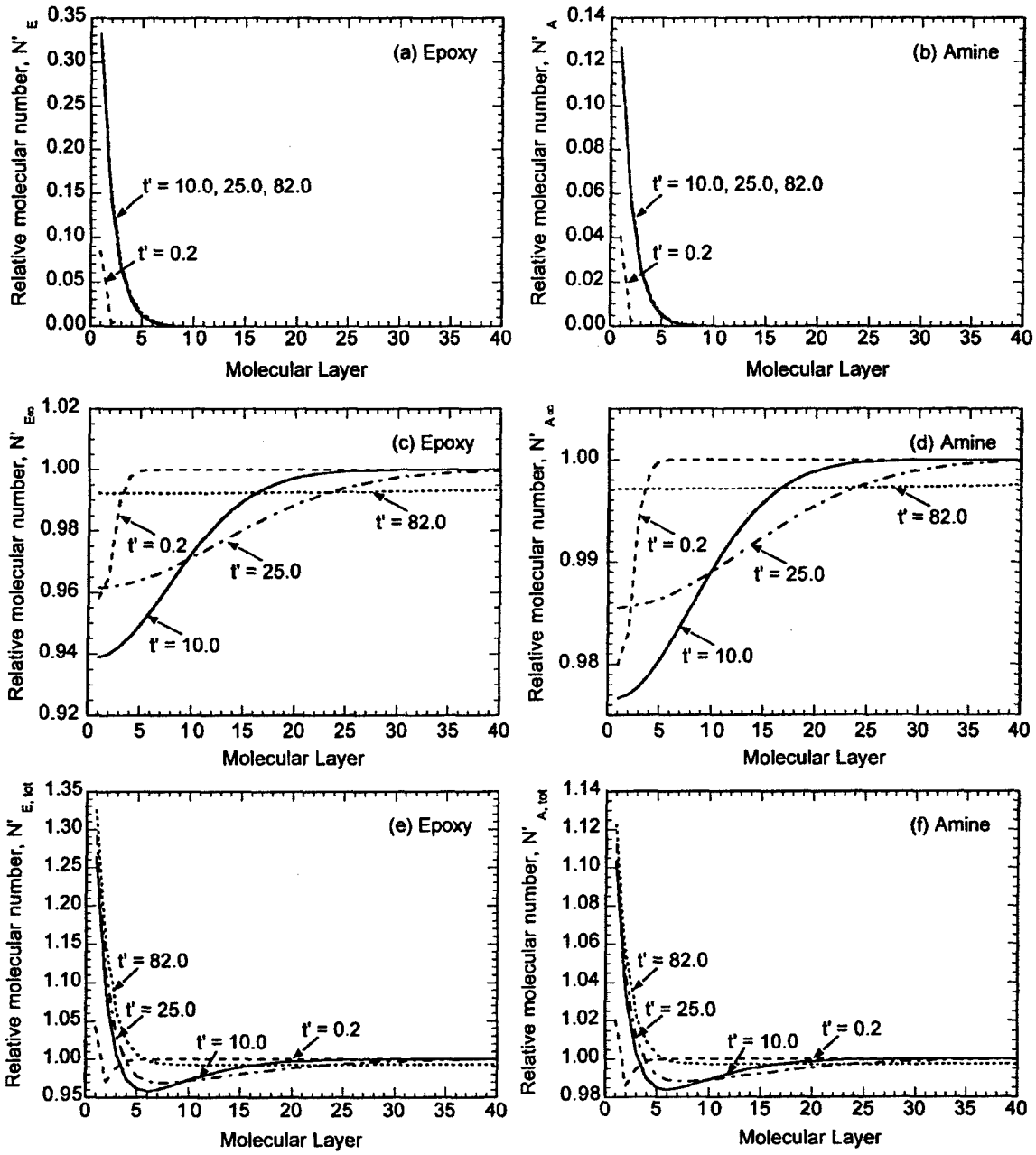

Figure 4 Interphase concentration profiles in terms of the relative number of (a) epoxy molecules in the adsorbed state, and (b) amine molecules in the adsorbed state; (c) epoxy molecules in the bulk state, and (d) amine molecules in the bulk state; (e) total epoxy molecules in both states, and (f) total amine molecules in both states, as a function of the molecular layer at four different times during the isothermal cure process. The parameter combination corresponds to a unsized system with weak adsorption effect and zero reaction rate.

and then decreased to a smaller value governed by the adsorbed state gradients at time $t' = 82.0$, when the diffusion gradients were zero. This scenario is in contrast to what is shown in Figure 3, where a strong force field by the fiber surface penetrated the entire resin domain. Through an increase in β_A and β_E and a decrease in α_A, the desorption process was strengthened with respect to adsorption, which corresponded to a relatively weak force field by the fiber surface that could only penetrate into a few molecular layers.

The parametric studies presented so far pertained to concentration evolution of a resin/fiber system without sizing layers on the fiber surface. The application of an epoxy sizing on the fiber surface is a common

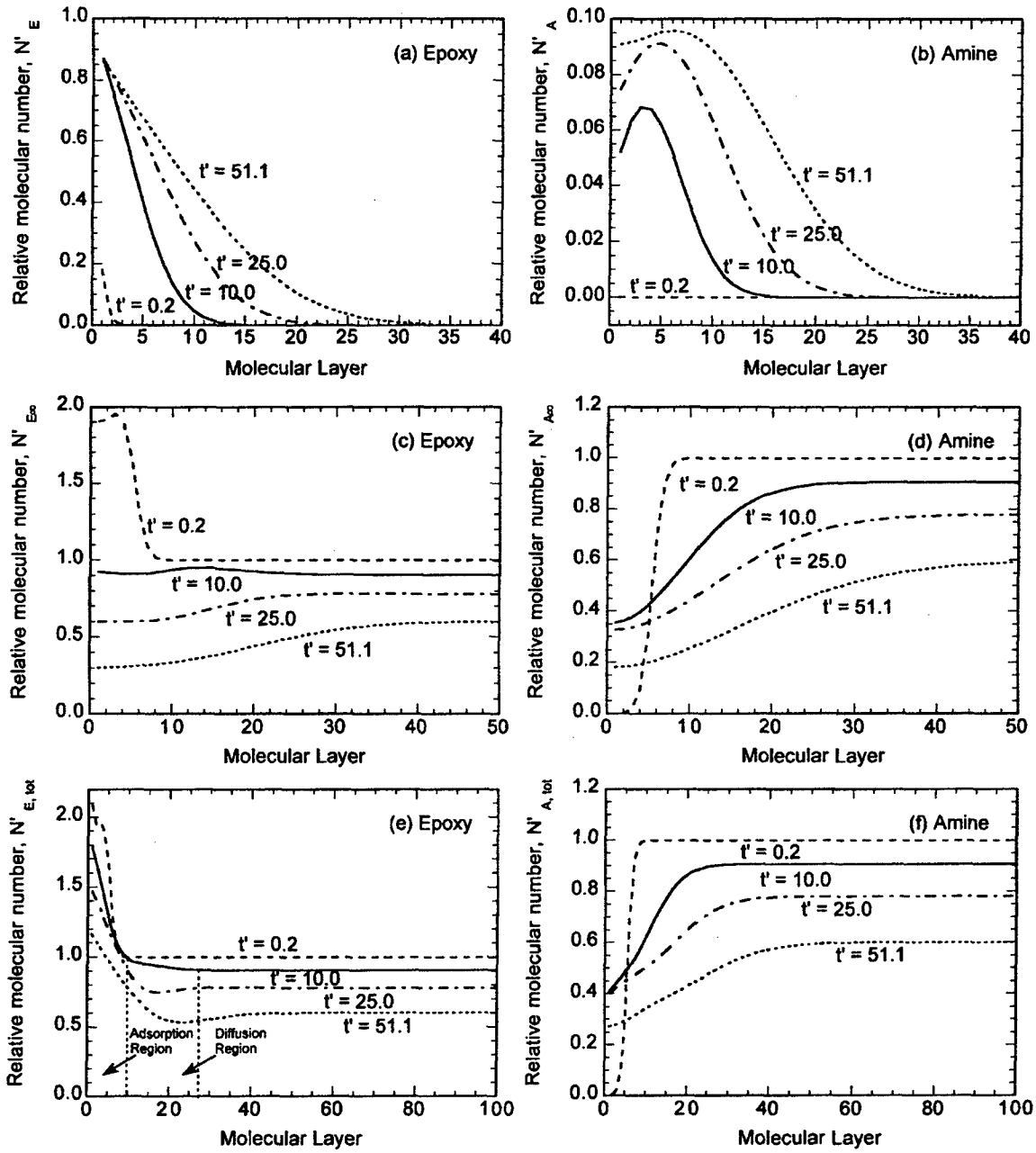

Figure 5 Interphase concentration profiles in terms of the relative number of (a) epoxy molecules in the adsorbed state, and (b) amine molecules in the adsorbed state; (c) epoxy molecules in the bulk state, and (d) amine molecules in the bulk state; (e) total epoxy molecules in both states, and (f) total amine molecules in both states, as a function of the molecular layer at four different times during the isothermal cure process. The parameter combination corresponds to a sized system with relative large reaction rate.

practice in the manufacturing process, and we were interested in examining its effect on the interphase evolution. Figure 5 follows the same presentation format as Figures 3 and 4 to show the concentration profiles evolution of a system with sizing. The result corresponds to the parameter combination of $N_S = 5$, $\gamma = 5.0$, $\beta_E = 0.5$, $\alpha_A = 1.5$, and $\beta_A = 0.5$, and all other parameters retained the same values as previously stated for Figure 3. Recall that the mass transfer through the adsorption, desorption, and diffusion processes is dramatically slowed when the reacting resin system reaches the gelation point, and the final concentration profiles can be approximated by the profiles at the gelation point. Because γ de-

termines the gelation time and, in turn, the available time for the mass transfer processes, as γ increases, the available time decreases. In Figure 5, γ is set to be relatively large, providing only a limited time for the mass transfer processes to develop.

The concentration of epoxy in the adsorbed state increased with time, and the growth was stopped by the reaction at the gelation time $t' = 51.1$, as shown in Figure 5(a). The amine concentration profiles, shown in Figure 5(b), had maxima near the fiber surface, which may be explained as follows: because the epoxy sizing directly contacted the fiber surface, epoxy molecules occupied most of the adsorption sites near the fiber surface, and most of the amine molecules could only be adsorbed on top of the epoxy molecules. Therefore, the amine concentration was small at the fiber surface, followed by an increase within a few molecular layers around the fiber due to adsorption and then a decrease as the net adsorption diminished in the region away from the fiber. As shown in Figure 5(c,d), the initially large concentration of epoxy and zero concentration of amine (at $t' = 0.2$) near the fiber surface correspond to the epoxy sizing layer applied on the fiber. At the gelation time ($t' = 51.1$), the concentration gradients in the bulk were small but greater than zero because the gelation time is not long enough for the diffusion process to reach equilibrium.

At time $t' = 10.0$, the total epoxy profile [Fig. 5(e)] had two distinct regions: a large gradient region near the fiber surface, followed by a small gradient region. An examination of the concentration profiles of the epoxy species in the adsorbed state [Fig. 5(a)] and bulk state [Fig. 5(c)] separately revealed that the large gradient region came from the profile in the adsorbed state, whereas the small gradient region was determined by the profile in the bulk state. These are shown in Figure 5(e) as the adsorption region and the diffusion region, respectively, for the particular time instant $t' = 10.0$. These regions grew away from the fiber with time, with the gradients in the diffusion region approaching zero because the tendency of the diffusion to equilibrate the concentration, whereas the gradient in the adsorption region approached an equilibrium value, corresponding to the net balance of the adsorption and desorption effects. Two minima of the epoxy concentration are shown in Figure 5(e), at $t' = 25.0$ and $t' = 51.1$, respectively, which can be explained by the fact that epoxy molecules were adsorbed onto the fiber surface from the neighborhood, resulting in the deficiency of the epoxy species, which was not sufficiently replenished through the diffusion process. Figure 5(f) presents the amine concentration evolution with time. In this case, the diffusion and adsorption mass transfer were in the same direction, toward the fiber surface, as opposed to that in Figure 5(e), where the adsorption caused epoxy migration

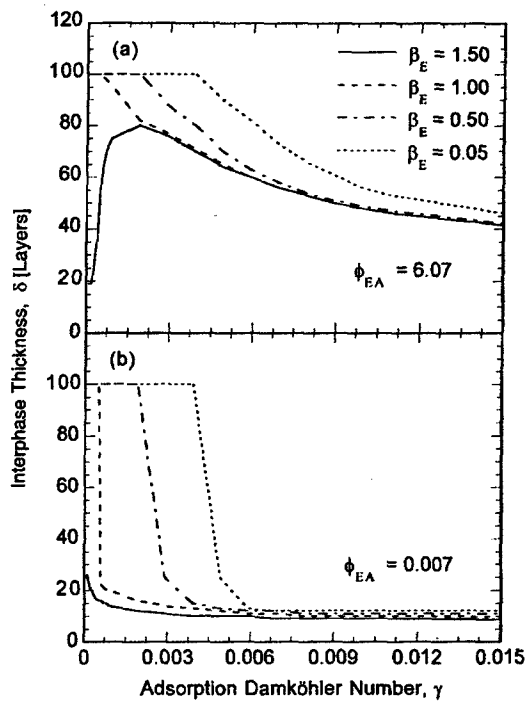

Figure 6 Interphase thickness as a function of adsorption Damköhler number, γ, at various epoxy desorption ratios, β_E, for (a) $\phi_{EA} = 6.07$ and (b) $\phi_{EA} = 0.007$.

toward the fiber, and diffusion tended to move the epoxy molecules away from the fiber.

An interphase thickness could be identified on the basis of the total concentration profiles, as shown in Figure 3(e). The interphase thickness is a concise representation of the interphase concentration profiles. As discussed previously, it critically influences the composite properties and constitutes an important input in the micromechanical models.[1,7] It is, therefore, instructive to examine the influence of each mechanism studied in the model on the interphase thickness. Figures 6–8 illustrate the roles of the various mechanisms involved and provide insight on the overall process. In Figure 6(a), the interphase thickness at the gelation time is plotted as a function of γ for different values of β_E. The result corresponded to the parameter combination of $\alpha_A = 1.0$, $\beta_A = 1.0$, $\phi_{EA} = 6.07$, and $N_S = 5$, and all of the other parameters retained their values as in Figure 3. In the parametric studies of the epoxy–amine system, the maximum thickness value was taken to be $N_L = 100$ layers. For the case of no reaction (i.e., $\gamma = 0$), which corresponded to an infinitely long interphase growth time, the diffusion process was fully developed, and the interphase concentration gradient and thickness were only determined by the net adsorption. For the case of $\beta_E = 0.05$, the small value indicated that the fiber surface had a strong net adsorption, which may have penetrated to

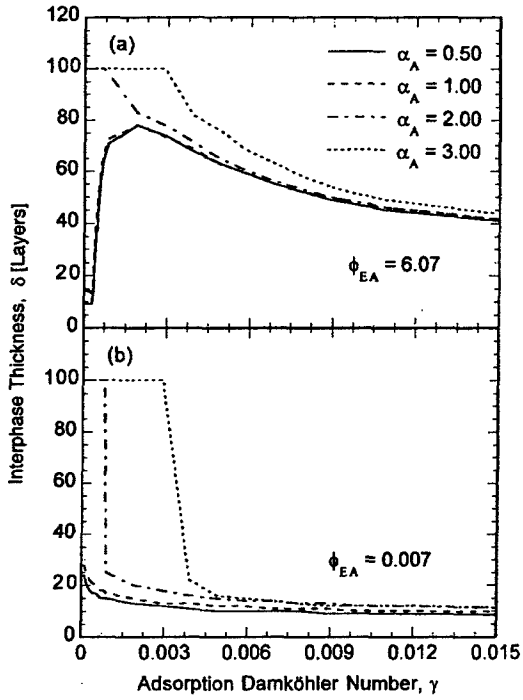

Figure 7 Interphase thickness as a function of adsorption Damköhler number, γ, at various amine adsorption ratios, α_A, for (a) ϕ_{EA} = 6.07 and (b) ϕ_{EA} = 0.007.

the entire resin domain given enough time. Therefore, when $\gamma = 0$, the curve started at the maximum thickness—100 layers. As γ increased, less time was available for the interphase development, and the thickness decreased monotonically. The same trend was observed for β_E = 0.50 and 1.00, which also had relatively strong net adsorptions.

With the increase in γ from zero, the increased reaction rate corresponded to less time available for the transport processes prior to gelation. The diffusion profile was, therefore, arrested before completion, which led to a thick diffusion. Because the adsorption/desorption concentration gradients were confined to a region near the fibers, the overall interphase thickness was governed by the diffusion profile, which led to an increased interphase thickness, as shown in Figure 6(a) for a β_E of 1.50. The increase in the interphase thickness from $\gamma = 0$ to a nonzero value was primarily due to the shift in the contribution to the interphase gradient from that of adsorption/desorption only (for $\gamma = 0$) to that of diffusion (for a small γ not equal to zero). With a further increase in the reaction rate (i.e., an increase in γ), the progressive decrease in the available time for the transport processes led to a monotonic decrease in the interphase thickness. In fact, as γ approaches infinity (the case of an infinitely fast reaction), the interphase composition should be that of the initial condition, and the interphase thickness should be the sizing thickness, N_S. As shown in the trend in Figure 6(a), all of the curves asymptotically approach this value (beyond the range of the plot). Furthermore, for a fixed γ, the interphase thickness decreased monotonically with increasing β_E because more molecules were desorbed from the interphase region.

Figure 6(b) has the same parameter combination as Figure 6(a) except that the diffusion ratio was set to ϕ_{EA} = 0.007 to show the effect of sluggish diffusion. The interphase thicknesses predicted in Figure 6(b) reflect the negligible contribution of the diffusion process and were always smaller than or equal to the corresponding values shown in Figure 6(a). Also, for the weak net adsorption cases, Figure 6(b) did not exhibit the peaks shown in Figure 6(a), again due to the small diffusion.

Figure 7(a) presents the interphase thickness as a function of γ and α_A. The result corresponded to the parameter combination β_A = 2.0, β_E = 1.0, ϕ_{EA} = 6.07, and N_S = 5, with all the other parameters retaining the same values as in Figure 3. The diffusion ratio ϕ_{EA} of 6.07 denoted a relatively active diffusion process. The parameter α_A reflected the relative attraction strength of the fiber surface to the epoxy and amine molecules, with $\alpha_A > 1$ denoting a preferential adsorption of the amine molecules. Through an increase in α_A, surface attraction to amine molecules was strengthened, which led to a thicker interphase rich in amine concentration. The influence of γ can be discussed by

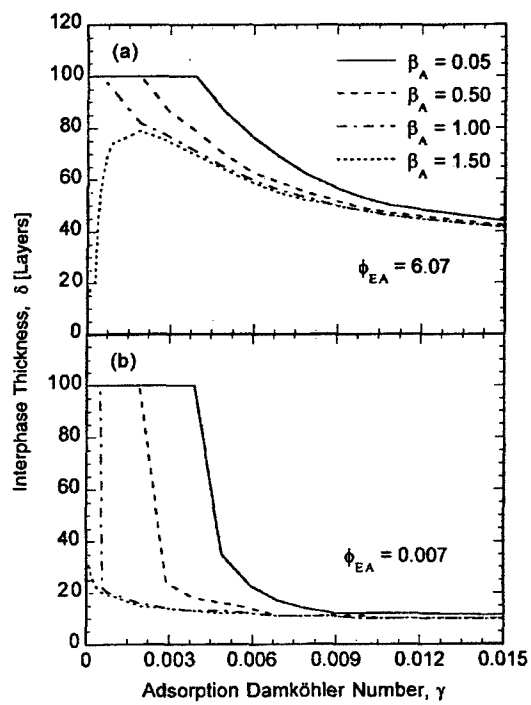

Figure 8 Interphase thickness as a function of adsorption Damköhler number, γ, at various amine desorption ratios, β_A, for (a) ϕ_{EA} = 6.07 and (b) ϕ_{EA} = 0.007.

similar considerations to those for the β_E effect in Figure 6. For strong net adsorption (corresponding to $\alpha_A = 2.0$ and 3.0), the thickness decreased monotonically from the maximum thickness of 100 layers with the increase of γ, whereas in the cases of weak net adsorption (corresponding to $\alpha_A = 0.5$ and 1.0), the thickness increased first due to the contribution of the diffusion and then decreased gradually. All the curves tended to the initial sizing thickness for $\gamma \rightarrow \infty$. At a constant value of γ, the interphase thickness increased monotonically with the increase in α_A because of the enhancement of the net adsorption.

Figure 7(b) represents the interphase thickness variation for the same parameter combination as in Figure 7(a) except for a ϕ_{EA} of 0.007 to illustrate the effect of weak diffusion. Similar to the discussion of Figure 6(b), the interphase thicknesses predicted in Figure 7(b) did not have a significant contribution of the diffusion process and were always smaller than or equal to the corresponding values shown in Figure 7(a). Again, for the weak net adsorption cases, Figure 7(b) does not exhibit the peaks shown in Figure 7(a) due to the lack of diffusion.

In Figure 8(a,b), the interphase thickness is presented as a function of γ and β_A. The result corresponded to the parameter combination of $\alpha_A = 1.0$, $\beta_E = 1.0$, $\phi_{EA} = 6.07$, and $N_S = 5$, with all the other parameters retaining the same values as in Figure 3. From eqs. (2) and (8), it follows that β_A had the same parametric effect as β_E, in that large values of β_A and β_E corresponded to weak net adsorption effects. Because the trends in Figure 8 were similar to those in Figure 6, the reader may examine to the corresponding discussion earlier. Although Figures 6 and 8 give similar thickness variations with corresponding desorption rates, the interphase compositions in the two cases were different; that is, a large β_E value corresponded to an epoxy-deficient interphase, whereas a large β_A value corresponded to an amine-deficient interphase. These two types of interphase would, therefore, lead to completely different properties of the overall composite.

The predicted interphase composition and thickness are important input data to the models that calculate the overall composite material properties. A significant step in a future work will be to determine the parameters involved in the kinetics model. Within the framework of the current model, the parameters may be evaluated by following the procedure outlined in the correlation study. In this case, the EELS measurements must be conducted systematically on the desired materials and temperatures to provide the concentration data in the interphase region. The current model is based on phenomenological descriptions of the kinetics of the governing transport processes without resorting to the calculations of the driving forces. Alternatively, the development of the thermodynamic or statistical models mentioned previously[1,10] involved detailed consideration of the driving forces (e.g., the enthalpy forces or entropy forces) and the complex motion and configuration of polymer molecules under these forces. The thermodynamic and kinetics approaches are equivalent if a relationship between the driving forces and the kinetics parameters can be established.

In this study, the temperature was taken as a given constant, whereas the real temperature field during a cure process needs to be solved by coupling to the energy equation for the whole composite domain. The cure cycles in the manufacturing processes act as boundary conditions for the energy equation to influence the temperature field, which in turn, controls the adsorption–desorption–diffusion–reaction processes and interphase formation. Therefore, through optimization of the cure cycle, the interphase can be tailored for a specific material system's requirements. These issues are presently under investigation to enhance the capabilities of the current model.

CONCLUSIONS

An adsorption–desorption–diffusion–reaction model was developed to predict the evolution of the interphase during isothermal cure of thermosetting resin systems. The parameters of the model were determined through a correlation to available experimental data on a DGEBA/PACM20 system. Parametric studies revealed that the concentration profiles showed minima or maxima instead of following simple monotonical patterns. In the case of strong net adsorption, as indicated by large values of adsorption rates and small values of desorption rates, the interphase thickness decreased monotonically with increasing reaction rate. Weak net adsorption resulted in peaks in the interphase thickness curves with respect to the reaction rate, due to the influence of the diffusion. A notable contribution of this study was the ability to predict the time evolution of the interphase. The predicted interphase composition and thickness may be used as input data for the finite element analysis of the overall composition properties, eliminating the need to assume input data values. The model may be combined with a macroscopic thermochemical model to establish the influence of the cure cycle on the interphase formation. This, in turn, will lead to the capability to tailor the interphase via optimal cure cycle selection.

NOMENCLATURE

b_D	empirical constant in the diffusion coefficient expression in eq. (13)
D_0	constant in the diffusion coefficient expression in eq. (13) (m^2/s)
D_{EA}	mutual diffusion coefficient in the binary epoxy–amine structure (m^2/s)

E_a	activation energy in the reaction rate expression in eq. (15) (J/kg)
$E_{a,A}$	adsorption activation energy of amine molecules (J/kg)
$E_{a,E}$	adsorption activation energy of epoxy molecules (J/kg)
E_D	activation energy in the diffusion coefficient expression in eq. (13) (J/kg)
$E_{d,A}$	desorption activation energy of amine molecules (J/kg)
$E_{d,E}$	desorption activation energy of epoxy molecules (J/kg)
E_x/E_m	constant in the DiBenedetto expression in eq. (14)
f_g	constant in the diffusion coefficient expression in eq. (13)
F_x/F_m	constant in the DiBenedetto expression in eq. (14)
$k_{a,A}$	adsorption rate of amine molecules (s^{-1})
$k_{a,E}$	adsorption rate of epoxy molecules (s^{-1})
$k_{d,A}$	desorption rate of amine molecules (s^{-1})
$k_{d,E}$	desorption rate of epoxy molecules (s^{-1})
k_r	reaction rate (s^{-1})
k_{r0}	Arrhenius preexponential constant in the reaction rate expression in eq. (15) (s^{-1})
M	molecular weight (kg/kmol)
M_A	molecular weight of PACM20 (kg/kmol)
M_E	molecular weight of DGEBA (kg/kmol)
n_1	number of moles of epoxy molecules (mol)
n_2	number of moles of amine molecules (mol)
N'_a	Avogadro's number
N_0	number of adsorption sites available for adsorption on the fiber surface
N'_0	dimensionless variable ($N_0/N_{E,0}$)
N_i	total number of adsorbed resin molecules in the ith layer
$N_{\infty,i}$	total number of resin molecules in the bulk state in the ith layer
$N_{A,0}$	initial number of amine molecules at the far region layers
$N_{A,i}$	number of adsorbed amine molecules in the ith layer
$N'_{A,i}$	dimensionless variable ($N_{A,i}/N_{E,0}$)
$N_{A\infty,i}$	number of amine molecules in the bulk state in ith layer
$N'_{A,\infty}$	dimensionless variable ($N_{A,\infty}/N_{E,0}$)
$N'_{A,\mathrm{tot}}$	total concentration of amine
$N_{E,0}$	initial number of epoxy molecules at the far region layers
$N_{E,1}$	initial number of epoxy molecules in the sizing layer
$N_{E,i}$	number of adsorbed epoxy molecules in the ith layer
$N'_{E,i}$	dimensionless variable ($N_{E,i}/N_{E,0}$)
$N_{E\infty,i}$	number of epoxy molecules in the bulk state in the ith layer
$N'_{E,\infty}$	dimensionless variable ($N_{E,\infty}/N_{E,0}$)
$N'_{E,\mathrm{tot}}$	total concentration of epoxy
N_L	the number of the far region layer where all of the resin molecules are at the bulk state and where the composition becomes constant beyond this layer
$N_{P,i}$	number of product segments in the ith layer due to the reaction in the adsorbed state
$N'_{P,i}$	dimensionless variable ($N_{P,i}/N_{E,0}$)
$N_{P\infty,i}$	number of product segments in the ith layer due to the reaction in the bulk state
$N'_{P,\infty}$	dimensionless variable ($N_{P,\infty}/N_{E,0}$)
N_S	number of sizing layers
R	Universal gas constant (J/kg k)
$R_{a,A}(i-1, i)$	rate term of the adsorption of amine molecules from the $(i-1)$th bulk layer to the ith adsorption layer (s^{-1})
$R_{a,A}(i, i)$	rate term of the adsorption of amine molecules from the ith bulk layer to the ith adsorption layer (s^{-1})
$R_{a,A}(i+1, i)$	rate term of the adsorption of amine molecules from the $(i+1)$th bulk layer to the ith adsorption layer (s^{-1})
$R_{d,A}(i-1, i)$	rate term of the desorption of amine molecules from the ith adsorption layer to the $(i-1)$th bulk layer (s^{-1})
$R_{d,A}(i, i)$	rate term of the desorption of amine molecules from the ith adsorption layer to the ith bulk layer (s^{-1})
$R_{d,A}(i+1, i)$	rate term of the desorption of amine molecules from the ith adsorption layer to the $(i+1)$th bulk layer (s^{-1})
$R_{a,E}(i-1, i)$	rate term of the adsorption of epoxy molecules from the $(i-1)$th bulk layer to the ith adsorption layer (s^{-1})
$R_{a,E}(i, i)$	rate term of the adsorption of epoxy molecules from the ith bulk layer to the ith adsorption layer (s^{-1})
$R_{a,E}(i+1, i)$	rate term of the adsorption of epoxy molecules from the $(i+1)$th bulk layer to the ith adsorption layer (s^{-1})

$R_{d,E}(i-1, i)$ rate term of the desorption of epoxy molecules from the ith adsorption layer to the $(i-1)$th bulk layer (s^{-1})

$R_{d,E}(i, i)$ rate term of the desorption of epoxy molecules from the ith adsorption layer to the ith bulk layer (s^{-1})

$R_{d,E}(i+1, i)$ rate term of the desorption of epoxy molecules from the ith adsorption layer to the $(i+1)$th bulk layer (s^{-1})

$\Re_{a,A}$ total adsorption rate of amine species into the ith adsorption layer from the neighboring bulk layers [eq. (8)] (s^{-1})

$\Re_{a,E}$ total adsorption rate of epoxy species into the ith adsorption layer from the neighboring bulk layers [eq. (2)] (s^{-1})

$\Re_{d,A}$ total desorption rate of amine species into the ith adsorption layer from the neighboring bulk layers [eq. (8)] (s^{-1})

$\Re_{d,E}$ total desorption rate of epoxy species into the ith adsorption layer from the neighboring bulk layers [eq. (2)] (s^{-1})

$\Re_{r,A}$ depletion rate of amine species due to the crosslinking chemical reaction [eq. (8)] (s^{-1})

$\Re_{r,E}$ depletion rate of amine species due to the crosslinking chemical reaction [eq. (2)] (s^{-1})

T temperature (K)

T_0 isothermal processing temperature considered in the parametric studies (K)

T_g glass-transition temperature (K)

T_g^0 constant in the DiBenedetto expression in eq. (14) (K)

t time (s)

t' dimensionless time in the parametric study

v volume

v_m molecular volume

X_A molar fraction of PACM20

Greek symbols

α_A $(k_{a,A}/k_{a,E})e^{-(E_{a,A}-E_{a,E}/RT_0)}$, the ratio of the adsorption rates of amine and epoxy molecules

α_f constant in the diffusion coefficient expression in eq. (13) (K^{-1})

β_A $(k_{d,A}/k_{a,E})e^{-(E_{d,A}-E_{a,E}/RT_0)}$, the ratio of the desorption rate of amine molecules to the adsorption rate of epoxy molecules

β_E $(k_{d,E}/k_{a,E})e^{-(E_{d,E}-E_{a,E}/RT_0)}$, the ratio of the desorption rate of epoxy molecules to the adsorption rate of epoxy molecules

δ interphase thickness in terms of molecular layers

δ_0 coordination sphere reaction parameter in the reaction rate expression in eq. (15) (cm^2/s)

δ_A interphase thickness based on the amine concentration profile

δ_E interphase thickness based on the epoxy concentration profile

ΔL physical size of a molecular layer (m)

ϕ_{EA} $(D_{EA}/\Delta L^2 k_{a,E})e^{(E_{a,E}/RT_0)}$, the ratio of the mutual diffusion rate to the adsorption rate of epoxy molecules

Φ_A volume fraction of PACM20

γ $(k_r/k_{a,E})e^{(E_{a,E}/RT_0)}$, adsorption Damköhler number, or the ratio of the chemical reaction rate to the adsorption rate of epoxy molecules

ρ density (kg/m^3)

ρ_A density of PACM20 (kg/m^3)

ρ_E density of DGEBA (kg/m^3)

ε reaction extent, $N_E/N_{E,0}$

References

1. Palmese, G. R. Origin and Influence of Interphase Material Property Gradients in Thermosetting Composites; Technical Report Number 92-25; University of Delaware Center for Composite Materials, Newark, DE 1992.
2. Subramanian, S.; Lesko, J. J.; Reifsnider, K. L.; Stinchcomb, W. W. J Compos Mater 1996, 30, 309.
3. Rydin, R. W.; Varelidis, P. C.; Papaspyrides, C. D.; Karbhari, V. M. J Compos Mater 1997, 31, 182.
4. Drzal, L. T. Adv Polym Sci 1986, 75, 1.
5. Madhukar, M. S.; Drzal, L. T. J Compos Mater 1991, 25, 958.
6. Dong, Z.; Wu, Y. J Mater Sci 1996, 31, 4401.
7. Liu, Y. J.; Xu, N.; Luo, J. F. J Appl Mech 2000, 67, 41.
8. Garton, A.; Stevenson, W. T. K.; Wang, S. Br Polym J 1987, 19, 459.
9. Sellitti, C.; Koenig, J. L.; Ishida, H. Mater Sci Eng A 1990, 126, 235.
10. Hrivnak, J. Interphase Formation in Reacting Systems; Technical Report Number 97-05; University of Delaware Center for Composite Materials, Newark, DE 1997.
11. Scheutjens, J. M. H. M.; Fleer, G. J. J Phys Chem 1979, 83, 1619.
12. Sergeyeva, L. M.; Todosiychuk, T. T.; Fabulyak, F. G. Geterogennye Polim Mater 1974, 79.
13. Ko, Y. S.; Forsman, W. C.; Dziemanowicz, T. S. Polym Eng Sci 1982, 22, 805.
14. Arayasantiparb, D.; McKnight, S.; Libera, M. J Adhes Sci Technol 2001, 15, 1463.
15. Hill, T. L. J Chem Phys 1946, 14, 268.
16. Ponec, V.; Knor, Z.; Cerny, S. Adsorption on Solids; Butterworth: London, 1974.
17. Sanford, W. M. Ph. D. Thesis, University of Delaware, 1987.
18. Press, W. H.; Teukolsky, S. A.; Vetterling, W. T.; Flannery, B. P. Numerical Recipes in FORTRAN; Cambridge University Press; New York, 1986.
19. Mawardi, A.; Pitchumani, R. ASME J Heat Transfer 2003, 125(1), 126.

Available online at www.sciencedirect.com
SCIENCE DIRECT
Composites Science and Technology 64 (2004) 1437–1452
COMPOSITES SCIENCE AND TECHNOLOGY
www.elsevier.com/locate/compscitech

Effects of interphase formation on the modulus and stress concentration factor of fiber-reinforced thermosetting-matrix composites

F. Yang, R. Pitchumani *

Composites Processing Laboratory, Department of Mechanical Engineering, University of Connecticut, 191 Auditorium Road, Unit 3139, Storrs, CT 06269-3139, USA

Received 19 May 2003; received in revised form 2 September 2003; accepted 11 September 2003
Available online 21 January 2004

Abstract

Experimental and theoretical studies in the literature have shown that a fiber surface perturbs its surrounding polymer to create a three-dimensional interphase zone with property gradients. Micromechanical stress analysis and evaluation of the effective properties of composites need the interphase material properties as input information. Since relatively scant information is available on the prediction of interphase formation as function of processing conditions, current micromechanical analyses have resorted to using assumed interphase property profiles. In this paper, a thermodynamic model for interphase formation is adopted to predict the interphase material properties, which, in turn, are used in the finite element analysis of overall composite properties. Relevant numerical results are presented for the first time where two major composite properties, modulus and stress concentration factor, are directly linked to the interphase formation parameters without assumed structures or properties of the interphase. The results provide guidelines for selecting material components and processing parameters to achieve desired overall composite properties.
© 2004 Elsevier Ltd. All rights reserved.

1. Introduction

Fabrication of thermosetting-matrix composites is based on a critical step of cure, which involves applying predefined temperature cycle to a fiber–resin matrix mixture. The elevated temperatures initiate an irreversible crosslinking chemical reaction among the species in the matrix. The presence of fibers has been found to significantly influence the cure reaction, resulting in the formation of a third phase known as the interphase which possesses property gradient distinct from those of the bulk fiber and the matrix. The interphase resides in a region between the original constituents of the composite with a size of a few to a few thousand nanometers [1–4]. Although the region has a sub-microscopic scale, it directly influences the ability of the matrix to transfer load to the reinforcing fiber. The structure and properties of the interphase are therefore dominant factors governing the overall composite properties and performance.

Several physical and chemical mechanisms contribute simultaneously to the interphase formation and very few of them have been described rigorously in mathematical models. Garton et al. [5] showed that the carbon surfaces influence the cross-linking reaction in an anhydride–epoxy system by adsorbing the tertiary amine catalyst and forming amine rich interphase regions near the carbon surfaces. Similarly, Sellitti et al. [6] used Fourier transform IR attenuated total reflection spectroscopy to characterize the interphase phenomena in an epoxy–anhydride-catalyst system, and showed that the surface species introduced on graphitized carbon fibers can promote or inhibit the cross-linking process by the preferential adsorption of the catalyst. Other possible interphase mechanisms are proposed by Drzal [4].

The effects of interphase property gradients on the overall composite properties are extensively investigated in the literature [7–15]. However, the studies are commonly based on assumed or empirical interphase

* Corresponding author. Tel.: +1-860-486-0683; fax: +1-860-486-5088.
E-mail address: r.pitchumani@uconn.edu (R. Pitchumani).

0266-3538/$ - see front matter © 2004 Elsevier Ltd. All rights reserved.
doi:10.1016/j.compscitech.2003.09.027

Nomenclature

c	characteristic constant for the polymer in Eq. (6)
C_{ij}	component of the stiffness matrix of the equivalent material (GPa)
c_{ij}	component of the stiffness matrix of the RVE (GPa)
E	Young's modulus (GPa)
k	Boltzmann constant (J/K)
K_s	stress concentration factor
l	bond length (m)
l^0	lattice layer thickness (m)
N_L	number of lattice layers in a sub-lattice
p	adhesion factor
pph	weight percentage of PACM20 to DGEBA in a resin mixture
q	single chain partition function
r	radius from the center of a fiber (m)
T	temperature (K)
U	strain energy of the RVE (J)
U^{eq}	strain energy of the equivalent material (J)
u	horizontal displacement (m)
V	volume of the RVE (m^3)
V^{eq}	volume of the equivalent material (m^3)
v	volume fraction; or vertical displacement (m)
x	chain length in terms of number of monomer segments
X	variable used in Eq. (8), equal to pph − 1/pph
z	number of lattice layer

Greek symbols

α	constant in Eq. (2)
χ	chain/chain interaction parameter
δ_2	boundary displacement in x-direction (m)
δ_3	boundary displacement in y-direction (m)
ϵ	microstrain of the RVE
Φ	macrostrain of the equivalent material
κ	scaling factor in Eq. (3)
ν	Poisson's ratio
ρ	density (kg/m^3)
ω	surface potential (J)

Subscripts

A	Amine or PACM20
E	Epoxy or DGEBA
f	fiber
i	interphase
m	matrix

property variation. Tsai et al. [7] used an axisymmetric finite element model to study the interface stress, displacement, and fracture toughness. An elastic shear lag analysis was developed and correlated with the micro-debonding test data to determine the thickness and material properties of the interphase. Boundary element method was adopted by Liu et al. [8] to predict transverse moduli of fibrous composites. Tsui et al. [9] studied the effects of different interphase properties on Young's modulus, maximum stress concentration factor, and stress distribution in particle-filled polymer composites. Transverse Young's storage/loss moduli and physical aging of a viscoelastic composite with fiber reinforcement were investigated by Fisher and Brinson [10]. All the studies in [8–10] assumed interphase thickness and modulus.

Some empirical relations have also been proposed for the interphase property gradients. By assuming that the rate of change of a property is proportional to the value of the property, the interphase modulus variation with radius, $E_i(r)$, was given as [11,12]:

$$E_i(r) = E_m\left[1 + (pE_f/E_m - 1)\frac{1 - r e^{1-r/r_i}/r_i}{1 - r_f e^{1-r_f/r_i}/r_i}\right], \quad (1)$$

where E_i is the interphase modulus, r is the radius, the subscripts i, m, and f refer to interphase, matrix, and fiber, respectively, and r_f is the radius of the fiber. The parameter p is called an adhesion factor, which is the ratio between the interphase modulus at $r = r_f$ and the fiber modulus

$p = E_i(r_f)/E_f$.

Similar expressions were applied to other properties, such as the Poisson's ratio. Thermal stresses due to the interphase property gradients are predicted by Sottos et al. [13], where the elastic constants are assumed to vary *linearly* within the interphase. A power-law relation was used by Wacker et al. [14] to calculate transverse Young's modulus of composites

$$E_i(r) = (\alpha E_f - E_m)\left[\frac{r_i - r}{r_i - r_f}\right]^n + E_m, \quad (2)$$

where $0 \leqslant \alpha \leqslant 1$, and $n = 2, 3, \ldots$ A review on the empirical interphase models and their features was given by Jayaraman et al. [15].

Due to complexities of the molecular level mechanisms that occur in the vicinity of the fibers during the process, prediction of the interphase evolution as function of processing parameters from first principles has been the subject of little attention. To the authors' knowledge, the first work on modeling interphase formation in thermosetting materials was presented by Palmese [1]. The model predicted the interphase composition profile under thermodynamic equilibrium con-

ditions of a non-reacting epoxy–amine resin system. The principle of minimum free energy was invoked to set up the equilibrium state, accounting for enthalpy interaction between fiber surface and resin components, and the calculation of Gibbs free energy was based on a Flory–Huggins type lattice structure. Hrivnak [16] extended Palmese's model to a reacting system by using renewal theory models to construct the assembly Gibbs free energy and the associated chemical potential. In an alternative approach, a kinetics-based description of the governing phenomena was developed by the authors to predict the interphase development during thermosetting composite processing [17,18]. In this method, mass conservation principle was employed to describe the transport processes of multilayer adsorption, desorption and diffusion near a fiber surface, which are accompanied by simultaneous cure reaction between the resin components. The time evolution of interphase concentration profile gradients before the gelation of the thermosetting system was predicted as function of material and process parameters.

The goal of this work is to use an existing interphase concentration evolution model to predict the interphase composition profiles, which are subsequently mapped to modulus profiles using an experimental correlation between compositions and moduli. To this end, the model of Hrivnak [16] is used for the interphase composition prediction, while the kinetics-based description [17,18] will be explored in a future work. The modulus profiles mapped from the interphase concentration gradients are used in finite element analyses to calculate the modulus and stress concentration factor of fiber reinforced epoxy/amine composites. A systematic study is conducted to show the effects of different processing and geometry related parameters on the overall composite properties.

2. Modeling

2.1. Interphase formation model

To eliminate the need for assumed interphase properties in micromechanical analyses, the interphase formation model by Hrivnak [16] is adopted to describe the concentration profiles in the interphase region. The model examines the chain/surface and chain/chain interactions of an epoxy/amine binary thermosetting-resin mixture in the vicinity of a fiber surface. The interaction of a single polymer chain with a surface is described by an analytical molecular partition function, which is incorporated into a sub-lattice model to derive the Gibbs free energy of the chain assembly. By minimizing the assembly Gibbs free energy, the volume fraction of the amine species at the (z)th lattice layer, $v_A(z)$, is obtained as follows.

$$v_A(z) = \kappa v_A(\infty)\underbrace{q(x_A,z)\exp[S_A(z)]}_{\text{chain/surface interaction}}\underbrace{\exp\left[\chi\left(v_E^2(\infty)-v_E^2(z)\right)\right]}_{\text{chain/chain interaction}} \times \underbrace{\exp\left[\frac{v_A(z)-v_A(\infty)}{N_L}(1-x_A/x_E)\right]}_{\text{excess mixing}}, \quad (3)$$

where

$$q(x_A,z) = 1-\sqrt{2/\pi x_A}\left(1-e^{\omega_A/kT}\right)\operatorname{erfc}(z/\sigma_A), \quad (4)$$

$$S_A(z) = \frac{\omega_A}{kT}\exp\left(\frac{\omega_A}{kT}\right)\sqrt{\frac{2}{\pi x_A}}\operatorname{erfc}\left(\frac{z}{\sigma_A}\right), \quad (5)$$

$$\sigma_A^2 = c\frac{x_A l^2}{3}. \quad (6)$$

Similar expressions for the epoxy species may be obtained by switching the subscripts A (amine) and E (epoxy) in the above equations.

The parameter κ is introduced as a normalization constant to ensure that volume fractions $v_A(z)$ and $v_E(z)$ sum up to unity, and $v_A(\infty)$ is the volume fraction of amine in the far region. Eqs. (4) and (5) and similar equations for the epoxy species show that chain/surface interaction depends on the surface potentials, ω_A and ω_E, chain lengths, x_A and x_E, number of the lattice layer from the surface, z, Boltzmann constant, k, and the temperature, T. Positive, negative, and zero values of ω_A (and ω_E) correspond to attractive, repulsive, and neutral surfaces to the amine (and epoxy) species, respectively. The second exponential term in Eq. (3) accounts for the chain/chain interaction between the two species in the binary resin mixture, where χ is the interaction parameter. For $\chi > 0$, the two species are repulsive to each other. If the surface prefers to adsorb amine, a positive chain/chain interaction pushes the epoxy molecules further away from the surface, leading to enhanced preferential adsorption of amine. The last exponential term in Eq. (3) represents the effect of excess mixing caused by different chain lengths (x_A and x_E) of the two species. The quantity N_L is the number of lattice layers, each of thickness l^0, contained within a sub-lattice, and may be treated as a weighting factor of the excess mixing. Note that large values of N_L reduce the effect of excess mixing. The parameters c and l in Eq. (6) are the characteristic constant and the C–C bond length of the polymer chain, respectively.

Fig. 1 presents two sample concentration profiles predicted by the above model. The thermosetting mixture consists of an aliphatic bis(p-aminocyclohexyl) methane (PACM20) curing agent and an aromatic diglycidyl ether of bisphenol-A (DGEBA) epoxy resin. In the following discussion, the subscripts A and E denote the resin components PACM20 and DGEBA, respectively. Note that the volume fraction of PACM20 is converted to a parts per hundred (i.e., pph) concentration,

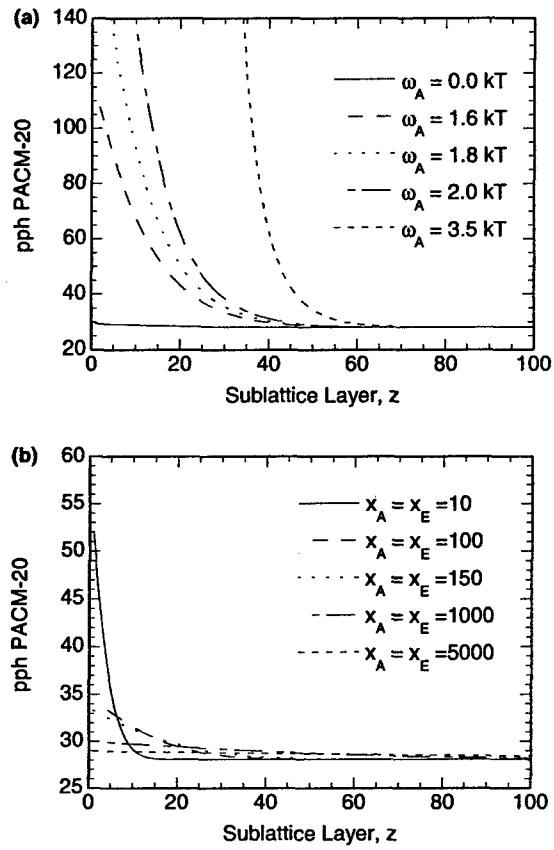

Fig. 1. Interphase concentration profiles predicted from the model by Hrivnak [16] for different: (a) surface potentials, and (b) chain lengths. The default values of the parameters are: $\omega_E = -0.28kT$, $\chi = 1.0$, $N_L = 2.5$: (a) $x_E = x_A = 150$, (b) $\omega_A = 0.43kT$.

defined as the weight percentage of PACM20 to DGEBA in the mixture.

$$\text{pph} = 100\frac{\rho_A v_A}{\rho_E(1 - v_A)}, \tag{7}$$

where v_A is the volume fraction of PACM20, and ρ_A and ρ_E are density of PACM20 and DGEBA, respectively.

Fig. 1(a) shows the distribution of pph PACM20 from the fiber surface (Layer 0) to the far region (Layer 100) for different amine surface potentials ω_A. The results correspond to the parameter combination of $\omega_E = -0.28kT$, $x_E = x_A = 150$, $\chi = 1.0$, $N_L = 2.5$, as determined by Hrivnak [16] for the DGEBA/PACM20 system. For a neutral surface, the pph PACM20 values near the fiber surface are close to the bulk value of 28. The surface concentrations increase as the surface becomes more attractive to PACM20, and sharp increases are observed for $\omega_A > 1.6kT$. As the distance increases, the pph PACM20 decreases asymptotically to the bulk value (28) for all the values of ω_A. Fig. 1(b) presents the effect of chain lengths, x_A and x_E, following the presentation format of Fig. 1(a), for $\omega_A = 0.43kT$; all other parameters retain their values as in Fig. 1(a). Fig. 1(b) shows that the surface may easily adsorb shorter chains, and the pph concentration at the surface is almost doubled as compared to the bulk value for the case of $x_E = x_A = 10$. However, the magnitudes of the surface concentration increases are not as significant as those in Fig. 1(a). It is also observed that the region perturbed by the surface becomes smaller as the chain length decreases.

The discussion on the interphase formation model in this subsection only provides the necessary information for the development of the micromechanical analysis in this paper, and the readers are referred to Hrivnak [16] for other details.

2.2. Interphase modulus profiles

Since matrix modulus is determined by the resin component compositions, the concentration profiles such as those in Fig. 1 may be mapped to corresponding interphase modulus profiles. Fig. 2 presents experimental data on matrix modulus as a function of the parameter $X = \text{pph} - 1/\text{pph}$ for the DGEBA/PACM20 system at 30 °C as reported by VanLandingham et al. [19]. Two peaks in the modulus variation are observed: one around 18 pph PACM20 with a value of 3.2 GPa, and the other between 48 and 56 pph PACM20 having a value of 2.4 GPa. Similar twin peak profiles were reported in [19] for a variety of other epoxy–amine systems and was explained in terms of the relationship of the matrix modulus to an effective chain aspect ratio, defined as the ratio of the length to the effective diameter of the polymer chains, and the volume fraction of the microgel structures in the cured matrix. Larger values of the effective aspect ratio and the microgel volume fraction result in higher matrix modulus. At the stoichiometric point of the thermosetting system, the effective aspect ratio and the microgel volume fraction were argued to exhibit minimum and maximum, respectively. Consequently, the modulus is not monotonic with respect to the pph values near the stoichiometric ratio. The interested reader is referred to [19] for more details. For concentrations between 18 and 56 pph, the value of

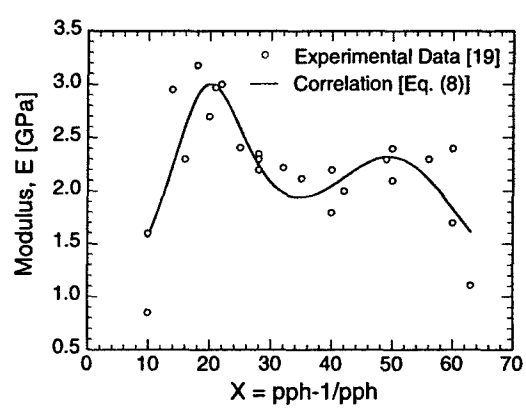

Fig. 2. The Young's modulus (measured at $T = 30°$) as a function of stoichiometry for the DGEBA/PACM20 system.

modulus varies about 60%. The modulus drops sharply on both ends of the concentration axis due to the fact that the matrix is in extreme deficit of either resin component and cannot be cured sufficiently. Based on these observations, a twin peak function is derived in the present analysis to fit the data as follows:

$$E = \frac{1}{(X-19.57)^2/214.42+0.42} + \frac{1}{(X-50.59)^2/803.09+0.47}. \quad (8)$$

Eq. (8), which has an asymptotic value of 0 as pph approaches 0 and infinity, is used in this study to map the concentration profiles, $v_A(z)$ or $v_E(z)$, to modulus profile, $E(r)$. Note that the radial distance from a fiber center, r, may be obtained from the fiber radius, r_f, and the lattice layer, z, as $r = r_f + zl^0$.

Since the interphase region is typically thin (around 10–500 nm), most micromechanical models consider only a single uniform interphase layer with thickness δ_i and effective modulus E_i [7–15]. An "interphase thickness" may be defined in a similar way as the boundary layer thickness in fluid mechanics, such that the PACM20 concentration is within 1% of the PACM20 concentration in the far region layers [17,18]. From the species concentration profiles, $v_A(z)$ or $v_E(z)$, the interphase thickness may be determined as $\delta_i = \Delta z l^0$, where Δz is the number of lattice layers within the interphase region. The modulus profile, $E(r)$, may be used to determine the effective interphase modulus by considering a series connection of infinite springs as follows [14].

$$E_i = \frac{r_i - r_f}{\int_{r_f}^{r_i} \frac{dr}{E(r)}}. \quad (9)$$

Fig. 3(a) shows the interphase thickness, δ_i, and the effective interphase modulus, E_i, as functions of the surface potential, ω_A. The results correspond to the same parameter combination as in Fig. 1(a). As the surface potential, ω_A, increases up to around $1.2kT$, the maximum pph PACM20 value in the interphase region changes from 28 to about 64. The corresponding interphase modulus profiles have relatively small variations from 1.6 to 2.3 GPa. Consequently, the effective interphase modulus evaluated from Eq. (9) has negligible changes as $\omega_A < 1.2kT$. Further increase in ω_A results in the formation of interphase region with very high PACM20 concentration, as shown by Fig. 1(a). The effective interphase modulus starts to drop and asymptotically approaches zero, which corresponds to the modulus of pure PACM20. Arayasantiparb et al. [20] reported a DGEBA/

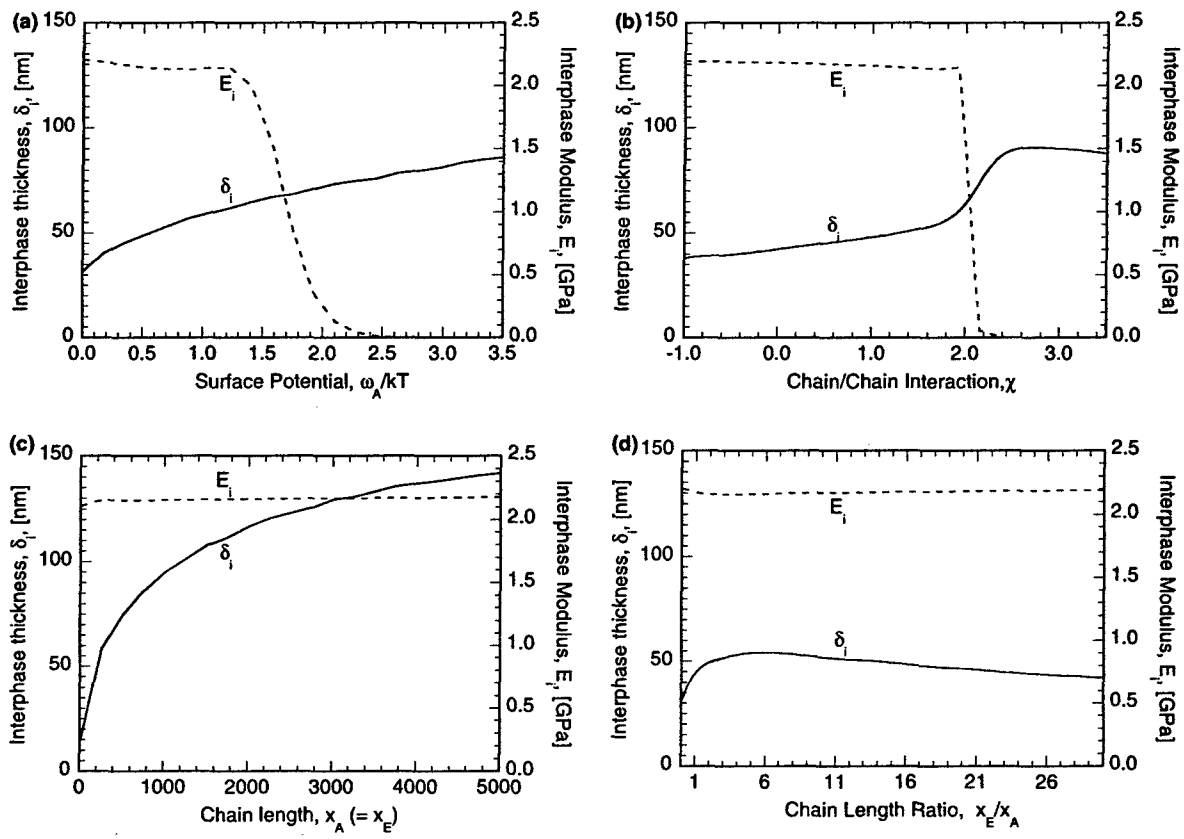

Fig. 3. Interphase thickness and modulus as functions of: (a) surface potential, ω_A, (b) chain/chain interaction, χ, (c) chain length of amine, x_A (= x_E), and (d) chain length ratio, x_E/x_A, for $x_A = 150$.

PACM20 interphase concentration profile with the maximum pph value as high as 1560, for which E_i may be determined to be 0.0022 GPa using Eqs. (8) and (9). The interphase thickness increases from 32 to 86 nm as ω_A increases from 0 to $3.5kT$, since more PACM20 molecules are adsorbed into the interphase region.

The influence of the chain/chain interaction parameter, χ, on the interphase properties is shown in Fig. 3(b). The results correspond to $\omega_A = 0.43kT$, and all other parameters retain their values as in Fig. 1(a). Recall that the positive chain/chain interaction enhances the preferential adsorption of PACM20; therefore, an increase in χ has the same effect as an increase in ω_A. Consequently, the overall trends in Fig. 3(b) are similar to those in Fig. 3(a). For $\chi < 2.0$, the interphase modulus profiles are characterized by relatively small variations and the effective interphase modulus exhibits little change with respect to χ. Further increase in χ causes significant adsorption of PACM20, and E_i decreases asymptotically to zero as in Fig. 3(a). A sharp increase in the interphase thickness is observed for the interaction parameter χ in the interval 1.8–2.6.

Fig. 3(c) illustrates the effect of the chain lengths, x_A and x_E, on E_i and δ_i, and the results correspond to the same parameter combination as in Fig. 1(b). The interphase thickness increases monotonically with increasing x_A and x_E, which is consistent with the concentration profiles shown in Fig. 1(b). It must be pointed out that the interphase modulus is almost independent of the chain lengths, owing to the small variation of the modulus in the pph range 28–55 as noted in Fig. 2. Fig. 3(d) presents the effect of increasing chain length x_E for a fixed chain length $x_A = 150$, and other parameters have the same values as in Fig. 3(c). Again, the effective interphase modulus is insensitive to x_E due to the small variation of the interphase modulus profiles. A non-monotonic trend is observed for the interphase thickness, and may be explained as follows. The increase in x_E results in an increase in the excess mixing term and a decrease in the chain/chain interaction term in Eq. (3). As x_E increases from 1 to around 900, the increase in the excess mixing term leads to more adsorption of PACM20 and increased interphase thickness. The decrease in the chain/chain interaction term overcomes the increase in the excess mixing term as x_E increases further, yielding less PACM20 adsorption and thinner interphase.

The interphase thickness and the effective interphase modulus were found to remain invariant with the number of lattice layers in a sub-lattice, N_L, and the lattice layer thickness, l^0. The corresponding plots are omitted here for brevity. The effective interphase modulus, the interphase thickness, and the properties of the fiber and the matrix constitute inputs to the numerical modeling of the effective composite properties discussed below.

2.3. Finite element analysis of laminae transverse moduli

The moduli of an apparent heterogeneous composite lamina, represented by a representative volume element (RVE), are defined as those of an equivalent macroscopic homogeneous medium. The equivalent material is generally anisotropic, and exhibits the same volume and deformation strain energy as the RVE [14,21]:

$$V^{eq} = V, \quad U^{eq} = U, \tag{10}$$

where V and U are the volume and strain energy of the RVE, and V^{eq} and U^{eq} are the same quantities for the equivalent material, respectively.

In order to investigate the effect of the fiber arrangement on the composite properties, two types of RVEs are considered in the present study. These correspond to a staggered and rectangular arrangement of fibers as depicted in Figs. 4(a) and 4(b), respectively. The cross-sections of the RVE in the x–y plane are rectangular with length a, height b, and array angle γ. In the model development, subscripts 2 and 3 are used to denote the in-plane transverse properties, as is conventionally adopted in the literature. To calculate the composite moduli, appropriate boundary conditions are essential to model different loading situations [21]. The following boundary conditions are considered to determine transverse Young's moduli [14,21].

$$\begin{aligned} &u(0,y) = 0, \\ &u(a,y) = \text{constant} = \delta_2, \\ &v(x,0) = 0, \\ &v(x,b) = \text{constant} = \delta_3, \end{aligned} \tag{11}$$

where u and v denote displacement in the x and y directions, respectively, and the subscripts 2 and 3 correspond to the directions x and y, respectively, as shown in Fig. 4.

The strain energy of the *equivalent material* subject to the loading conditions in Eq. (11) is given by

$$U^{eq} = \frac{1}{2}\int_v C_{ij}\Phi_i\Phi_j \mathrm{d}V = \frac{1}{2}C_{ij}\Phi_i\Phi_j V,$$

where C_{ij} are the components of stiffness matrix of the *equivalent material*, and Φ_i and Φ_j are macrostrains in the contracted notations. Note that the macrostrains are constants within the homogeneous *equivalent material*. Similarly, the strain energy of the RVE may be written as

$$U = \frac{1}{2}\int_v c_{ij}\epsilon_i\epsilon_j \mathrm{d}V,$$

where the stiffnesses, c_{ij}, and the microstrains ϵ_i and ϵ_j are functions of locations in the RVE. The RVE strain energy U is computed using ABAQUS V6.3, a commercial finite element package. Substituting the above two expressions into Eq. (10) yields

$$\frac{1}{2}C_{ij}\Phi_i\Phi_j V = \frac{1}{2}\int_v c_{ij}\epsilon_i\epsilon_j \mathrm{d}V. \tag{12}$$

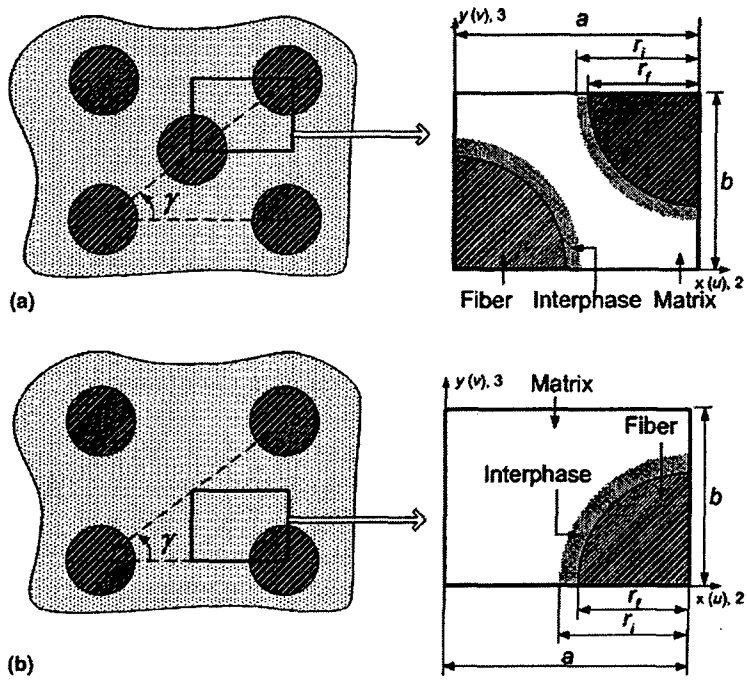

Fig. 4. Unit cells considered for the analysis.

By introducing sufficient number of admissible deformation states of the RVE, Eq. (12) may be used repetitively to form a set of linear algebraic equations which, in turn, can be used to determine all the stiffness components of the *equivalent* (or composite) material.

Three deformation states are configured by specifying the following requirements for the boundary conditions in Eq. (11):

$$\begin{aligned} &\text{state I}: \quad \delta_2 \neq 0, \quad \delta_3 = 0, \\ &\text{state II}: \quad \delta_2 \neq 0, \quad \delta_3 \neq 0, \\ &\text{state III}: \quad \delta_2 = 0, \quad \delta_3 \neq 0. \end{aligned} \tag{13}$$

The macrostrains in the *equivalent material* corresponding to the deformation states are:

$$\begin{aligned} &\text{state I}: \quad \Phi_2^{\mathrm{I}} = \frac{\delta_2}{a}, \quad \Phi_3^{\mathrm{I}} = 0, \quad \Phi_{23}^{\mathrm{I}} = 0, \\ &\text{state II}: \quad \Phi_2^{\mathrm{II}} = \frac{\delta_2}{a}, \quad \Phi_3^{\mathrm{II}} = \frac{\delta_3}{b}, \quad \Phi_{23}^{\mathrm{II}} = 0, \\ &\text{state III}: \quad \Phi_2^{\mathrm{III}} = 0, \quad \Phi_3^{\mathrm{III}} = \frac{\delta_3}{b}, \quad \Phi_{23}^{\mathrm{III}} = 0. \end{aligned} \tag{14}$$

Combining Eqs. (12) and (14) yields:

$$\begin{aligned} &\text{state I}: \quad \frac{1}{2} C_{22} (\Phi_2^{\mathrm{I}})^2 V = U_{\mathrm{I}}, \\ &\text{state II}: \quad \frac{1}{2} \left[C_{22} (\Phi_2^{\mathrm{II}})^2 + C_{23} \Phi_2^{\mathrm{II}} \Phi_3^{\mathrm{II}} + C_{33} (\Phi_3^{\mathrm{II}})^2 \right] V = U_{\mathrm{II}}, \\ &\text{state III}: \quad \frac{1}{2} C_{33} (\Phi_3^{\mathrm{III}})^2 V = U_{\mathrm{III}}, \end{aligned} \tag{15}$$

where U_{I}, U_{II}, U_{III} are the strain energies of the RVE (obtained from finite element analysis) for deformation states I, II and III, respectively. Eq. (15) may be used to solve the stiffnesses C_{22}, C_{23}, and C_{33}, which, in turn, are used to determine transverse Young's moduli of composite laminae.

In this study, the lamina is considered to be an orthotropic material, and has two independent transverse Young's moduli, E_2 and E_3, in the x and y directions in Fig. 4, respectively. Under plane stress conditions, the relationships between the stiffnesses and the elastic constants are [22,23]:

$$\begin{aligned} C_{22} &= \frac{E_2}{1 - \nu_{23}^2 E_3/E_2}, \\ C_{23} &= \frac{\nu_{23} E_3}{1 - \nu_{23}^2 E_3/E_2}, \\ C_{33} &= \frac{E_3}{1 - \nu_{23}^2 E_3/E_2}, \end{aligned} \tag{16}$$

where ν_{23} is the Poisson's ratio of the composite in the x–y plane. The three relationships in Eq. (16) may be rearranged to solve for the three unknowns, E_2, E_3, and ν_{23} as

$$\begin{aligned} E_2 &= C_{22} \left[1 - \frac{C_{23}^2}{C_{22} C_{33}} \right], \\ E_3 &= C_{33} \left[1 - \frac{C_{23}^2}{C_{22} C_{33}} \right], \\ \nu_{23} &= C_{23}/C_{33}. \end{aligned} \tag{17}$$

The composite properties, E_2, E_3, and ν_{23}, in Eq. (17) depend on interphase formation and fiber microarchitectural parameters. The interphase formation is governed by the following principal parameters: (1) surface potentials for chain/surface interaction, ω_A and ω_E, (2) the chain/chain interaction parameter, χ, (3) lattice layer thickness, l^0, (4) number of lattice layer within a sublattice, N_L, and (5) chain lengths, x_E and x_A. Geometric parameters pertaining to the fiber micro-architecture in the composite are the fiber volume fraction, v_f, the relative fiber arrangement – either rectangular or staggered – and for each arrangement, the array angle, γ. A systematic finite element analysis is carried out to study the effects of the two classes of parameters – interphase and fiber architectural – on the transverse Young's moduli, E_2 and E_3, and the stress concentration factor. For each combination of model parameters, Eq. (3) is used to determine the interphase composition profile, which is transformed to the interphase modulus profile $E(r)$ by Eq. (8), and the effective interphase modulus, E_i, is readily determined by Eq. (9). Stress fields of the three deformation states (given by Eqs. (11) and (13)) are calculated using ABAQUS, with $E(r)$ or E_i as input information. The stress field analyses provide the values of strain energies, which, in turn, are used to determine the stiffness components in Eq. (15). The composite moduli, E_2 and E_3, are subsequently evaluated using Eq. (15). Note that the stress concentration factor, K_s, may be defined from the stress field as the ratio between the maximum stress in the domain and the average applied stress. The results on the variation of E_2, E_3, and K_s with the interphase formation parameters and the geometric parameters are discussed in the following section.

3. Results and discussion

Toward validating the model, the predictions of the elastic moduli based on the finite element analysis of the representative volume elements were compared with calculations by Wacker et al. [14]. It must be pointed out that the assumption of transverse isotropy is used in [14], which is a special case of the orthotropic medium considered in this study. By considering a rectangular array and setting the array angle γ to 45°, the orthotropic solutions are reduced to the corresponding transverse isotropic solutions ($E_2 = E_3$). The RVE used in the comparison study is a rectangular array ($\gamma = 45°$) with 50% fiber volume fraction. The properties and the geometry of the constituent materials, epoxy matrix (m), E-glass fiber (f), and the interphase (i) are:

$$E_f = 84 \text{ GPa}; \quad \nu_f = 0.22; \quad r_f = 8.5\ \mu\text{m},$$
$$E_m = 4 \text{ GPa}; \quad \nu_f = \nu_i = 0.34; \quad r_i = 9.5\ \mu\text{m},$$

where ν denotes the Poisson's ratio. The finite element analysis used in this study employs eight-noded quadratic plane stress elements, and mesh convergence studies were conducted to ensure correct modulus values. Table 1 presents a comparison of the transverse composite modulus predicted from the present analysis and those reported by Wacker et al. [14] for different values of the interphase modulus, E_i. Good agreement between the finite element model predictions and the literature results is observed for all the values of the interphase modulus studied.

Table 1
Effect of the interphase modulus on the transverse elastic modulus of an epoxy/E-glass composite lamina. Validation of the present analysis with the data of Wacker et al. [14]

E_i (GPa)	Present FEM	Wacker et al. [14]
4	12.15	12.25
6	13.70	13.71
8	14.66	14.68
12	15.79	15.91

With the validated finite element formulation as basis, effects of the interphase and fiber architectural parameters on the composite properties are described in this section. A DGEBA epoxy/PACM20 curing agent thermosetting system is considered in the parametric studies; however, all the analyses are readily extended to a general two-component thermosetting system provided a mapping of the interphase composition to the properties is known. At the stoichiometric point (28 pph PACM20), the modulus of the DGEBA/PACM20 system, E_m, has a value of 2.3 GPa as obtained from Fig. 2. As mentioned previously, the interphase modulus profiles are obtained by combining Eqs. (3), (7), and (8), and the effective interphase modulus, E_i, is calculated from Eq. (9). Relevant numerical results are presented for the first time where two major composite properties, modulus and stress concentration factor are directly linked to the interphase formation parameters without assumed structures or properties of the interphase.

Fig. 5(a) shows a dimensionless composite transverse Young's modulus, E_2/E_m, as a function of fiber modulus ratio, E_f/E_m at different surface potentials ω_A. The results correspond to a rectangular array with a packing angle, $\gamma = 45°$, for which the fiber arrangement is identical in the 2- and the 3-directions, and consequently, $E_2/E_m = E_3/E_m$. For the case of $\omega_A = 0$, the fiber surface is neutral to PACM20, and its concentration near the surface is almost identical to that of the far region [see Fig. 1(a)]. Consequently, the composite material is similar to a two component (fiber and matrix) system without distinct interphase regions. When $E_f/E_m = 1$, the composite modulus ratio E_2/E_m $(= E_3/E_m) = 1$ since the material is essentially homogeneous. The composite modulus is seen to increase with increasing fiber modulus, as physically expected. However, the increase rate of E_2 $(= E_3)$ slows down at larger E_f/E_m

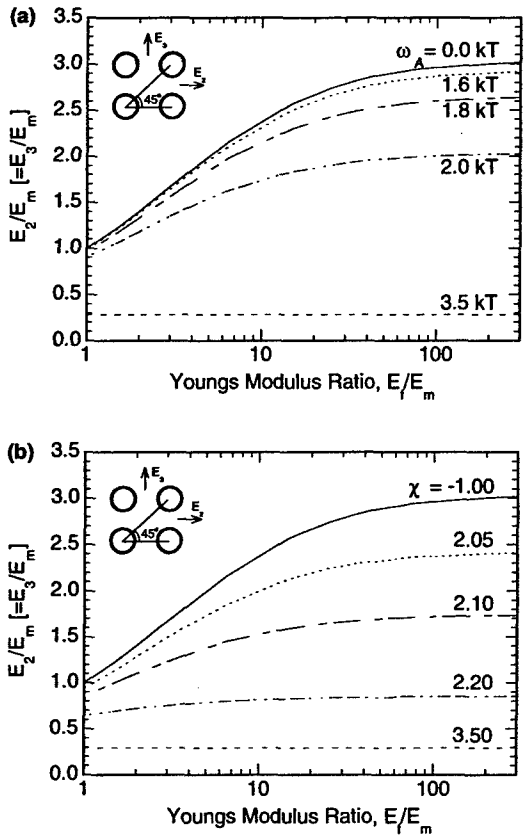

Fig. 5. Transverse Young's modulus of composite as a function of the ratio E_f/E_m for different: (a) surface potentials, and (b) chain/chain interaction parameters. The RVEs used in the finite element analysis are rectangular arrays. The default values of the parameters are: $\omega_E = -0.28kT$, $x_E = x_A = 150$, $l^0 = 15$ nm, $N_L = 2.5$, $v_f = 0.5$, $\gamma = 45°$: (a) $\chi = 1.0$, (b) $\omega_A = 0.43kT$.

values; as $E_f/E_m \to \infty$, E_2/E_m $(= E_3/E_m)$ approaches an asymptotic value corresponding to an ideal rigid body reinforcement.

Interphases richer in PACM20 are developed as ω_A increases. When ω_A increases from 0 to $1.6kT$, the pph PACM20 at the fiber surface increases from 28 to 115, while the interphase modulus E_i decreases 38% from 2.30 to 1.43 GPa (Fig. 2). Since the interphase thickness is small (about 120 nm), the composite modulus exhibits only a slight corresponding decrease. Further increase of surface potential to $1.8kT$ and $2.0kT$ yields a sharp decrease of E_i to 0.67 and 0.24 GPa, respectively, and a significant drop in the value E_2 $(= E_3)$ is observed. At $\omega_A = 3.5kT$, the interphase consists of almost pure PACM20, which corresponds to a near zero value of E_i. In this case, mechanical and thermal loads may cause the compressive interfacial contact between the fiber and matrix, which retains certain measure of load transfer.

In Fig. 5(b), the influence of the chain/chain interaction, χ, on the composite modulus is demonstrated. The result corresponds to $\omega_A = 0.43kT$, with all the other parameters retaining their values as in Fig. 5(a). Once again, by virtue of isotropy in the 2- and 3-directions corresponding to $\gamma = 45°$, $E_2/E_m = E_3/E_m$ as in Fig. 5(a). Recall that positive chain/chain interaction enhances the preferential adsorption of PACM20; therefore, the increase of χ has the same effect as the increase of surface potential ω_A. Since the fiber surface typically exhibits preferential adsorption of the PACM20 species [1–6], the values of ω_A are taken to be positive. However, both repulsive and attractive chain/chain interactions are considered, and χ can be positive or negative. Discussion of the trends with respect to increasing χ follows that presented with respect to increasing ω_A in Fig. 5(a), and similarly, E_2/E_m $(= E_3/E_m)$ increases with E_f/E_m as explained previously.

The influence of the other interphase formation parameters, i.e., x_1, x_2, l^0, and N_L on the transverse composite modulus ratio, E_2/E_m $(= E_3/E_m)$ is shown in Figs. 6 and 7. It was seen in Fig. 1(b) that the pph PACM20 at the fiber surface increases almost twice to 53 as chain lengths decrease from 5000 to 10. However, the interphase modulus has only a negligible corresponding change from 2.30 to 2.10 GPa, owing to the small

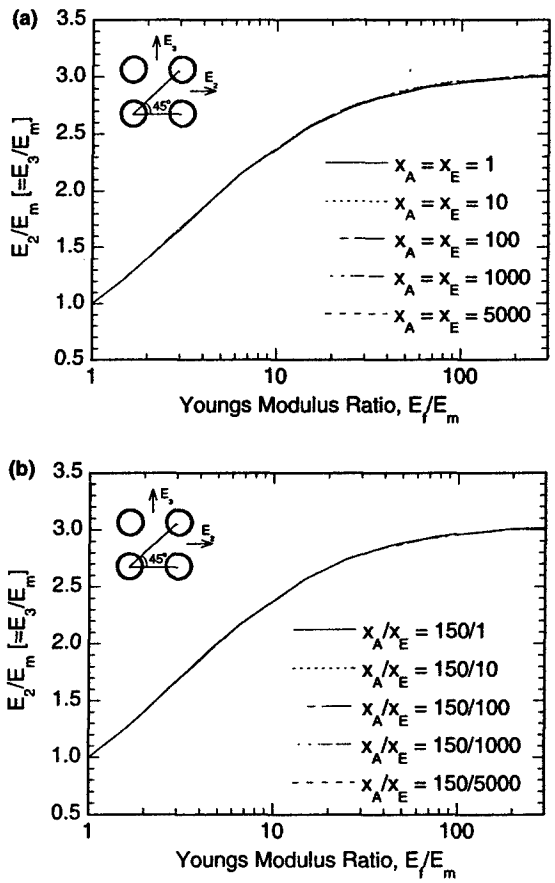

Fig. 6. Transverse Young's modulus of composite as a function of the ratio E_f/E_m for different: (a) chain lengths, and (b) chain length ratios. The default values of the parameters are: $\omega_E = -0.28kT$, $\omega_A = 0.43kT$, $\chi = 1.0$, $l^0 = 15$ nm, $N_L = 2.5$, $v_f = 0.5$, $\gamma = 45°$.

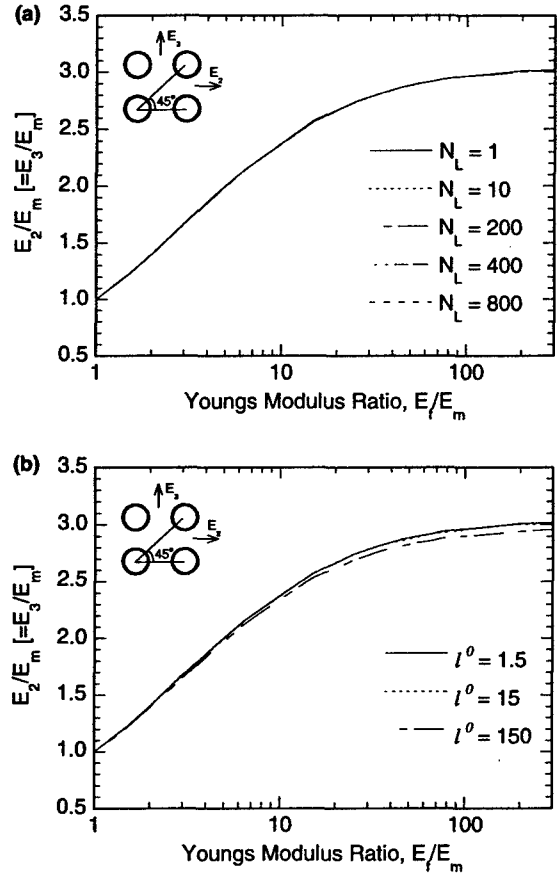

Fig. 7. Transverse Young's modulus of composite as a function of the ratio E_f/E_m for different: (a) number of lattice layers in a sublattice, and (b) thickness of a lattice layer. The default values of the parameters are: $\omega_E = -0.28kT$, $\omega_A = 0.43kT$, $\chi = 1.0$, $x_E = x_A = 150$, $v_f = 0.5$, $\gamma = 45°$: (a) $l^0 = 15$ nm, (b) $N_L = 2.5$,.

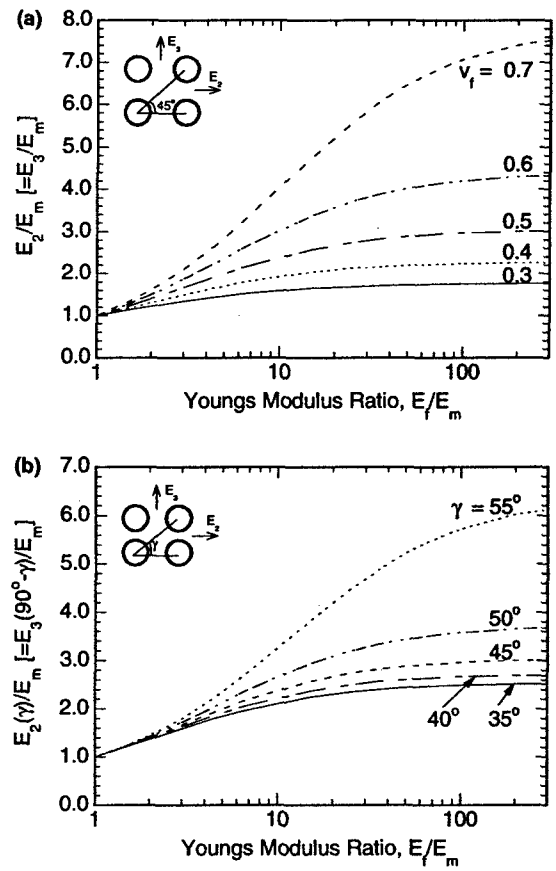

Fig. 8. Transverse Young's modulus of composite as a function of the ratio E_f/E_m for different: (a) fiber volume fractions, and (b) array angles. The default values of the parameters are: $\omega_E = -0.28kT$, $\omega_A = 0.43kT$, $\chi = 1.0$, $x_E = x_A = 150$, $l^0 = 15$ nm, $N_L = 2.5$: (a) $\gamma = 45°$, (b) $v_f = 0.5$.

variation of modulus in the pph range 28–55 as noted in Fig. 2. Consequently, the composite modulus E_2 $(= E_3)$ is almost independent of the chain lengths, x_E and x_A, as shown in Fig. 6(a) and (b), for a wide range of values. The interphase modulus also has a small change from 2.30 to 2.18 GPa for the range of N_L considered; consequently, the composite modulus is insensitive to N_L (Fig. 7(a)).

Recall that the interphase thickness may be calculated as $\Delta z l^0$, where Δz is the number of lattice layers within the interphase region. For fixed Δz, the value of lattice layer thickness l^0 governs the interphase thickness, and in turn, the composite modulus. However, for the parameter combination considered in Fig. 7(b), the effective interphase modulus, E_i, has a value of 2.15 GPa, which is close to the matrix modulus of 2.30 GPa. In this case, the lattice layer thickness (or the interphase thickness) has a limited influence on E_2 (and E_3). It must be pointed out that l^0 may be an important parameter if other combinations of parameters for which E_i differs considerably from E_m are considered.

The results in Figs. 5–7 pertain to the effects of the interphase parameters on the composite modulus. In the foregoing discussion, it is assumed that composite laminae consist of repeating rectangular RVEs with $v_f = 0.5$ and the transversely isotropic configuration of $\gamma = 45°$. Clearly, the microgeometry of the fiber arrangement in the matrix influences the overall composite properties, and to this end, it is of significance to investigate their effects. Furthermore, given that the real fiber arrangement in a composite cross section is random, a systematic analysis of the microgeometry parameters will yield insight on the range of property values expected of actual composites. Toward this objective, the effects of the fiber volume fraction, v_f, and array angle, γ, are investigated for the rectangular and the staggered fiber arrangements. The results are presented in Figs. 8–10 as described below.

Fig. 8(a) shows the influence of the fiber volume fraction, v_f, in the case of rectangular arrays with $\gamma = 45°$. For a fixed fiber–matrix modulus ratio E_f/E_m, the composite modulus E_2/E_m $(= E_3/E_m)$ increases

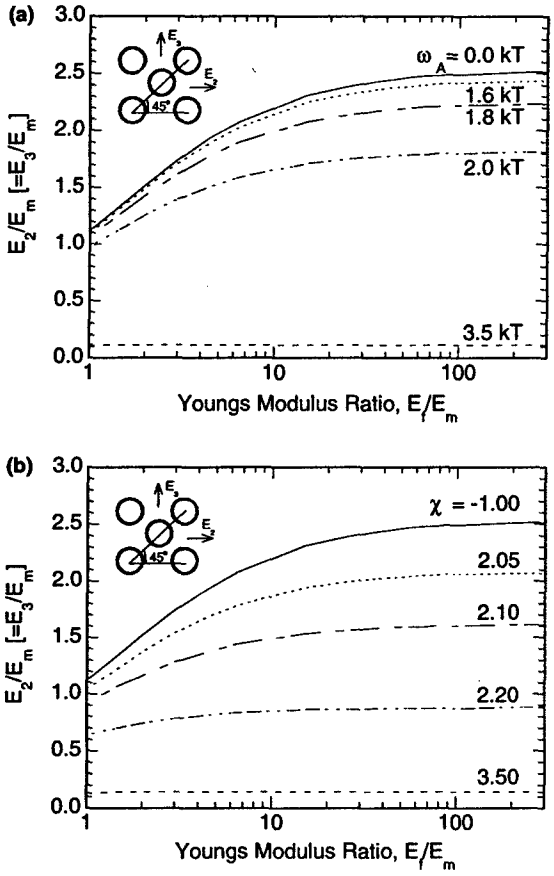

Fig. 9. Transverse Young's modulus of composite as a function of the ratio E_f/E_m for different: (a) surface potentials, and (b) chain/chain interaction parameters. The default values of the parameters are: $\omega_E = -0.28kT$, $x_E = x_A = 150$, $l^0 = 15$ nm, $N_L = 2.5$, $v_f = 0.5$, $\gamma = 45°$: (a) $\chi = 1.0$, (b) $\omega_A = 0.43kT$.

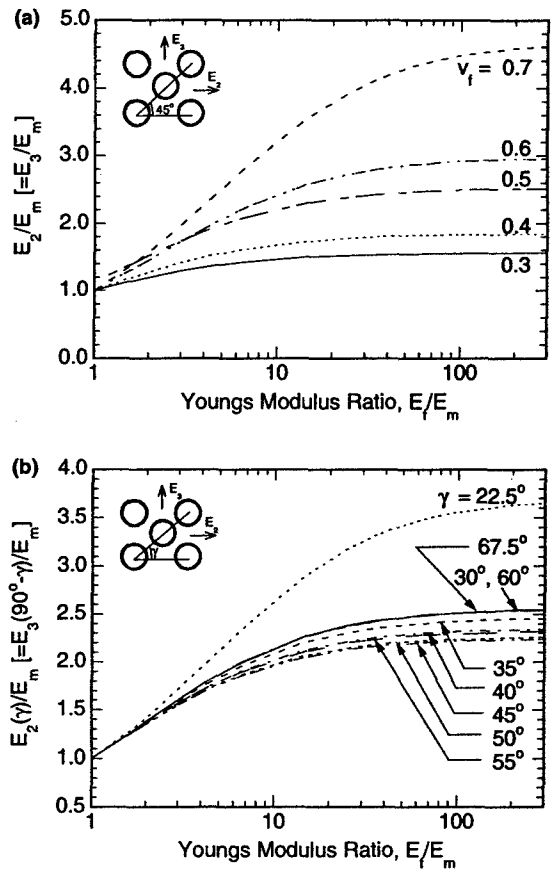

Fig. 10. Transverse Young's modulus of composite as a function of the ratio E_f/E_m for different: (a) fiber volume fractions, and (b) array angles. The default values of the parameters are: $\omega_E = -0.28kT$, $\omega_A = 0.43kT$, $\chi = 1.0$, $x_E = x_A = 150$, $l^0 = 15$ nm, $N_L = 2.5$: (a) $\gamma = 45°$, (b) $v_f = 0.5$.

monotonically with increasing fiber volume fraction, v_f. This is attributed to the increasing concentration of the stiffer fiber phase in the composite. For the range of values considered in the current study, it is observed that the geometric parameters have more significant effect on E_2/E_m $(= E_3/E_m)$ than the interphase parameters. For example, when $v_f = 0.7$, the asymptotic value of E_2/E_m $(= E_3/E_m)$ is around 7.6, which is more than twice the corresponding values shown in Fig. 5(a) for $\omega_A = 0$ or for $\chi = -1.00$ in Fig. 5(b).

Fig. 8(b) shows the modulus ratio, E_2/E_m at different array angle, γ, for a rectangular arrangement of fibers in the RVE. For any fiber array angle, γ, the values of E_3 may be derived from the results for E_2 by considering a complementary RVE constructed by rotating the original one by 90°. From geometric symmetry considerations, E_2 and E_3 are equal for the complementary RVEs, i.e., $E_2(\gamma) = E_3(90° - \gamma)$. In the special case of $\gamma = 45°$, $E_2(45°) = E_3(45°)$, as presented in the results so far. It is seen in Fig. 8(b) that for a fixed fiber–matrix modulus ratio, E_f/E_m, the transverse moduli $E_2(\gamma)/E_m$ $[= E_3(90° - \gamma)/E_m]$ increase monotonically with increasing fiber array angle, γ. A larger value of γ corresponds to a shorter inter-fiber distance in the 2-direction and a larger inter-fiber spacing in the 3-direction, which causes an increase of $E_2(\gamma)$ and a decrease in $E_3(\gamma)$. A relatively large increase in the composite modulus, by as much as a factor of 6, may be achieved at $\gamma = 55°$, as noted in Fig. 8(b).

The influence of the relative fiber arrangement on the composite moduli is examined by considering the staggered array, as presented in Figs. 9 and 10. The results are based on the same parameter combinations as in Figs. 5 and 8, respectively, except for the fiber microarchitecture. As shown in the results for rectangular arrays, the effects of the interphase formation parameters, x_E, x_A, N_L, and l^0, are less significant [Figs. 6 and 7] relative to the effects of ω_A and χ [Fig. 5(a) and (b)]. A similar result was obtained for the staggered arrays as well, and consequently the results presented in Fig. 9 elucidate only the effect of ω_A and χ for the staggered fiber arrangement. The trends in Fig. 9(a) and (b) follow those in Fig. 5(a) and (b), respectively, namely that E_2/E_m $(= E_3/E_m)$ increases with increasing ω_A and χ,

and with increasing E_f/E_m. However, it is observed that the values of E_2/E_m $(= E_3/E_m)$ for the staggered arrays are, in general, smaller than those for the corresponding rectangular arrays (cf. Fig. 5).

Fig. 10 presents the effects of the geometric parameters v_f and γ on the effective composite modulus, for a staggered fiber arrangement, following the same presentation format as in Fig. 8. It is seen from Fig. 10(a) that the transverse elastic modulus, E_2/E_m $(= E_3/E_m)$ increases monotonically with increasing fiber–matrix modulus ratio, E_f/E_m, and with increasing fiber volume fraction, v_f, a trend similar to that in Fig. 8, and explained similarly as in the related discussion. The notable distinction is once again in the magnitude of E_2/E_m $(= E_3/E_m)$ relative to the values for the corresponding rectangular array in Fig. 8.

The influence of the fiber array angle, γ, on the transverse moduli, $E_2(\gamma)/E_m$ $[= E_3(90° - \gamma)/E_m]$, is seen in Fig. 10(b). While the composite modulus increases monotonically with E_f/E_m as seen in previous result, the modulus exhibits a non-monotonic trend with respect to the staggered array angle, γ. The effective modulus initially decreases as γ increases from 25° to 45° and increases with further increase of γ. Note that the moduli for $\gamma = 30°$ and $\gamma = 60°$ are identical, reflecting the fact that the fiber arrangements are geometrically equivalent (corresponding to the hexagonal array) for these two configurations. The modulus variation for $\gamma = 67.5°$ [the solid line in Fig. 10(b)] is numerically distinct although close to the values for $\gamma = 30°$ and 60°. These trends are consistent with those reported for the effective transverse thermal conductivity of fibrous composites by Han and Cosner [24].

The discussion so far focused on the effective moduli of the composite. It is further instructive to explore the interphase effects on the maximum stress concentration factor, K_s, as considered in the remainder of this section. The stress concentration factor is one of the parameters influencing the failure of composite materials [25–27]. Boundary conditions used to calculate K_s are given by Eq. (11), where δ_3 is set to be zero. A maximum K_s is defined as the ratio of the maximum principal stress, σ_{max}, to the average applied stress, $\overline{\sigma}_x$, where both σ_{max} and $\overline{\sigma}_x$ are obtained from 2D finite element analysis under plane strain conditions. The mesh used in the evaluation of K_s was determined through a systematic convergence study where the mesh was refined until no significant change in the computed K_s value was noted. The convergence studies were carried out for the extreme values of the interphase modulus, $E_i = 0.01$ MPa and 2.4 GPa, respectively, used in the present analysis, and finer of the two mesh structures was used to compute the values reported in this section.

Three examples of maximum principal stress fields are presented in Fig. 11, for the parameter combination indicated in the caption. Fig. 11(a)–(c) correspond to

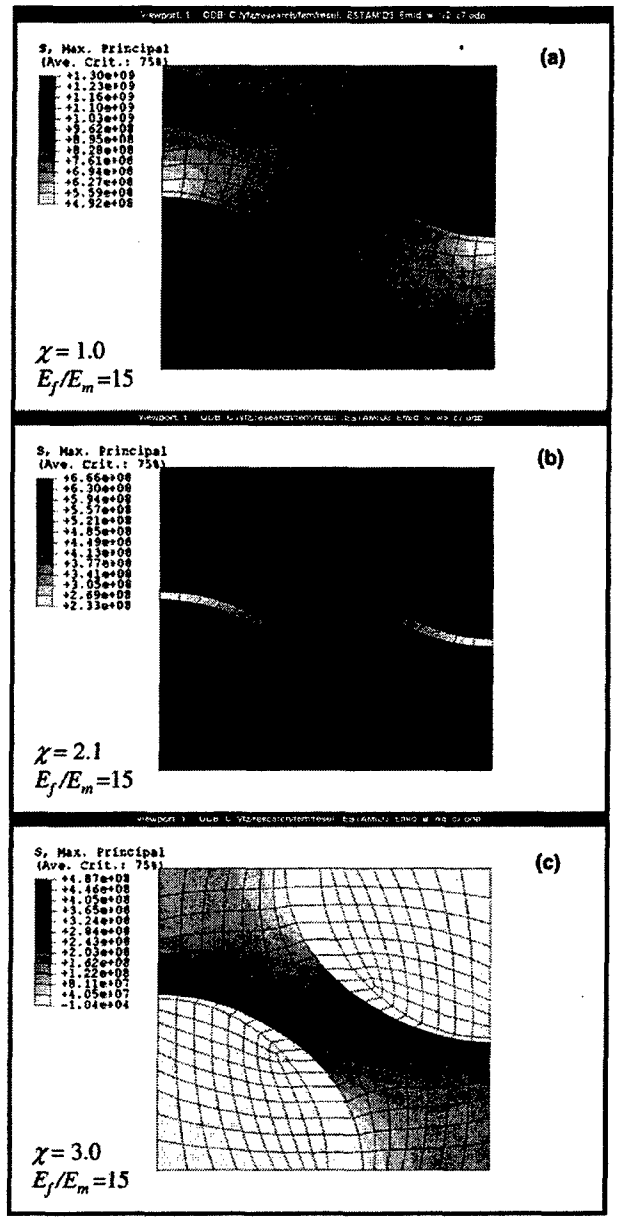

Fig. 11. Maximum principal stress distribution within a staggered RVE containing: (a) stiff, (b) media, and (c) soft interphase. The default values of the parameters are: $\omega_E = -0.28kT$, $\omega_A = 0.43kT$, $x_E = x_A = 150$, $l^0 = 15$ nm, $N_L = 2.5$, $v_f = 0.5$, $\gamma = 45°$.

stiff, moderate, and soft interphase regions, with $E_i = 2.159$ GPa, 0.157 GPa, and 0.620 MPa, respectively. The stiff interphase in Fig. 11(a) shows relatively strong capability to transfer load from matrix to the fiber, which leads to large stress concentrations in the fiber regions. For the interphase with moderate modulus in Fig. 11(b), load can still be transferred to the fiber through the interphase, however, the stress distribution appears more uniform since a bigger portion of the load is carried by the matrix as compared to Fig. 11(a). In Fig. 11(c), the interphase is too weak to transfer any load to the fiber, and the matrix assumes all the load.

Stress concentration is found within the matrix instead of the fibers. It is interesting to note that the fibers are in a compression (not tension) state, since the elongation of the matrix in x-direction causes a contraction in the y-direction, which, in turn, yields a transverse compression of the fibers.

From the predicted stress fields as exemplified in Fig. 11, K_s may be obtained for different combinations of interphase and geometric parameters. For the captioned parameter values, Fig. 12(a)–(c) presents nine curves corresponding to nine values of χ in the range −1.00–3.50, which is chosen to cover the range of interphase concentration values reported by Arayasantiparb et al. [20]. The interphase modulus values corresponding to the different values of χ are tabulated in Table 2. For the cases of $\chi = -1.00$, 1.00, 2.00 (Fig. 12(a)), the corresponding interphases are stiff, and the stress distributions are similar to that in Fig. 11(a). In this range of χ, it is noted from Table 2 that the values of E_i are close to that of E_m (= 2.30 GPa), therefore, the composite is similar to a two-component material. The stress concentration factor increases monotonically with increasing E_f/E_m in Fig. 12(a), which is consistent with the trend reported for a two-component composite in the literature [4]. At fixed E_f/E_m, a slight decrease of K_s is observed as χ increases to 2.00, which may be attributed to the relatively softer interphase.

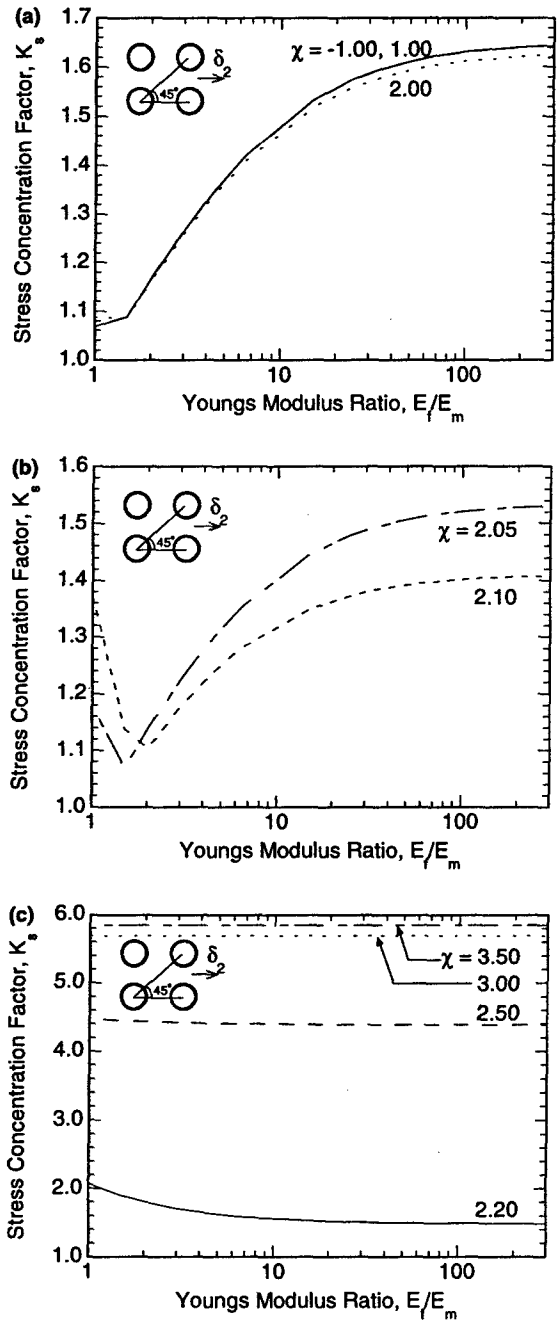

Fig. 12. Stress concentration factor of composite as a function of the ratio E_f/E_m for different chain/chain interaction parameters. The default values of the parameters are: $\omega_E = -0.28kT$, $\omega_A = 0.43kT$, $x_E = x_A = 150$, $l^0 = 15$ nm, $N_L = 2.5$, $v_f = 0.5$, $\gamma = 45°$.

Moderately stiff interphases similar to that in Fig. 11(b) are formed for χ in the range 2.05–2.10. Nonmonotonic trends are observed in the stress concentration factor, K_s, for the cases in Fig. 12(b), which may be explained as follows. As E_f/E_m increases from 1, the composite modulus, E_2, experiences a rapid initial increase (Fig. 5(b)), and the applied load, $\bar{\sigma}_x$, being directly proportional to E_2, increases at the same rate. On the other hand, the maximum principal stress in the fibers, σ_{max}, exhibits a relatively smaller increase since the load transfer through the interphase is not sufficient, causing an initial decrease in K_s with increasing E_f/E_m. Fig. 5(b) also indicates that further increase in E_f/E_m yields only limited gain in E_2, and the increase rate of σ_{max} exceeds that of $\bar{\sigma}_x$, which explains the later increase of K_s in Fig. 12(b).

As $\chi \geqslant 2.20$, the interphases in the composite belong to the soft type as in Fig. 11(c), where the maximum stress concentration occurs in the matrix region. For the case of $\chi = 2.20$, similar reasoning as in the cases of $\chi = 2.05$, 2.10 may be used to explain the decreasing trend with E_f/E_m. As χ increases from 2.20 to 3.50, the value of K_s at the ratio $E_f/E_m = 1$ increases sharply from 2.07 to 5.85, which may be explained by the increasing difference between the interphase and the matrix moduli. The fibers are weakly bonded to the matrix for the cases $\chi \geqslant 2.50$, and K_s is seen to be relatively

Table 2
Interphase moduli at different values of the interaction parameter χ in Fig. 11

χ	−1.00	1.00	2.00
E_i (GPa)	2.19	2.16	1.44
χ	2.05	2.10	2.20
E_i (GPa)	0.43	0.16	0.04
χ	2.50	3.00	3.50
E_i (MPa)	3.90	0.62	0.32

insensitive to the change in the fiber–matrix modulus ratio [Fig. 12(c)].

Detailed results on the effects of the other interphase formation parameters on K_s for rectangular arrays are omitted for brevity. However, it is found that the surface potential, ω_A, shows similar trends as χ in Fig. 12(a)–(c). As ω_A increases from 0 to $3.5kT$, the type of the interphase changes from stiff to moderate, and finally to soft; non-monotonic trends for the moderately stiff interphases (similar to Fig. 12(b)) and higher K_s values for the soft interphases (similar to Fig. 12(c)) are seen again. Since the parameters x_E, x_A, N_L, and l^0 do not have a significant influence on the interphase modulus (Figs. 6 and 7), their effects on the stress concentration factor K_s are also found to be negligible.

Fig. 13 shows the influence of geometric parameters of the fiber arrangement, v_f and γ, on K_s for rectangular arrays. The interphases involved are stiff ($E_i = 2.15$ GPa), therefore, K_s increases monotonically with increasing E_f/E_m. For a fixed ratio E_f/E_m, K_s increases as v_f or γ increases, since the inter-fiber distances in the loading direction become smaller in both cases. It is interesting to note that the influence of the geometric parameters on K_s is relatively smaller than that of the interphase formation parameter discussed in Fig. 12. The maximum values of K_s in Fig. 13(a) and (b) are 2.53 and 3.70, respectively, which are smaller than the value of 5.85 in Fig. 12(a). Recall that the geometric param-

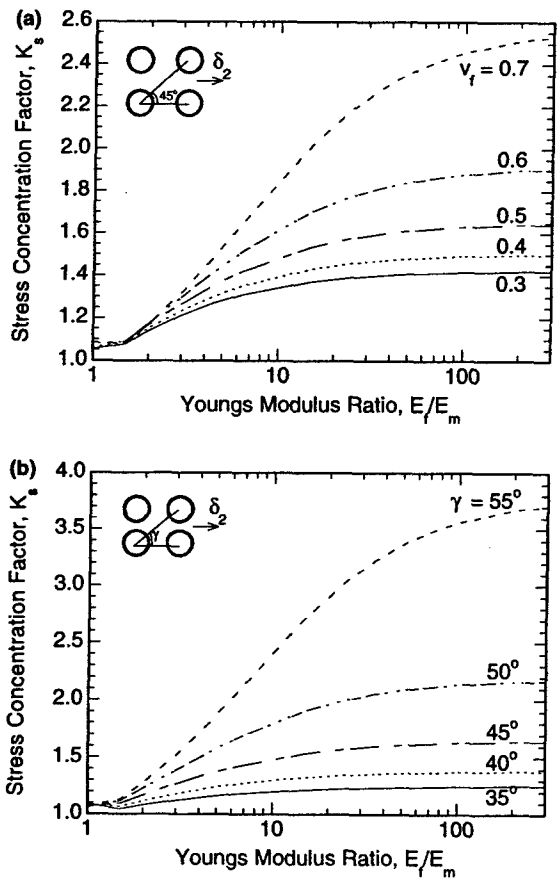

Fig. 13. Stress concentration factor of composite as a function of the ratio E_f/E_m for different: (a) fiber volume fractions, and (b) array angles. The default values of the parameters are: $\omega_E = -0.28kT$, $\omega_A = 0.43kT$, $\chi = 1.0$, $x_E = x_A = 150$, $l^0 = 15$ nm, $N_L = 2.5$: (a) $\gamma = 45°$, (b) $v_f = 0.5$.

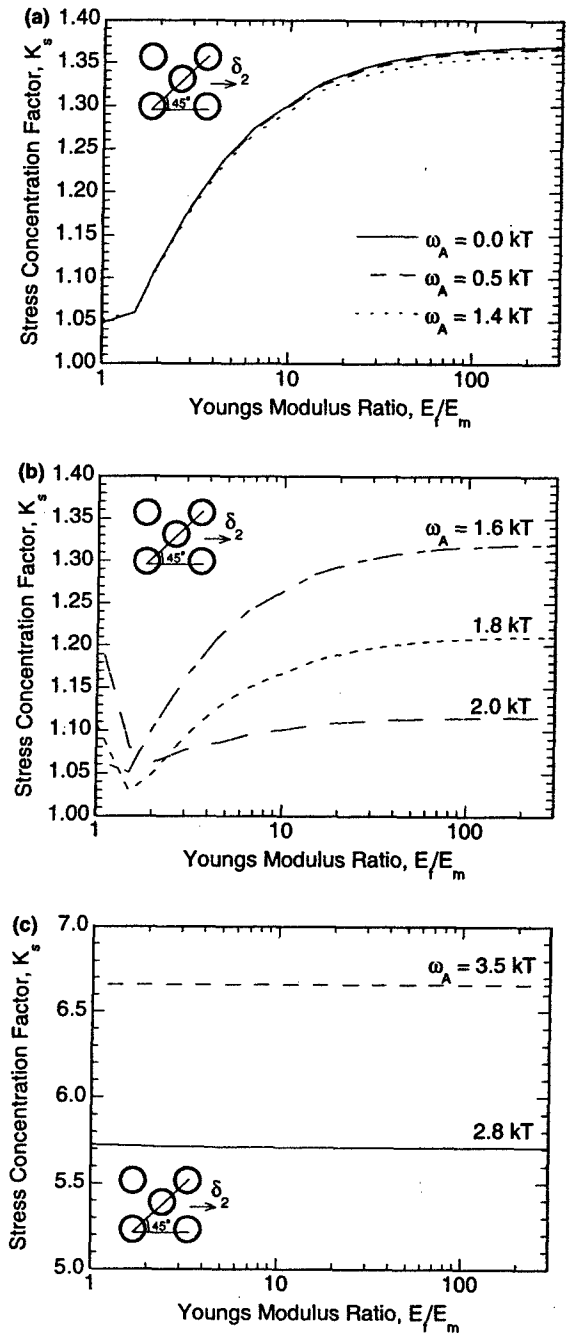

Fig. 14. Stress concentration factor of composite as a function of the ratio E_f/E_m for different surface potentials. The default values of the parameters are: $\omega_E = -0.28kT$, $\chi = 1.0$, $x_E = x_A = 150$, $l^0 = 15$ nm, $N_L = 2.5$, $v_f = 0.5$, $\gamma = 45°$.

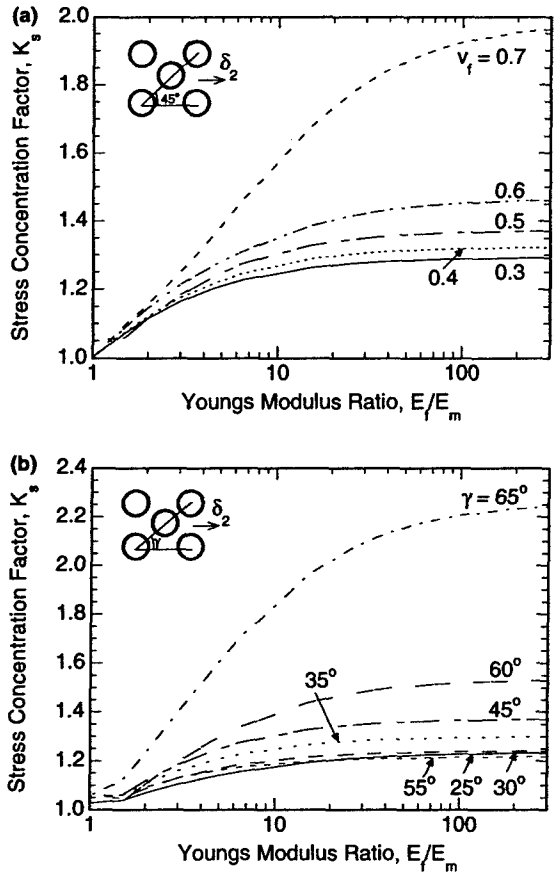

Fig. 15. Stress concentration factor of composite as a function of the ratio E_f/E_m for different: (a) fiber volume fractions, and (b) array angles. The default values of the parameters are: $\omega_E = -0.28kT$, $\omega_A = 0.43kT$, $\chi = 1.0$, $x_E = x_A = 150$, $l^0 = 15$ nm, $N_L = 2.5$: (a) $\gamma = 45°$, (b) $v_f = 0.5$.

eters have stronger effects on E_2 than the interphase formation parameters, as shown in Fig. 5.

The results of K_s for staggered arrangement of fibers in the composite are illustrated in Figs. 14 and 15. Fig. 14 follows the presentation format of Fig. 12, and depicts the effect of the surface potential, ω_A as an example interphase formation parameter. The interphase modulus values corresponding to the different values of ω_A are tabulated in Table 3. Fig. 14(a)–(c) correspond to the results of stiff, moderate, and soft interphase regions, respectively. As mentioned before, increases in ω_A and χ both lead to interphase regions richer in PACM20, therefore, the observations and explanations of trends in Fig. 14 are similar to those in Fig. 12. For $E_f/E_m > 10$ (typical range of practical interest), the stress concentration factor initially decreases with the increase of ω_A due to softer interphase; however, K_s increases as ω_A increases further to form weak interphases. Again, the influence of the other interphase parameters on K_s for the staggered arrays is similar to that outlined in the case of the rectangular arrays, and a detailed discussion is not included here.

Table 3
Interphase moduli at different values of the interaction parameter ω_A in Fig. 14

ω_A	0.0	0.5	1.4
E_i (GPa)	2.21	2.15	2.00
ω_A	1.6	1.8	2.0
E_i (GPa)	1.03	0.68	0.24
ω_A	2.8	3.5	
E_i (MPa)	1.14	0.01	

Fig. 15 illustrates the influence of the fiber volume fraction (v_f) and the fiber array angle (γ) for the case of staggered arrays. For fixed ratio E_f/E_m, K_s increases monotonically with the increase of fiber volume fraction, which is similar to the trend noted for rectangular arrays in Fig. 13. However, the values of K_s in Fig. 15(a) are smaller than those for the rectangular arrays of the same volume fraction. Recall from Fig. 10(b) that for a fixed ratio E_f/E_m, the effective composite modulus was observed to be minimum at $\gamma = 45°$. Similarly, a non-monotonic trend of the stress concentration factor is also noted in Fig. 15(b) with respect to γ. However, the stress concentration factor, K_s, reaches a maximum (not a minimum) at $\gamma = 45°$, decreases to a minimum at $\gamma = 55°$, and increases for $\gamma > 55°$. It is also observed that unlike the trend noted in Fig. 10(b), the values corresponding to $\gamma = 30°$ and 60° are not identical in Fig. 15(b).

Two important composite properties, transverse Young's modulus and normal stress concentration factor, are presented in this section as functions of processing and geometrical related parameters. Similarly, other composite properties such as transverse shear modulus and the shear stress concentration factor may be obtained for a more comprehensive analysis. For given material components and parameters, the approach presented in this article provides for predicting the composite properties without any assumed interphase properties. The results provide capabilities for tailoring composite properties and interphases via suitable material and processing parameter selection.

4. Conclusions

An interphase formation model obtained from first principles is adopted to predict the modulus and stress concentration factor of a fibrous composite, eliminating the need for assumed interphase properties. Interphase formation parameters such as the surface potentials and chain/chain interaction are directly linked for the first time to the overall composite properties. Parametric studies on DGEBA/PACM20 thermosetting composites reveal that transverse modulus and stress concentration factor of the composites strongly depend on the chain/surface and chain/chain interactions. The

transverse Young's modulus shows a monotonic decrease as surface potential ω_A or interaction parameter χ increases, due to softer interphases associated with the higher PACM20 concentration. On the other hand, the stress concentration factor initially decreases with increasing ω_A or χ because of the softer interphases. With further increase in ω_A or χ, the location of stress concentration transfer from the fiber to the matrix, and the stress concentration factor starts to increase. The study provides for linking the processing parameters to the composite properties, and in turn, for designing the process parameters to obtain tailored interphases and properties.

Acknowledgements

The work reported in this paper was carried out as part of the MEANS program funded by the Air Force Office of Scientific Research (Grant No. F496200110521). We are grateful to Prof. P. Zhang and Mr. W. Xie of University of Connecticut for their suggestions on the finite element modeling.

References

[1] Palmese GR. Origin and influence of interphase material property gradients in thermosetting composites. University of Delaware Center for Composite Materials, Technical Report Number 92-25; 1992.

[2] Subramanian S, Lesko JJ, Reifsnider KL, Stinchcomb WW. Characterization of the fiber–matrix interphase and its influence on mechanical properties of unidirectional composites. J Compos Mater 1996;30:309–32.

[3] Rydin RW, Varelidis PC, Papaspyrides CD, Karbhari VM. Glass fabric vinyl-ester composites: tailoring the fiber bundle/matrix interphase with nylon coating to modify energy absorption behavior. J Compos Mater 1997;31:182–209.

[4] Drzal LT. The interphase in epoxy composites. Adv Polym Sci 1986;75:1–32.

[5] Garton A, Stevenson WTK, Wang S. Interfacial reactions in carbon–epoxy composites. Br Polym J 1987;19:459–67.

[6] Sellitti C, Koenig JL, Ishida H. Surface characterization of carbon fibers and interphase phenomena in epoxy-reinforced composites. Mater Sci Eng A 1990;126:235–44.

[7] Tsai HC, Arocho AM, Gause LW. Prediction of fiber–matrix interphase properties and their influence on interface stress, displacement and fracture toughness of composite material. Mater Sci Eng A 1990;126:295–304.

[8] Liu YJ, Xu N, Luo JF. Modeling of interphases in fiber-reinforced composites under transverse loading using the boundary element method. J Appl Mech 2000;67:41–9.

[9] Tsui CP, Tang CY, Lee TC. Finite element analysis of polymer composites filled by interphase coated particles. J Mater Process Technol 2001;117:105–10.

[10] Fisher FT, Brinson LC. Viscoelastic interphases in polymer–matrix composites: theoretical models and finite-element analysis. Compos Sci Technol 2001;61:731–48.

[11] Papanocolaou GC, Michalopoulou MV, Anifantis NK. Thermal stresses in fibrous composites incorporating hybrid interphase regions. Compos Sci Technol 2002;62:1881–94.

[12] Anifantis NK. Micromechanical stress analysis of closely packed fibrous composites. Compos Sci Technol 2000;60:1241–8.

[13] Sottos NR, McCullough RL, Guceri SI. Thermal stresses due to property gradients at the fiber/matrix interface. In: Reddy JN, Teply JL, editors. Mechanics of composites materials and structures. American Society of Mechanical Engineers; 1989. p. 11–20.

[14] Wacker G, Bledzki AK, Chate A. Effect of interphase on the transverse Young's modulus of glass/epoxy composites. Compos Part A 1998;29:619–26.

[15] Jayaraman K, Reifsnider KL, Swain RE. Elastic and thermal effects in the interphase: part II. comments on modeling studies. J Compos Technol Res 1993;15:14–22.

[16] Hrivnak J. Interphase formation in reacting systems. University of Delaware Center for Composite Materials, Technical Report Number 97-05; 1997.

[17] Yang F, Pitchumani R. A kinetics model for interphase formation in thermosetting-matrix composites. J Appl Polym Sci 2003;89:3220–36.

[18] Yang F. Investigations on interface and interphase development in polymer–matrix composite materials. Ph.D. Dissertation, University of Connecticut, Department of Mechanical Engineering; 2002.

[19] VanLandingham MR, Eduljee RF, Gillespie Jr JW. Relationships between stoichiometry, microstructure, and properties for amine-cured epoxies. J Appl Polym Sci 1999;71:699–712.

[20] Arayasantiparb D, McKnight S, Libera M. Compositional variation within the epoxy/adherend interphase. J Adhes Sci Technol 2001;15:1463–84.

[21] Sun CT, Vaidya RS. Prediction of composite properties from a representative volume element. Compos Sci Technol 1996;56: 171–9.

[22] Yu YY. Vibrations of elastic plates: linear and nonlinear dynamical modeling of sandwiches, laminated composites, and piezoelectric layers. New York: Springer; 1996.

[23] Jones RM. Mechanics of composite materials. Taylor & Francis; 1999.

[24] Han LS, Cosner AA. Effective thermal conductivities of fibrous composites. J Heat Transfer 1981;103:387–92.

[25] Lane R, Hayes SA, Jones FR. Fibre/matrix stress transfer through a discrete. high volume fraction systems interphase: 2. Compos Sci Technol 2001;61:565–78.

[26] Fiedler B, Klisch A, Schulte K. Stress concentrations in multiple fibre model composites. Compos Part A 1998;29A: 1013–9.

[27] van den Heuvel PWJ, Wubbolts MK, Young RJ, Peijs T. Failure phenomena in two-dimensional multi-fibre model composites: 5. a finite element study. Compos Part A 1998;29A:1121–35.

Processing-Interphase-Property Relationship in Fiber-Reinforced Thermosetting-Matrix Composites

F. Yang, R. Pitchumani
Composites Processing Laboratory, Department of Mechanical Engineering, University of Connecticut, Storrs, Connecticut 06269-3139

Fabrication of thermosetting-matrix composites is based on a critical step of cure, which involves applying a predefined temperature cycle to a fiber-resin mixture. Several temperature-dependent mass transport processes occur in the vicinity of the reinforcement fiber, leading to the formation of an interphase region with different chemical and physical properties from the bulk resin. The cure cycles applied on the macroscopic boundaries of the composite govern the microscopic cure kinetics near the fiber surface, which in turn determines the interphase and composite properties. A predictive approach to directly linking the cure cycles and final composite properties is not presently available and is established for the first time in this paper. A multiscale thermochemical model is developed to predict the concentration profile evolution with time near fiber surfaces at various locations across the composite thickness. The concentration profiles at the gelation time are mapped to modulus profiles within the interphase region, and a finite element analysis is used to determine the overall composite modulus in terms of the constituent interphase, fiber, and matrix properties. Relevant numerical results are presented for the first time where the composite modulus is directly linked to the cure cycle and interphase formation parameters without assumed structures or properties of the interphase. The results provide useful information for selecting material components and cure cycles parameters to achieve desired interphase and composite properties. POLYM. COMPOS., 26:193–208, 2005. © 2005 Society of Plastics Engineers

INTRODUCTION

During the cure of thermosetting-matrix polymer composites, the presence of reinforcing fibers significantly alters the resin composition in the vicinity of the fiber surface via several microscale processes, forming an interphase region with different chemical and physical properties from the bulk resin. The interphase resides in a region between the original constituents of the composite with a size of one to a few thousand nanometers [1–4]. The performance of the composite is determined by the ability of the matrix to transfer load to the reinforcing fiber and is thus controlled by the interphase region. The structure and properties of the interphase are the dominant factors governing the overall composite properties and performance.

Several physical and chemical mechanisms contribute simultaneously to the interphase formation and very few of them have been described rigorously in mathematical models. Garton et al. [5] showed that the carbon surfaces influence the cross-linking reaction in an amine catalyzed anhydride-epoxy system by adsorbing the tertiary amine catalyst and forming amine rich interphase regions near the carbon surfaces. Similarly, Sellitti et al. [6] used Fourier transform IR attenuated total reflection spectroscopy to characterize the interphase phenomena in an epoxy-anhydride-catalyst system, and showed that the surface species introduced on graphitized carbon fibers can promote or inhibit the cross-linking process by the preferential adsorption of the catalyst. Other possible interphase mechanisms are proposed by Drzal [4].

Many studies in the literature on interphase have focused on the experimental determination of the influence of interphase on the mechanical behavior of the composite materials (for example, Refs. 2–4, 7). Fiber surface modifications, such as high temperature treatment and sizing, are commonly implemented to tailor the structure of the interphase regions and to investigate their effects on the mechanical and other properties of the composite materials. Numerical prediction of the interphase effects on the overall composite properties are also frequently seen in the literature (for example, Refs. 8–10). However, the studies are commonly based on assumed or empirical interphase property variation. Tsai et al. [8] used an axisymmetric finite element model to study the interface stress, displacement, and fracture toughness. An elastic shear lag analysis was developed and correlated with the micro-debonding test data to determine the thickness and material properties of the interphase. Boundary element method was adopted by Liu et al. [9] to

Correspondence to: R. Pitchumani; e-mail: r.pitchumani@uconn.edu
Contract grant sponsor: Air Force Office of Scientific Research; contract grant number: F496200110521.
DOI 10.1002/pc.20089
Published online in Wiley InterScience (www.interscience.wiley.com).
© 2005 Society of Plastics Engineers

predict transverse moduli of fibrous composites. Tsui et al. [10] studied the effects of different interphase properties on Youngs modulus, maximum stress concentration factor, and stress distribution in particle-filled polymer composites. All the studies in Refs. 9, 10 assumed interphase thickness and modulus.

Due to complexities of the molecular level mechanisms that occur in the vicinity of the fibers during the processing, prediction of the interphase evolution as a function of processing parameters has been the subject of little attention. Palmese [1] presented a model for predicting the interphase composition profile under thermodynamic equilibrium conditions of a nonreacting epoxy-amine resin system. The principle of minimum free energy was invoked to set up the equilibrium state, accounting for enthalpy interaction between fiber surface and resin components, and the calculation of Gibbs free energy was based on a Flory-Huggins type lattice structure. Hrivnak [11] extended Palmese's model to a reacting system by using renewal theory models to the construction of the assembly Gibbs free energy and the associated chemical potential. In an alternative approach, a kinetics-based description of the governing phenomena was developed by the authors to predict the interphase development during thermosetting composite processing [12–15]. In this method, a mass conservation principle was employed to describe the transport processes of multilayer adsorption, desorption, and diffusion near a fiber surface, which are accompanied by simultaneous cure reaction between the resin components. The time evolution of interphase concentration profile gradients before the gelation of the thermosetting system was predicted as a function of material and process parameters. Furthermore, to eliminate the need for assumed interphase properties in the prediction of overall composite properties, the interphase model of Hrivnak was adopted by the authors to describe the concentration profiles in the interphase region [16]. The interphase concentration profiles were subsequently mapped to modulus profiles, which in turn were used in finite element analyses to calculate the modulus and stress concentration factor of fiber reinforced epoxy/amine composites [16].

The foregoing discussion suggests that although processing-interphase and interphase-property relationships have been attempted individually under special conditions, a complete processing-interphase-property linkage has not been established so far. This is in part due to the complexities of the inherent mechanisms involved as well as those of integrating the phenomena across a cascade of length scales ranging from the interphase scale (on the order of nm) to the laminate scale. The goal of this work is to address this challenge and to establish the complete processing-interphase-property relationship for a fiber reinforced epoxy/amine composite system. To this end, the microscale kinetics model developed by the authors in previous studies [12–15] is coupled with the macroscale energy equation to predict the interphase concentration profile evolution with time near fiber surfaces, as a function of the cure temperature cycle and different locations across the composite cross section. An experimental correlation between interphase composition and modulus is used to map the concentration profiles to modulus profiles, which in turn are used in a finite element analysis to calculate the transverse modulus of the composite. A systematic study is conducted to show the effects of different cure cycles and interphase formation parameters on the overall composite property.

MODELING

Thermosetting-matrix composites fabrication via an autoclave process is considered in the study. In this process, a laminate consisting of multiple layers of the fiber-resin mixture is inserted between two layers of tooling material and placed in an autoclave oven [17–19]. The assembly is exposed to a cure temperature cycle, and the elevated temperatures initiate an exothermic crosslinking cure reaction among the species in the resin, which transforms the soft initial mixture to a structurally hard product. The dominant physical and chemical phenomena are: 1) the heat transfer associated with the heating of the composite, and 2) the chemical reaction leading the cure process [17–19].

Modeling of the heat transfer in the laminate has been well established in the literature, as, for example, in Ref. 18 and in the references therein. Most of the mathematical descriptions of the cure reactions are based on the assumption of uniform reactant concentration throughout the laminate domain (e.g., Ref. 18), while the influence of the reinforcement on the cure process is commonly ignored. An interphase kinetics model was developed by the authors to account for the fiber surface effects on the cure reaction, and was used to predict the reactant concentration evolution with time in the vicinity of a fiber surface for the case of isothermal cure process [12–15]. In this study, the heat transfer model is coupled with the interphase kinetics model to predict the cure evolution at various locations across the thickness of the laminate under the influence of nonisothermal cure cycles. The processing conditions are linked first with the local interphase structure and properties, which in turn are used to predict the overall composite modulus.

Macroscale Thermal Model

The heat transfer in the autoclave is assumed to be uniform across the length and width of the assembly (y- and z-directions in Fig. 1), and the lay-up thickness is small in comparison to the laminate length and width. It is further assumed that symmetric boundary conditions are imposed on the top and bottom surfaces of the lay-up. The problem domain is thus reduced to one half of the assembly thickness, and the one-dimensional heat transfer equations for the laminate and tooling materials may be written as:

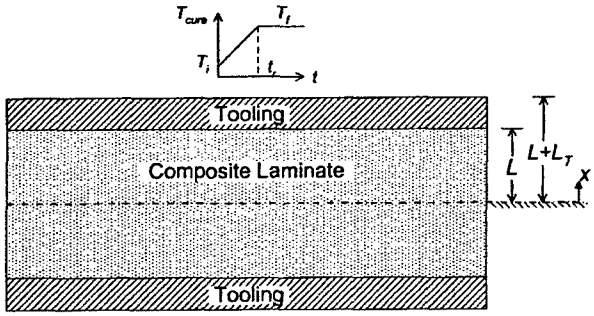

FIG. 1. Schematic of a laminate cross section sandwiched between tooling layers in an autoclave process for manufacturing thermosetting composites.

$$\frac{\partial[(\rho c_p T)_L]}{\partial t} = \frac{\partial}{\partial x}\left(k_L \frac{\partial T_L}{\partial x}\right) + C_{E0}\Delta H_r(1 - v_f)\frac{d\epsilon}{dt}; \quad 0 \le x \le L \text{ (Laminate)} \quad (1)$$

$$\frac{\partial[(\rho c_p T)_T]}{\partial t} = \frac{\partial}{\partial x}\left(k_T \frac{\partial T_T}{\partial x}\right); \quad L < x \le L + L_T \text{ (Tooling)}$$

where the variables t and x are the time and location coordinates, respectively, ΔH_r is the heat of the cure reaction, C_{E0} is the initial concentration of the epoxy resin, v_f is the fiber volume fraction, and T is the local temperature of the lay-up assembly. The subscripts L and T refer to the laminate and tooling, respectively. Note that a heat source term is present in the laminate equation to account for the heat of the exothermic cure reaction in the composite. The three material properties of the laminate, namely, the thermal conductivity, k_L, the density, ρ_L, and the specific heat, c_{pL}, are evaluated based on the weight fraction of the fiber in the fiber-resin mixture [17]. The term $d\epsilon/dt$ is the local reaction rate, and its determination is the focus of the remaining discussion in this section.

The initial temperature field in the laminate and tooling for the governing equation, *Eq. 1*, is given by:

$$T_L(x, 0) = T_T(x, 0) = T_{ini}. \quad (2)$$

The boundary conditions associated with *Eq. 1* are convective heating of the top tooling surface by the cure cycle $T_{cure}(t)$ in the autoclave ($x = L + L_T$ in Fig. 1) and an insulated condition at the symmetry line of the lay-up ($x = 0$ in Fig. 1). Furthermore, temperature and heat flux must be continuous at the laminate-tooling interface ($x = L$). The mathematical expressions for these conditions may be written as follows:

$$-k_T \frac{\partial T_T}{\partial x} = h[T_T - T_{cure}(t)]; \quad \text{at } x = L + L_T$$

$$\frac{\partial T_L}{\partial x} = 0; \quad \text{at } x = 0 \quad (3)$$

$$T_T = T_L; \quad k_T \frac{\partial T_T}{\partial x} = k_L \frac{\partial T_L}{\partial x}; \quad \text{at } x = L$$

where h is the heat transfer coefficient and all the other terms in the above equations are defined previously. The cure cycle $T_{cure}(t)$ considered in this paper begins with a linear ramp from $T = T_i$ to T_f within a ramp time t_r, followed by a hold stage with a constant temperature T_f, as shown schematically in Fig. 1.

Microscale Cure Kinetics Model

The cure reaction rate, $d\epsilon/dt$ in *Eq. 1*, is commonly modeled by empirical correlations, which are obtained using data from the bulk reactions with uniform mixing of the reacting species in the absence of the reinforcing fibers [16]. The presence of fibers, however, has been found to cause concentration gradients in the vicinity of the fiber surfaces through the preferential adsorption mechanism [1, 12]. Consequently, the reaction kinetics is significantly changed by the spatial variation of the stoichiometric ratio, i.e., the nonuniform mixing of the reacting species. A model of the microscale cure kinetics near the fiber surfaces has been developed by the authors [12], and is modified in this subsection to determine the cure reaction rate $d\epsilon/dt$.

The geometry considered in the cure kinetics model is the inter-fiber space in a composite having a typical staggered fiber arrangement (Fig. 2a). The domain in the model development is idealized as the region between two identical infinite planes representing the fiber surfaces (Fig. 2b), which may be justified by the fact that the interphase thickness is often small in comparison to the fiber diameter. A

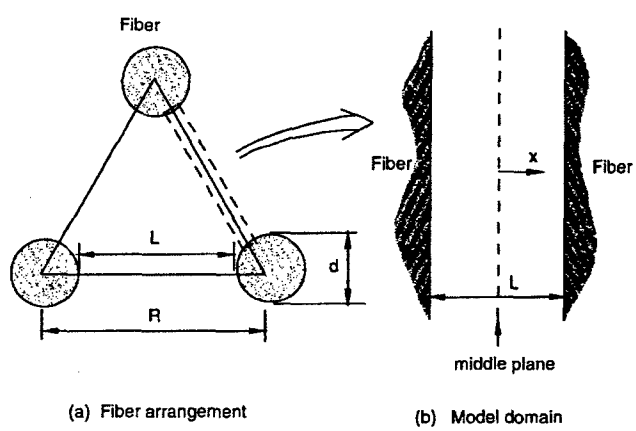

FIG. 2. (a) A representative fiber arrangement in the composite, and (b) schematic of the domain between two fiber surfaces considered in the modeling.

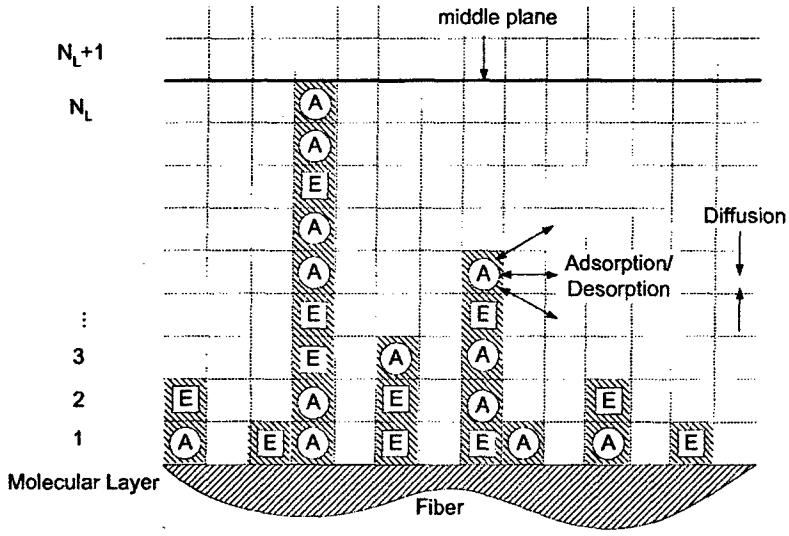

FIG. 3. Schematic of the adsorption, desorption, and diffusion processes near a fiber surface in a fiber-epoxy-amine system.

graphite fiber/epoxy-amine thermosetting system is considered in the model development; however, all the derivations and results are applicable to a general two-component thermosetting system. The domain between the two fiber surfaces is divided into molecular layers, such that there are N_L layers in the half domain. Each layer is further discretized along the fiber direction, as shown in Fig. 3, and a molecule of epoxy or amine can occupy only one of these discretized cells.

Due to the interaction between resin molecules and the fiber surface, as well as those among resin molecules themselves, epoxy and amine molecules can move from layer to layer. The solid surface can adsorb molecules from a "bulk" state into an "adsorbed" state, and conversely, molecules in the "adsorbed" state may be desorbed into the "bulk" state. Molecules in the "adsorbed" state are treated to be fixed in the space and are not permitted to diffuse, while molecules in the "bulk" state may diffuse within the resin mixture. Figure 3 shows the molecular layers in the model domain, where the shaded cells denote contained molecules in the "adsorbed" state, while the blank cells hold molecules in the "bulk" state. Chemical reaction between epoxy (E) and amine (A) happens simultaneously during the adsorption, desorption, and diffusion processes, resulting in a continuously evolving concentration profile that is "frozen" in space upon gelation of the thermosetting system. The reaction equation may be written as

$$n_1E + n_2A \rightarrow P$$

where P denotes the product and n_1 and n_2 are the molar numbers of the reactants needed to produce 1 mol of product.

The mass balance for the epoxy molecules in the "adsorbed" state in any (i)th molecular layer yields [12]:

$$\underbrace{\frac{dN_{E,i}}{dt}}_{storage} = \underbrace{R_{a,E}(i-1,i) + R_{a,E}(i,i) + R_{a,E}(i+1,i)}_{adsorption,\ \Re_{a,E}(i)} - \underbrace{R_{d,E}(i-1,i) - R_{d,E}(i,i) - R_{d,E}(i+1,i)}_{desorption,\ \Re_{d,E}(k)} - \underbrace{\Re_{r,E}(i)}_{depletion\ (reaction)} \quad (4)$$

In *Eq. 4*, $dN_{E,i}/dt$ is the rate of change of total number of adsorbed epoxy molecules in the (i)th molecular layer, and the subscripts E and i denote epoxy and (i)th layer, respectively. Epoxy molecules in the bulk state in the ($i - 1$)th, (i)th, and ($i + 1$)th layers may be adsorbed into the (i)th molecular layer, denoted by the rate terms $R_{a,E}(i - 1, i)$, $R_{a,E}(i, i)$, and $R_{a,E}(i + 1, i)$, respectively. In a reverse process, the adsorbed epoxy molecules in the (i)th layer can also be desorbed into the bulk in the ($i - 1$)th, (i)th, and ($i + 1$)th layers through the rate terms $R_{d,E}(i - 1, i)$, $R_{d,E}(i, i)$, and $R_{d,E}(i + 1, i)$. Further, the depletion of adsorbed epoxy in the (i)th molecular layer through chemical reaction is determined by the rate term $\Re_{r,E}(i)$.

The adsorption of epoxy molecules from ($i - 1$)th layer of the bulk state to (i)th layer of the adsorbed state is given as:

$$R_{a,E}(i-1,i) = k_{a,E}(N_{i-1} - N_i)\exp\left(-\frac{E_{a,E}}{RT}\right)\frac{N_{E\infty,i-1}}{N_{\infty,i-1} + N_{\infty,i} + N_{\infty,i+1}}.$$

The parameter, $k_{a,E}$, in the above equation is the frequency factor in the adsorption rate of epoxy molecules, and N_i is the total number of epoxy and amine molecules adsorbed in

the (i)th layer, i.e., $N_i = N_{E,i} + N_{A,i}$. Because a molecule adsorbed into the (i)th layer must adjoin an adsorbed epoxy or amine molecule in the $(i - 1)$th layer, the term $N_{i-1} - N_i$ yields the number of available sites in the $(i - 1)$th layer which are open for adsorption. Note that for $i = 1$, the term $N_0 - N_1$ denotes the available sites in the first adsorption layer, where N_0 is the number of adsorption sites on the bare fiber surface. The activation energy of adsorption for the epoxy molecules is denoted as $E_{a,E}$, which defines the energy barrier to be crossed for an epoxy molecule to be adsorbed. The parameters $N_{E\infty,i}$ and $N_{A\infty,i}$ are the number of epoxy and amine molecules in the bulk state in the (i)th molecular layer, and $N_{\infty,i} = N_{E\infty,i} + N_{A\infty,i}$. Since the epoxy molecules adsorbed into the (i)th layer come from the $(i - 1)$th, (i)th, and $(i + 1)$th layers, the fraction $\frac{N_{E\infty,i-1}}{N_{\infty,i-1}+N_{\infty,i}+N_{\infty,i+1}}$ in the above equation denotes the probability that a site can capture an epoxy molecule from the $(i - 1)$th layer of the bulk state.

The "depletion" term, $\Re_{r,E}$, is determined by the crosslinking chemical reaction between epoxy and amine, and may be defined as:

$$\Re_{r,E}(i) = n_1 k_r N_{E,i}$$

where k_r is the reaction rate. The other rate terms and the mass conservation analysis of the amine and product in the adsorbed state (i.e., $N_{A,i}$ and $N_{P,i}$) may be discussed in a similar way, and the readers are referred to Ref. 12 for details.

The adsorbed state exchanges mass with the bulk state, in which the molecules undergo diffusion in addition to the adsorption, desorption, and reaction processes. Evidently, the following processes are responsible for the change in the number of the epoxy molecules in the bulk state in the (i)th layer: 1) diffusion of epoxy molecules in the "bulk" state from $(i + 1)$th and $(i - 1)$th layers to (i)th layer, which increases $N_{E\infty,i}$; 2) desorption of epoxy molecules in the "adsorbed" state in the $(i - 1)$th, (i)th, and $(i + 1)$th layers to the (i)th layer of the "bulk" state, which increases $N_{E\infty,i}$; 3) epoxy molecules in the "bulk" state in the (i)th layer being adsorbed to the $(i - 1)$th, (i)th, and $(i + 1)$th layers of the "adsorbed" state, which reduces $N_{E\infty,i}$; and 4) chemical reaction in the bulk in (i)th layer, which depletes $N_{E\infty,i}$. Furthermore, it is assumed that any discrete cell within a molecular layer is filled with one and only one resin molecule at any time instant, which assures a constant number density of resin molecules near the surface. Consequently, the transfer (caused by either adsorption or desorption) of one molecule (epoxy or amine) from the (i)th layer to a neighborhood layer j (where $j = i - 1$, i, or $i + 1$) creates a vacant square box in (i)th layer, which is assumed to be filled by molecules in the bulk state from the (j)th layer. The probability that the vacant site is filled by an epoxy molecule in the bulk state from the (j)th is $\frac{N_{E\infty,j}}{N_{\infty,j}}$. Conversely, the transfer (caused by either adsorption or desorption) of a molecule (epoxy or amine) from a neighborhood (j)th layer into the (i)th molecular layer repeals one of the molecules in the bulk state in the (i)th layer to the (j)th layer, and the epoxy molecules are reduced with the probability $\frac{N_{E\infty,i}}{N_{\infty,i}}$.

The mass balance for the epoxy molecules in the "bulk" state in any (i)th molecular layer yields:

$$\begin{aligned}\frac{dN_{E\infty,i}}{dt} = {} & \frac{D_{EA}}{\Delta L^2}\left(N_{E\infty,i+1}\frac{N_0 - N(i)}{N_0} - N_{E\infty,i}\frac{N_0 - N(i+1)}{N_0}\right) + \frac{D_{EA}}{\Delta L^2}\left(N_{E\infty,i-1}\frac{N_0 - N(i)}{N_0} - N_{E\infty,i}\frac{N_0 - N(i-1)}{N_0}\right) \\ & + R_{d,E}(i, i-1) + R_{d,E}(i, i) + R_{d,E}(i, i+1) - R_{a,E}(i, i-1) - R_{a,E}(i, i) - R_{a,E}(i, i+1) - n_1 k_r N_{E\infty,i} \\ & + \sum_{j=i-1,i+1}\left[\frac{N_{E\infty,j}}{N_{\infty,j}}(R_{d,E}(j, i) + R_{d,A}(j, i) + R_{a,E}(i, j) + R_{a,A}(i, j))\right] - \frac{N_{E\infty,i}}{N_{\infty,i}}\sum_{j=i-1,i+1}[R_{a,E}(j, i) + R_{a,A}(j, i) \\ & + R_{d,E}(i, j) + R_{d,A}(i, j)] \quad (5)\end{aligned}$$

where the mutual diffusion coefficient D_{EA} in the binary epoxy-amine mixture is a function of temperature and degree of cure [12], ΔL corresponds to the physical size of a molecular layer, and k_r is the reaction rate.

It must be pointed out that *Eq. 5* has two principal modifications from the corresponding equation in Ref. 12: 1) The terms in the last two lines of *Eq. 5* are added to account for the constant number density consideration, and 2) the diffusion term is modified to consider the blockage effect of the adsorbed molecules. Since molecules in the adsorbed state are assumed to be fixed in the space, a molecule can diffuse into the (i)th layer only into an available space that is unoccupied by an adsorbed molecule. Consequently, the diffusion rate of epoxy molecules from $(i + 1)$th layer to (i)th layer is $\frac{D_{EA}}{\Delta L^2} N_{E\infty,i+1} \frac{N_0 - N(i)}{N_0}$, where $\frac{N_0 - N(i)}{N_0}$ denotes the probability of the above-mentioned diffusion. Similar considerations are incorporated in *Eq. 5* for the other diffusion terms, i.e., from (i)th to $(i + 1)$th layer, and those between (i)th and $(i - 1)$th layers.

The subscripts E and A in *Eq. 5* may be switched to obtain the rate equation for $N_{A\infty,i}$, and the equation for $N_{P\infty,i}$ follows that in Ref. 12. In summary, the current cure kinetics model

inherits the four rate equations for the four unknowns, $N_{E,i}$, $N_{A,i}$, $N_{P,i}$, and $N_{P\infty,i}$ in Ref. 12, and the two equations for the two unknowns, $N_{E\infty,i}$ and $N_{A\infty,i}$, follow the form given by *Eq. 5*. All the rate equations of the microscale kinetics model are summarized in the appendix. The symmetry of the geometry in Fig. 2b suggests the following conditions:

$$\begin{aligned} &[\text{adsorbed state}]\, N_{E,N_L} = N_{E,N_L+1}; \quad N_{A,N_L} = N_{A,N_L+1}; \\ &\qquad\qquad N_{P,N_L} = N_{P,N_L+1} \\ &[\text{bulk state}]\, N_{E\infty,N_L} = N_{E\infty,N_L+1}; \\ &\qquad\qquad N_{A\infty,N_L} = N_{A\infty,N_L+1}; \quad N_{P\infty,N_L} = N_{P\infty,N_L+1}. \end{aligned} \tag{6}$$

For a thermosetting system with fiber sizing thickness of N_S molecular layers, the initial conditions associated with the species rate equations are: 1) the number of molecules for each species in the adsorbed state and the number of product in the bulk state are zero; 2) within the epoxy sizing layer, the number of epoxy is a constant, $N_{E,1}$, while the number of amine is zero; and 3) beyond the sizing layer, the numbers of epoxy and amine species are constants, $N_{E,0}$ and $N_{A,0}$, respectively. The mathematical expressions for the initial conditions may be written as:

$$\begin{aligned} &N_{E,i} = N_{A,i} = N_{P,i} = N_{P,\infty} = 0; \quad (i = 1, 2, \cdots, N_L) \\ &N_{E\infty,i} = N_{E,1}; \quad N_{A\infty,i} = 0; \quad (i = 1, 2, \cdots, N_S) \\ &N_{E\infty,i} = N_{E,0}; \quad N_{A\infty,i} = N_{A,0}; \quad (i = N_S + 1, \cdots, N_L). \end{aligned} \tag{7}$$

For a given temperature history, the microscale cure kinetics model (*Eqs. 4–6*) may be used to predict the evolution of the concentration profiles (e.g., $N_{E,i}$, $N_{A,i}$) with time near a fiber surface. Note that the microscale cure kinetics model and the macroscale thermal model (*Eq. 1*) exhibit a two-way coupling via 1) the temperature dependence of the rate terms (e.g., $R_{a,E}$), and 2) the relationship between the bulk reaction rate $d\epsilon/dt$ in *Eq. 1* and the microscale rates of change of species (e.g., $dN_{E,i}/dt$). The next subsection establishes the linkage between the micro/macroscale models presented above.

Multiscale Thermochemical Model

The kinetics model discussed in the previous subsection paves the way for the assembling of the multiscale thermochemical model, which involves the determination of the term $d\epsilon/dt$ in *Eq. 1* from the microscale species rate equations. The degree of cure, ϵ, is defined as:

$$\epsilon = \frac{N_{E,0} - N_E}{N_{E,0}} \tag{8}$$

where $N_{E,0}$ is the initial number of epoxy molecules in the half domain between two fiber surfaces (Fig. 3), and N_E is the instantaneous number of epoxy molecules in the half domain:

$$N_E = \sum_{i=1}^{N_L} (N_{E,i} + N_{E\infty,i}). \tag{9}$$

Differentiating *Eqs. 8* and *9* with respect to time yields:

$$\frac{d\epsilon}{dt} = -\frac{1}{N_{E,0}}\frac{dN_E}{dt} = -\frac{1}{N_{E,0}}\sum_{i=1}^{N_L}\left(\frac{dN_{E,i}}{dt} + \frac{dN_{E\infty,i}}{dt}\right) \tag{10}$$

where the rates of change, $dN_{E,i}/dt$ and $dN_{E\infty,i}/dt$, are given by *Eqs. 4* and *5*, respectively. The energy equation, *Eq. 1*, for the macroscale composite domain in Fig. 1 and the reaction rate equation, *Eq. 10*, for the microscale model domain in Fig. 3 together constitute a multiscale thermochemical model. Note that *Eqs. 1* and *10* are coupled through the temperature dependence of the rate terms in *Eqs. 4* and *5*.

The governing equations, *Eqs. 1, 10,* and the rate equations of the cure kinetics model, along with the initial and boundary conditions in *Eqs. 2, 3, 6,* and *7*, were solved numerically using an implicit finite-difference scheme with a control volume formulation [17]. The mesh for the macroscopic composite domain contained 64 numerical grids along the x-direction, and the time step Δt was determined such that the mesh Fourier number $k\Delta t/\rho c_p \Delta x^2$ is less than unity. Depending on the fiber volume fraction, each computational grid may consist of a large number of fiber surfaces with the adsorption-desorption-diffusion-reaction processes such as that illustrated in Fig. 3 occurring near each surface. All the fibers within a computational grid experience the same temperature history, and, hence, the same concentration profile evolution history. Within each time step, the temperature field obtained from *Eq. 1* is used to calculate the cure reaction rate $d\epsilon/dt$ in *Eq. 10*, which in turn is substituted into *Eq. 1* to update the temperature field; and the procedure is performed until the temperature field is converged. Note that the calculation of $d\epsilon/dt$ in *Eq. 10* involves the evaluation of the microscale rate of change of species (e.g., $dN_{E,i}/dt$), which are determined by the microscale cure kinetics model, *Eqs. 4–6*. The rate equations in the microscale kinetics model were solved using a fourth-order Runge-Kutta method [12]. The stopping criterion for the numerical simulation is that all the sections of the composite are completely cured, which corresponds to $\epsilon = 0.95$.

Interphase-Composite-Property Relationship

The concentration profiles predicted by the multiscale thermochemical model are used to determine the interphase and composite material properties, following the steps in a micromechanical model reported by Yang and Pitchumani [16]. First, concentration profiles are mapped to modulus

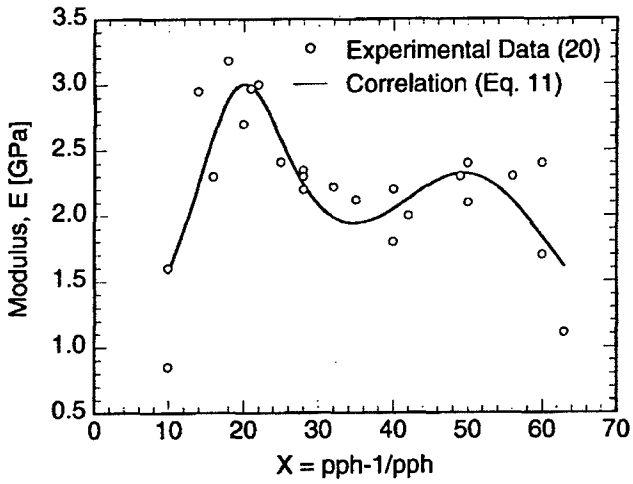

FIG. 4. Measured Youngs modulus (at $T = 30°$) as a function of amine concentration for a DGEBA/PACM20 system.

profiles using available experimental data. Figure 4 presents the experimental data on matrix modulus as a function of the parameter X = pph − 1/pph for the DGEBA/PACM20 system at 30°C as reported by VanLandingham et al. [20]. Note that pph is the parts per hundred concentration defined as the weight percentage of PACM20 to DGEBA in the mixture, and ranges from 0 (denoting pure DGEBA) to infinity (denoting pure PACM20). Two peaks in the modulus variation are observed: one around 18 pph PACM20 with a value of 3.2 GPa, and the other between 48 and 56 pph PACM20 having a value of 2.4 GPa. A twin peak function was derived to fit the data as follows [16]:

$$E = \frac{1}{(X - 19.57)^2/214.42 + 0.42} + \frac{1}{(X - 50.59)^2/803.09 + 0.47}. \quad (11)$$

Equation 11, which has an asymptotic value of 0 as pph approaches 0 and infinity, is used in this study to map the concentration profiles, $N_{E,i}$ and $N_{A,i}$, to modulus profile. Note that the concentration in terms of the number of molecules (e.g., $N_{E,i}$) may be converted to the pph concentration as:

$$\text{pph} = 100\frac{(N_{A,i} + N_{A\infty,i} + n_1 \cdot N_{P,i})M_A}{(N_{E,i} + N_{E\infty,i} + n_2 \cdot N_{P,i})M_E} \quad (12)$$

where M_E and M_A are the molecular weight of epoxy and amine molecules, respectively.

Since the interphase region is typically thin (around 10–500 nm), the micromechanical model considers only a single uniform interphase layer with thickness, δ_i, and effective modulus, E_i. An "interphase thickness" may be defined as that distance from the fiber surface where the amine concentration is within 1% of the amine concentration in the far region layers. The modulus profile within the interphase thickness is averaged to determine the effective interphase modulus [16]. The transverse composite modulus, E_2, is determined by a finite element analysis using δ_i and E_i as inputs, and by considering representative volume elements with a staggered array configuration of fibers. The readers are referred to Ref. 16 for the details of the micromechanical analysis.

RESULTS AND DISCUSSION

The thermochemical model developed in the previous section is used to calculate the molar concentration of the resin components as a function of the molecular layers at different locations in the composite for various cure cycles. The model was correlated to experimental data on the interphase concentration profiles or moduli to determine the parameters of the model [12, 21]. Good agreement between the model and experimental data was observed in Refs. 12 and 21, which demonstrated the ability of the model to reflect the physical trends. With this preliminary validation of the model as basis, parametric studies are conducted in this section to illustrate the effects of different interphase formation and cure cycle parameters on the interphase and composite properties. A nondimensional form of the governing thermochemical equation (*Eq. 1*) and the associated boundary and initial conditions is obtained by introducing the dimensionless temperature, location, and time as: $\theta = (T - T_0)/T_0$, $x' = x/L$, $t' = k_{d,E}\exp(-E_{d,E}/RT_0)t$, where T_0 is a reference temperature; while the dimensionless form of the reaction rate equation, *Eq. 10,* and its initial conditions is derived by introducing the dimensionless time t' and dividing all the number of molecules (e.g., $N_{E,i}$, $N_{A,i}$) by the initial number of epoxy molecules in the layer next to the middle plane $N_{E,0}$ (e.g., $N'_{E,i} = N_{E,i}/N_{E,0}$).

The principal dimensionless groups that govern the interphase concentration evolution at various locations in a composite are identified as follows: 1) the adiabatic reaction temperature $\theta_{ad} = \Delta H_r C_{E0}(1 - v_f)/\rho c_p T_0$; 2) dimensionless epoxy adsorption energy, $E'_{a,E} = E_{a,E}/RT_0$; 3) dimensionless epoxy desorption energy, $E'_{d,E} = E_{d,E}/RT_0$; 4) epoxy adsorption ratio $\alpha_E = k_{a,E}e^{-(E_{a,E}-E_{d,E})/RT_0}/k_{d,E}$; 5) mutual diffusion ratio $\phi_{EA} = D_{EA}(T_0, \epsilon_0)e^{E_{d,E}/RT_0}/\Delta L^2 k_{d,E}$; 6) dimensionless amine adsorption energy, $E'_{a,A} = E_{a,A}/RT_0$; 7) dimensionless amine desorption energy, $E'_{d,A} = E_{d,A}/RT_0$; 8) amine desorption ratio $\beta_E = k_{d,A}e^{-(E_{d,A}-E_{d,E})/RT_0}/k_{d,E}$; 9) amine adsorption ratio $\alpha_A = k_{a,A}e^{-(E_{a,A}-E_{d,E})/RT_0}/k_{d,E}$; and 10) desorption Damköhler number $\gamma = k_r e^{E_{d,E}/RT_0}/k_{d,E}$. In this study, the number of molecular layers in the model domain is kept fixed at $N_L = 200$, the reference temperature is kept at $T_0 = 80°C$, the half thickness of the laminate $L = 0.00635$ m, the fiber volume fraction $v_f = 0.5$, the tooling thickness $L_T = 0.00318$ m, the number of sizing layers $N_S = 5$, $N'_{E,0} = N'_{A,0} = 1$, $N'_0 = 2$ ($N'_0 = N_0/N_{E,0}$, where N_0 is the number of adsorption sites at the fiber surface), the adsorption and desorption activation energies are $E'_{a,E} = E'_{a,A}$

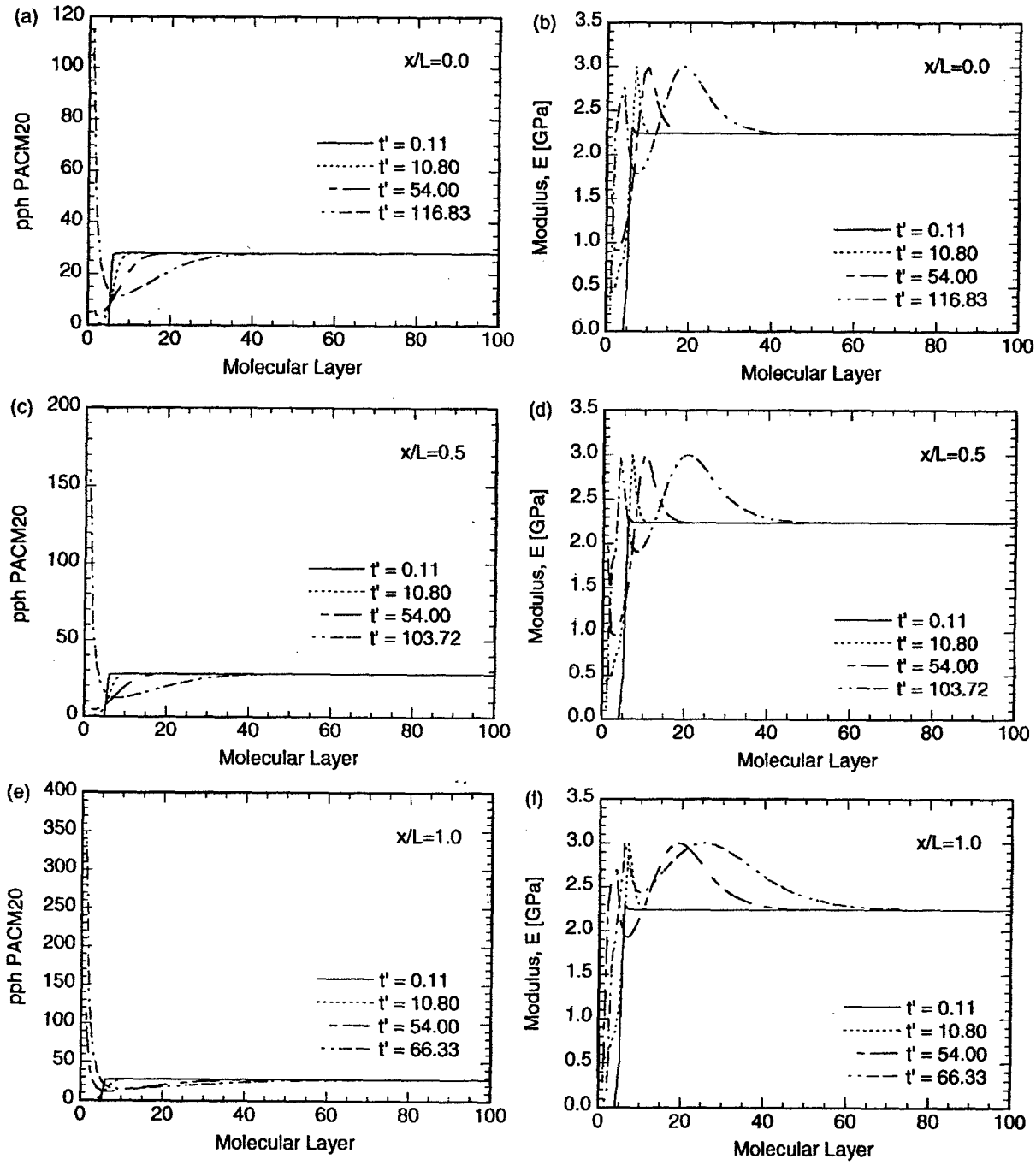

FIG. 5. Interphase concentration and modulus profiles predicted from the multiscale thermochemical model at various locations in the composite: (a) concentration profiles at $x/L = 0.0$; (b) modulus profiles at $x/L = 0.0$; (c) concentration profiles at $x/L = 0.5$; (d) modulus profiles at $x/L = 0.5$; (e) concentration profiles at $x/L = 1.0$; and (f) modulus profiles at $x/L = 1.0$. The results correspond to the parameter combination of: $\alpha_E = 0.01$, $\alpha_A = 1.0$, $\beta_A = 0.1$, $\phi_{EA} = 0.1$, $\theta_{ad} = 0.072$, $\gamma = 0.0044$, $\theta_f = 0.25$, and $t'_r = 80$.

$= 3.39$, $E'_{d,E} = E'_{d,A} = 6.78$, and the physical size of the molecular layer $\Delta L = 1$ nm. Furthermore, the cure cycles begin with a linear ramp from $\theta_i = -0.33$ to θ_f within a ramp time t'_r, followed by a hold stage with a constant temperature θ_f. The effects of the processing parameters on the interphase composition and properties (i.e., interphase thickness δ_i and interphase modulus E_i) and the composite property (transverse modulus E_2) are described in the following subsections.

Interphase Concentration and Properties

Figure 5a, b presents the amine concentration distributions in pph and modulus within a microscopic representa-

tive volume element (shown in Fig. 2) at different nondimensional times during the cure process. The location of the RVE is at the center line of the composite, i.e., $x/L = 0.0$. The results correspond to the parameter combination of: $\alpha_E = 0.01$, $\alpha_A = 1.0$, $\beta_A = 0.1$, $\phi_{EA} = 6.0$, $\theta_{ad} = 0.072$, $\gamma = 0.01$, $\theta_f = 0.25$, and $t'_r = 80$. The amine desorption ratio, α_A, is chosen to be larger than the epoxy adsorption ratio, α_E, indicating a preferential adsorption of the amine molecules onto the fiber surface.

In Fig. 5a, the PACM20 concentration profile at an early time $t' = 0.11$ is close to a step function, which represents an epoxy sizing layer on the fiber surface. The amine concentration is zero within the sizing layer ($N_S = 5$), and equals 28 in the bulk matrix at the far region. Due to the diffusion and adsorption processes, amine molecules migrate in the direction toward the surface. Consequently, the pph concentration increases with time in the original sizing region. At $t' = 54.00$, the strong adsorption of amine molecules from the vicinity of the fiber onto the fiber surface leads to a minimum in the amine concentration profile in the neighborhood of the fiber surface. Since the parameter combination in this case pertains to a preferential adsorption of amine molecules, the surface concentration pph = 116.58 is well above the bulk value of 28 at the gelation time $t' = 116.83$, and a relatively deep minimum is also observed at the seventh molecular layer. Recalling that the mass transfer through the adsorption, desorption, and diffusion processes is dramatically slowed when the reacting resin system reaches the gelation point, the final concentration profiles can be approximated by the profiles at the gelation point.

Prediction of the composite properties such as transverse moduli needs the information of interphase modulus; therefore, the concentration profiles in Fig. 5a are mapped to modulus profiles in Fig. 5b by using *Eq. 11*. Similar to the corresponding concentration profile, the modulus profile at $t' = 0.11$ in Fig. 5b exhibits a near step variation—the modulus is zero for pure epoxy within the sizing layer, and equals 2.24 GPa for the bulk matrix. *Equation 11* suggests that the matrix modulus has a peak value of 3.00 GPa at pph = 20. At $t' = 10.80$, the amine concentration reaches pph = 20 at the (7)th molecular layer, which is the location of the corresponding maximum in Fig. 5b. A peak for the modulus profile at $t' = 54.00$ is also observed at the (10)th molecular layer. It is interesting to note that the modulus profile at the gelation time $t' = 116.83$ has two peaks, since the corresponding concentration profile reaches pph = 20 twice at the (4)th and (19)th molecular layer, respectively. The final twin-peak modulus profile predicted by the current model deviates from the monotonic interphase modulus profiles assumed in the literature (e.g., Ref. 22], and may have significant influence on the overall composite properties.

Figure 5c–f shows the concentration and modulus evolution at two other locations in the composite, i.e., the middle location between the laminate center line and surface, $x/L = 0.5$, and the laminate outer surface $x/L = 1.0$; all the parameters retain the values as in Fig. 5a. For the parameter combination considered, resin materials at a larger x-value experience higher temperatures. Consequently, the gelation time decreases from $t' = 116.83$ at the center line to $t' = 103.72$ at the middle point (Fig. 5c, d). The concentration evolution in Fig. 5c follows a similar trend in Fig. 5a, however, significant changes are observed for the final pph profiles. Due to enhanced preferential adsorption of amine at higher temperatures, the final pph value at the fiber surface increases to 163.15 in Fig. 5c from a value of 116.58 in Fig. 5a. It is also noted that the nonzero amine concentration gradient zone in Fig. 5c is extended, leading to a thicker interphase region than that in Fig. 5a. Similarly, the modulus profiles shown in Fig. 5d are close to those in Fig. 5b except at the gelation times. The final modulus at the fiber surface decreases to 0.072 GPa in Fig. 5d from 0.192 GPa in Fig. 5b, and larger final interphase thickness is seen again in Fig. 5d.

At the outer surface $x/L = 1.0$, the effects of higher temperatures are significantly pronounced. Figure 5e shows that the preferential adsorption of amine leads to a surface pph value of 130.00 at $t' = 54.00$, and the final surface concentration (pph = 354.55) is more than three times the value at the center line. The concentration curve at $t' = 54.00$ also shows a minimum, which is not seen for the corresponding profiles in Fig. 5a and c. Consequently, two modulus profiles in Fig. 5f show twin peaks, i.e., $t' = 54.00$ and $t' = 66.33$. The final modulus at the fiber surface drops to 0.010 GPa, and a very large interphase thickness is observed in Fig. 5f. Figure 5a–f demonstrates that both the final concentration and modulus profiles are dramatically different at various locations of the composite. Particularly, when the location approaches the outer surface, thicker interphase with higher amine concentration and lower modulus is obtained. Different temperature histories experienced by the resin materials at different locations is responsible for the concentration and modulus variations, which suggests that desirable composite properties may be achieved via an optimization of the cure cycles.

The results in Fig. 5 pertain to one combination of the interphase formation and cure cycle parameters. A systematic parametric study is presented in the following discussion to illustrate the influence of the different parameters on the interphase and composite properties. Figure 6a shows the final (or gelation) concentration profiles at the center line location for three values of the epoxy adsorption ratio, α_E; all other parameters retain their values as in Fig. 5. The modulus profiles and the concentration profiles before the gelation time are omitted for the purpose of brevity since the interphase and overall composite properties are readily derived from the final concentration profiles. For the two cases of small epoxy adsorption ratios (i.e., $\alpha_E = 0.001$ and 0.1), the fiber surface exhibits preferential adsorption of the amine molecules, and relatively large pph values on the fiber surface are observed. The strong adsorption of amine also results in the minima near the fiber surface, which was

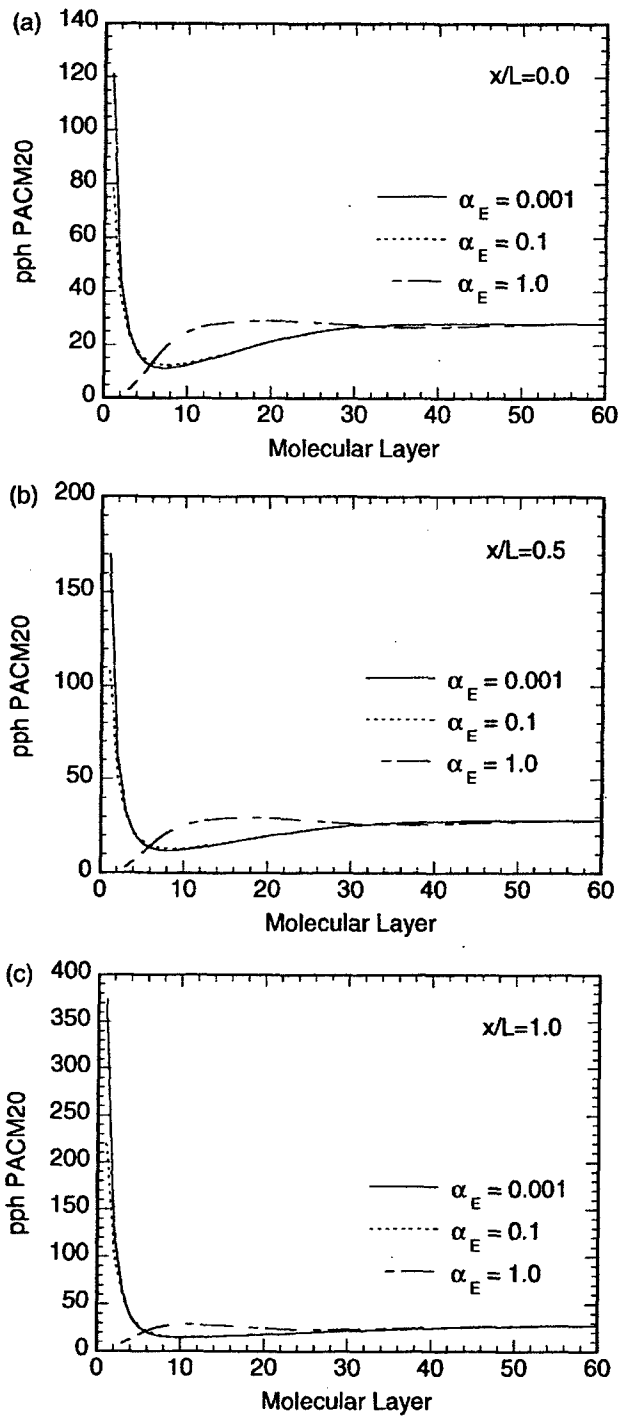

FIG. 6. The final interphase concentration profiles for three values of α_E at the locations (a) $x/L = 0.0$, (b) $x/L = 0.5$, and (c) $x/L = 1.0$. The default values of the parameters are: $\alpha_A = 1.0$, $\beta_A = 0.1$, $\phi_{EA} = 0.1$, $\theta_{ad} = 0.072$, $\gamma = 0.0044$, $\theta_f = 0.25$, and $t'_r = 80$.

previously observed in Fig. 5a. As α_E increases from 0.001 to 0.1, the surface pph value decreases from 121.26 to 78.29 since more epoxy molecules are adsorbed on the fiber surface. When $\alpha_E = 1.0$, the majority of the molecules adsorbed on the surface are epoxy from the sizing layer, forming an epoxy-rich interphase with low pph concentration. The interphase thickness increases with the increase in α_E, since more epoxy molecules are adsorbed into the interphase region.

Figure 6b and c presents the effects of the epoxy adsorption ratio, α_E, on the final concentration profiles at two other locations in the composite. The trends in Fig. 6b and c follow those in Fig. 6a, i.e., with increasing α_E, the pph concentration at the surface decreases while the interphase thickness increases. The notable distinction is once again the significant increase in surface pph value for the outer locations due to higher temperature effects. In general, the results in Fig. 6 suggest that the interphase material transitions from being amine rich to being epoxy rich as α_E increases, and the final gelation profiles may show large variations from one location to another in the composite domain.

A significant objective—and contribution—of current work is the establishment of the direct linkage for the first time between cure cycles and the interphase/composite properties. In Fig. 7, the influence of the cure cycle ramp time, t'_r, on the final composition profile is demonstrated; all other parameters retain the values in Fig. 5. The decrease in cure cycle ramp time has the same effect as an increase of the cure temperature. For the parameter combinations considered in this study, increased temperature leads to enhanced preferential adsorption of the amine species. Since the parameter combination indicates that the surface has preferential adsorption of amine, each curve in Fig. 7a has a minimum near the fiber surface, as previously seen in Fig. 5a. When t'_r decreases from 160 to 20, the pph value on the fiber surface increases from 92.75 to 170.00, and the interphase thickness also increases from 34 nm to 44 nm due to more active adsorption processes (Fig. 7a).

Interphases richer in amine are developed as x/L increases. When t'_r decreases from 160 to 20, the pph value at the surface increases from 110.21 to 249.23 at the middle point $x/L = 0.5$ (Fig. 7b), and from 191.89 to 514.84 at the outer surface $x/L = 1.0$ (Fig. 7c). The uniformity of the composite properties may be represented by the maximum difference of the surface pph values within the composite domain, which for the cases studied in this paper is the difference between the pph at the outer surface and that at the center line location. It is noted that the maximum difference of the surface pph value within the composite increases from 99.14 to 344.84 as t'_r decreases from 160 to 20. The numerical results in Fig. 7 clearly show that shorter cure ramp time (equivalent to higher cure temperature) results in amine rich interphases, which may correspond to low interphase modulus. Furthermore, the maximum temperature difference in the composite also increases at higher cure temperatures, and the property gradient in the composite is magnified. Since composites with high modulus and uniform properties are typically desirable, the above results indicate that a lower limit should be imposed for the cure ramp time. However, the increase in cure ramp time causes an increase in processing time and cost. Consequently, an optimal cure ramp may be determined to simultaneously satisfy the material property requirements and processing cost constraints.

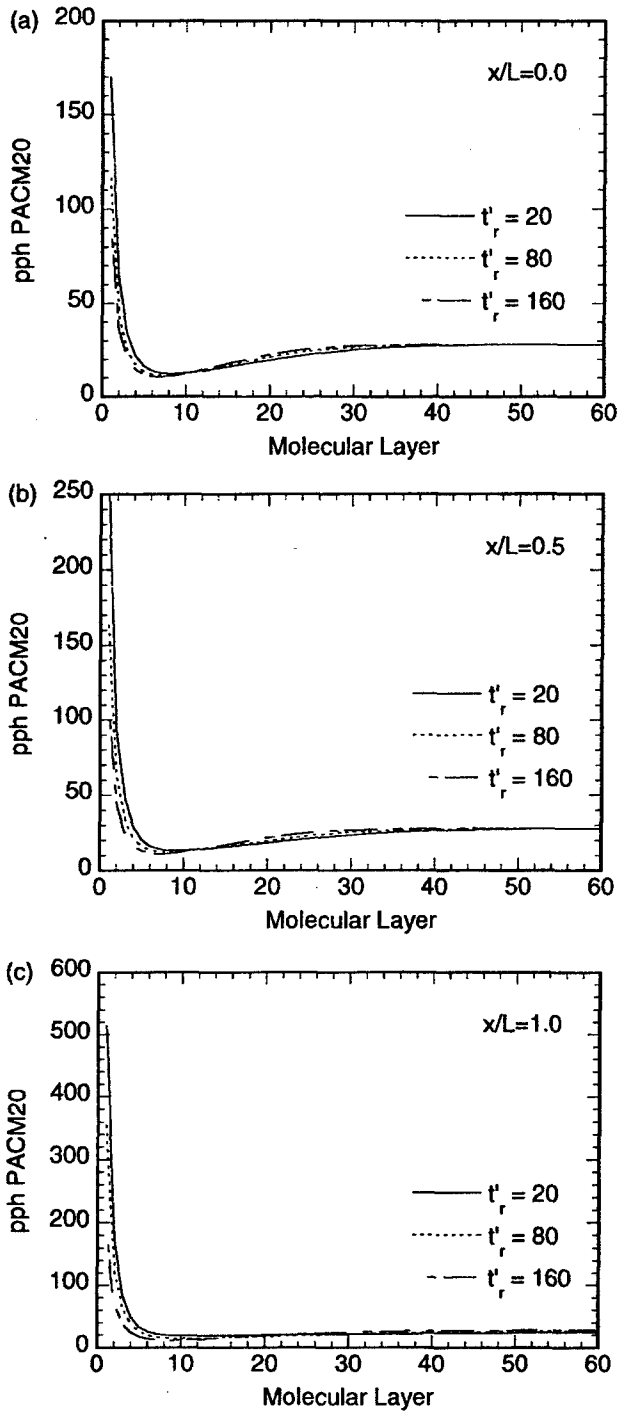

FIG. 7. The final interphase concentration profiles for three values of t'_r at the locations (a) $x/L = 0.0$, (b) $x/L = 0.5$, and (c) $x/L = 1.0$. The default values of the parameters are: $\alpha_E = 0.01$, $\alpha_A = 1.0$, $\beta_A = 0.1$, $\phi_{EA} = 0.1$, $\theta_{ad} = 0.072$, $\gamma = 0.0044$, and $\theta_f = 0.25$.

The effects of the interphase formation parameter, α_E, and the cure cycle parameter, t'_r, on the final interphase concentration profiles are seen in Figs. 6 and 7, respectively. In Fig. 8, the influence of several principal interphase formation and cure cycle parameters on the interphase properties are illustrated. Note that the final interphase concentration profiles used in Figs. 6 and 7 are replaced in Fig. 8 by the two parameters, interphase thickness, δ_i, and interphase modulus, E_i, which are a concise representation of the corresponding concentration profiles. Figure 8a presents the interphase thickness as a function of epoxy adsorption ratio, α_E, at three locations in the composite. For the locations $x/L = 0.0$ and 0.5, δ_i increases monotonically with the increase in α_E since more epoxy molecules are adsorbed into the interphase region. At the outer surface $x/L = 1.0$, a relatively large value of δ_i is observed as $\alpha_E = 0.001$, which is attributed to the pronounced adsorption of amine molecules (see Fig. 6c), and the additional adsorption of epoxy molecules does not have significant influence on δ_i as α_E increases. For a fixed epoxy adsorption ratio, δ_i increases with x/L due to enhanced adsorption processes at the higher temperatures at the outer locations.

Figure 8b shows the interphase modulus E_i as a function of α_E at different values of x/L. The average pph value decreases monotonically with increasing α_E, which indicates that an E_i versus α_E curve should follow a nonmonotonic trend similar to that of the fitting curve in Fig. 4. For the location $x/L = 0.0$, the average pph in the interphase region decreases from 60 to 28 when $\alpha_E =$ increases from 0.001 to 0.1, which corresponds to the initial increase of interphase modulus from $E_i = 1.77$ GPa to 2.32 GPa. When α_E increases to 1.0 and 2.0, the average pph value decreases to 12.8 and 12.0, and E_i is seen to decrease to 2.02 GPa and 1.86 GPa, respectively. Note that the twin-peak shape in Fig. 4 is not exactly duplicated since relatively small number of α_E values are investigated; however, the range of α_E is sufficiently large to cover a comprehensive range of interphase modulus values. At the other two locations, $x/L = 0.5$ and 1.0, it is also seen that E_i reaches maxima as α_E increases. As $\alpha_E \to \infty$, all the curves in Fig. 8b are expected to approach zero modulus corresponding to a pure epoxy interphase. It is observed that the curve at $x/L = 1.0$ intersects with the other two curves, which is again caused by the twin-peak nature of the experimental modulus data. The interphase modulus at the outer surface may be either larger (e.g., as $\alpha = 1.0$) or smaller (e.g., as $\alpha = 0.1$) than that at the center line location.

The influences of reaction Damköhler number, γ, and cure cycle hold temperature, θ_f, on the interphase thickness, δ_i, and interphase modulus, E_i, are illustrated in Fig. 8c–f. The reaction Damköhler number determines the speed of the cure process. As γ increases, less time is available for the interphase development, and the thickness decreases monotonically at each location of the composite (Fig. 8c). Significant drops of δ_i are observed as γ increases from 0.0011 to 0.011 (e.g., from 170 nm to 27 nm at the outer surface). When $\gamma = 0.0011$, the interphase regions consist of nearly pure amine due to excessive adsorption of the amine species, and the E_i is close to zero at all the locations (Fig. 8d). The interphase modulus increases with increasing γ due to reduced amine adsorption. Note that the curve at $x/L = 1.0$ crosses the other two curves, which may be explained by similar discussions in Fig. 8b.

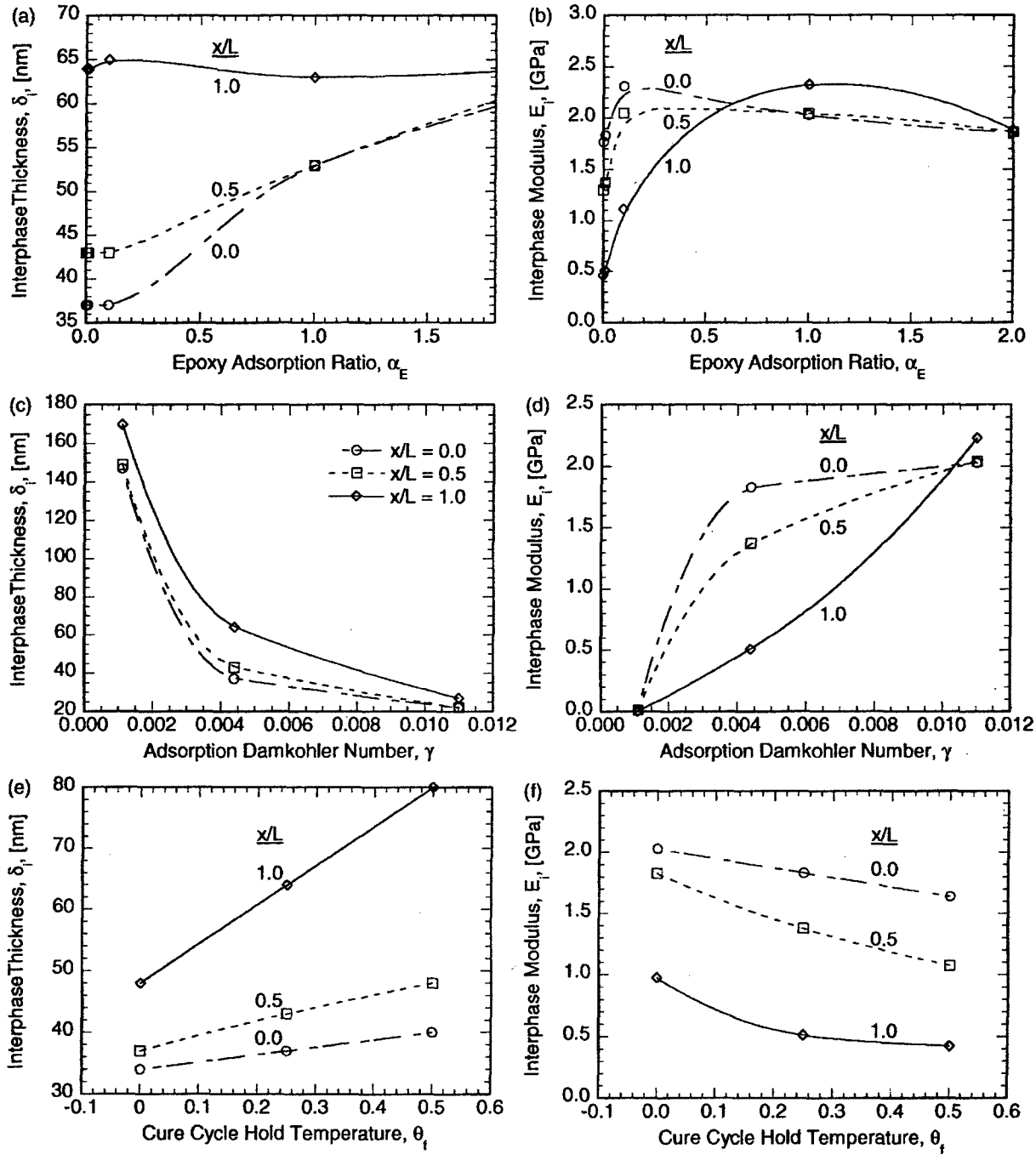

FIG. 8. Interphase thickness and modulus as functions of the interphase formation parameters and the location in the composite: (a) δ_i and (b) E_i as a function of α_E; (c) δ_i and (d) E_i as a function of γ; and (e) δ_i and (f) E_i as a function of θ_f. The default values of the parameters are: $\alpha_A = 1.0$, $\beta_A = 0.1$, $\phi_{EA} = 0.1$, $\theta_{ad} = 0.072$, $t'_r = 80$; (a, b) $\gamma = 0.0044$, $\theta_f = 0.25$, (c, d) $\alpha_E = 0.01$, $\theta_f = 0.25$, and (e, f) $\gamma = 0.0044$, $\alpha_E = 0.01$.

The effects of the cure cycle parameter (i.e., θ_f) on the interphase thickness and modulus are presented in Fig. 8e and f, where all the interphase formation parameters retain the values as in Fig. 5. Note that Fig. 8e and f represents the first time that the cure cycle parameters are directly related to the interphase properties in a predictive manner. Figure 8e shows the interphase thickness as a function of the cure cycle hold temperature at three locations of the composite. The interphase thickness, δ_i, increases monotonically with increasing θ_f for a fixed x/L and with increasing x/L for a fixed θ_f, owing to enhanced adsorption of amine molecules at higher temperatures. A large increase in δ_i from 48 nm to 80 nm is observed at the outer surface location as θ_f increases from 0 to 0.5, while the increases in δ_i are moderate at the other two locations. The interphase modulus decreases with θ_f at a fixed location due to more adsorption of

amine molecules into amine rich interphase regions (Fig. 8f). For the parameter combination, the maximum interphase modulus at the outer surface location equals to 0.98 GPa as $\theta_f = 0$, which is only 44% of the bulk matrix modulus. Thus, a lower cure cycle hold temperature ($\theta_f < 0$) is needed to improve the modulus at the outer surface location. A large difference of modulus is observed at different locations due to the cure temperature gradient in the composite. It is, therefore, desirable to adopt uniform temperature through the thickness of the composite laminate during the cure process, which may be achieved via cure cycle optimization [18] or via an embedded resistive heating configuration, where the inner locations are subjected to a heat source that allows them to cure in synchronization with the outer locations [17, 19].

Composite Transverse Modulus

The results presented so far pertain to the interphase properties, i.e., the effective interphase modulus, E_i, and the interphase thickness, δ_i. To complete the processing-interphase-property relationship, the interphase properties are used as inputs in this section to a finite element analysis as reported in a previous publication to predict the effective composite properties [16]. The heterogeneous composite is modeled by a representative volume element (RVE) with a staggered array configuration of fibers. The array angle, fiber volume fraction, and fiber modulus are chosen to be 45°, 50%, and 223 GPa, respectively. Relevant numerical results are presented for the first time where the composite transverse modulus, E_2, is directly linked to the interphase formation and cure cycle parameters without assumed structures or properties of the interphase.

Figure 9a shows the composite transverse Youngs modulus, E_2, as a function of epoxy adsorption ratio, α_E, at different locations in the composite. The results correspond to the same parameter combination as in Fig. 8b. Evidently, both the interphase thickness and interphase modulus are important factors influencing the composite transverse modulus, E_2, of a fiber/interphase/matrix system. Current calculations reveal that extremely thin interphases, with thickness between 30 nm and 170 nm, are present in the composite. The composite transverse modulus does not show distinctive changes for the thickness variation in this small range, and E_2 is only strongly influenced by the interphase modulus E_i. Consequently, Fig. 9a has the same pattern as Fig. 8b, and the similarity of the results between E_2 and E_i is observed throughout the parametric studies. For the case $x/L = 0.0$, as α_E increases from 0.001 to 2, E_2 increases slightly from 5.52 GPa to 5.62 GPa, and then drops down to 5.54 GPa (Fig. 9a), which corresponds the variation of E_i from 1.77 GPa to 2.32 GPa and to 1.86 GPa. It is noted that a 24% decrease of E_i from the bulk matrix modulus (2.32 GPa) causes only a 1.8% decrease of the composite modulus, which is attributed to the small fraction of the interphase in the matrix. Significant decrease of E_2 is observed only at the outer surface location when $\alpha_E < 0.1$,

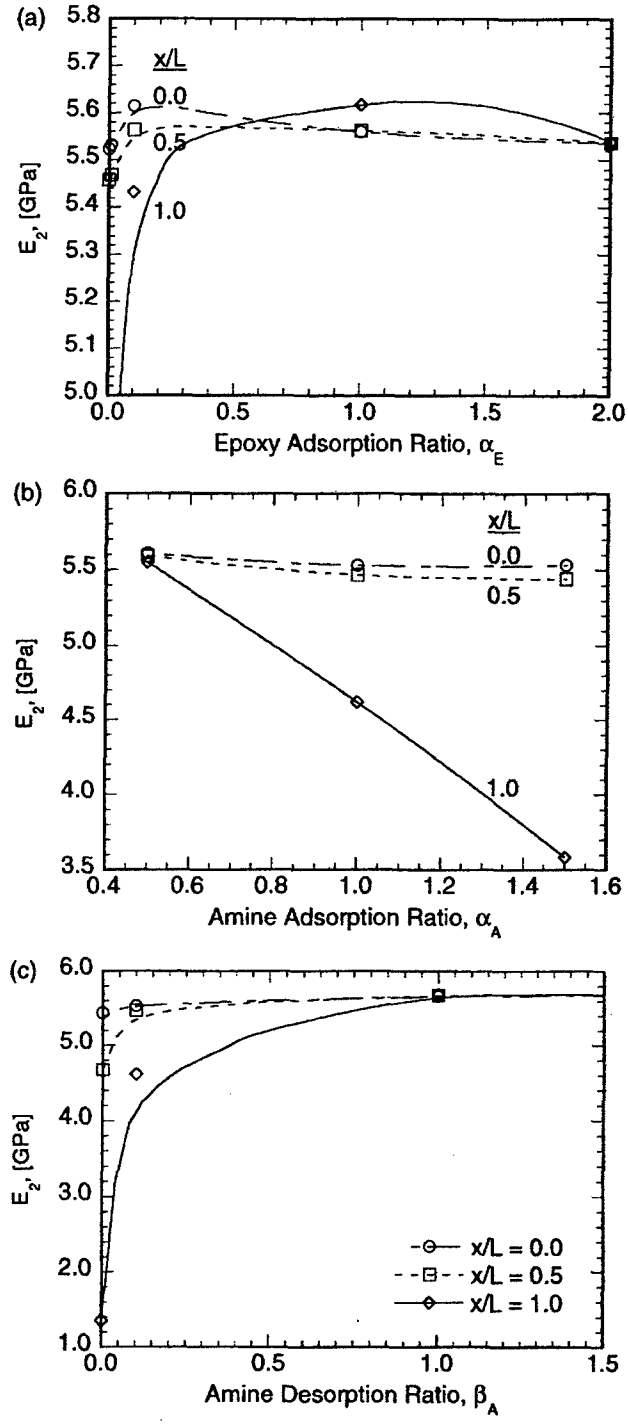

FIG. 9. Composite transverse modulus as a function of (a) α_E, (b) α_A, and (c) β_A. The default values of the parameters are: $\phi_{EA} = 0.1$, $\theta_{ad} = 0.072$, $\gamma = 0.0044$, $\theta_f = 0.25$, $t'_r = 80$; (a) $\alpha_A = 1.0$, $\beta_A = 0.1$, (b) $\beta_A = 0.1$, $\alpha_E = 0.01$, and (c) $\alpha_A = 1.0$, $\alpha_E = 0.01$.

which correspond to amine rich interphases with $E_i < 0.52$ GPa.

The effects of amine adsorption ratio, α_A, and amine desorption ratio, β_A, on the composite transverse modulus are illustrated in Fig. 9b and c, respectively. At the center line and at $x/L = 0.5$, E_2 has a limited variation between

5.60 to 5.44 GPa in Fig. 9b, which corresponds to the change of E_i between 2.29 and 1.19 GPa. At the outer surface, $x/L = 1.0$, a large decrease in E_2 is seen with increasing α_A, owing to enhanced adsorption of amine and the resulting amine rich interphase. In Fig. 9c, the composite modulus increases with increasing β_A for a fixed x/L, and with decreasing x/L for a fixed β_A, due to increased desorption of amine species from an amine rich interphase. When $\beta_A > 1.0$, the composite modulus has a uniform distribution within the composite domain.

Figure 10 follows the presentation format of Fig. 9 to show the effects of the mutual diffusion ratio ϕ_{EA} (Fig. 10a), the adsorption Damköhler number γ (Fig. 10b), and the adiabatic reaction temperature θ_{ad} (Fig. 10c) on the composite transverse modulus. The composite transverse modulus, E_2, decreases with increasing ϕ_{EA} for a fixed x/L, and with increasing x/L for a fixed ϕ_{EA}, owing to the enhanced adsorption of amine into amine rich interphases (Fig. 10a). Extremely low E_2 (<1.0 GPa) is obtained throughout the composite domain when $\phi_{EA} = 1.0$.

The composite transverse modulus increases monotonically with increasing γ at each location x/L since fewer amine molecules are adsorbed into the interphase region (Fig. 10b). The distribution of E_2 in the composite domain is quite uniform for both fast $\gamma = 0.011$ and slow $\gamma = 0.0011$ reactions. However, a composite with very low E_2 (<0.6 GPa) is obtained when $\gamma = 0.0011$, while a composite with high modulus, $E_2 = 5.6$ GPa, is achieved for $\gamma = 0.011$. Since different values of γ correspond to different material systems, the results in Fig. 10b demonstrate the capability of tailoring the interphase and composite properties via appropriate material selection. For the locations $x/L = 0.0$ and 0.5, E_2 decreases monotonically with increasing θ_{ad} due to enhanced adsorption of amine species (Fig. 10c). At the outer surface location, E_2 remains constant with respect to θ_{ad}, owing to negligible variation in the interphase modulus E_i.

The effects of the cure cycle parameters, t'_r and θ_f, on the effective composite modulus are presented in Fig. 11a and b, respectively. The results provide the direct linkage between the cure cycle and composite properties for the first time and demonstrate the feasibility of tailoring the composite property via cure cycle selection. In Fig. 11a, E_2 increases monotonically with increasing t'_r at all the locations, owing to increasing interphase modulus. For the case $t'_r = 20$, the composite transverse modulus ($E_2 = 4.4$ GPa) is relatively small at the outer surface location; however, when t'_r is increased to 160, a composite with uniform transverse modulus (about 5.5 GPa) across the thickness is obtained. Figure 11b shows that the composite transverse modulus decreases monotonically with increasing θ_f, which is in agreement with the trend in Fig. 8f. For the two locations, $x/L = 0.0$ and 0.5, E_2 has limited variation from 5.56 GPa to 5.42 GPa, while a significant drop to 4.44 GPa is observed at the outer surface, $x/L = 1.0$.

An important composite property, transverse Youngs modulus E_2, was presented in this section as a function of

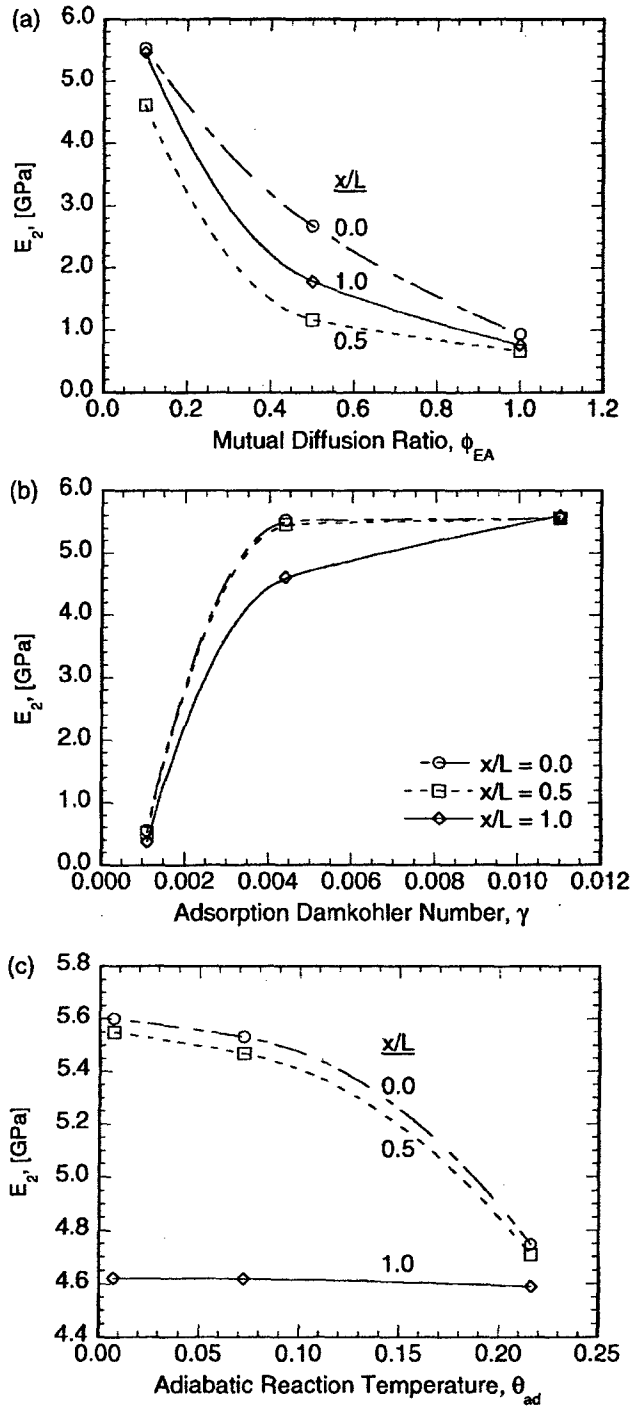

FIG. 10. Composite transverse modulus as a function of (a) ϕ_{EA}, (b) γ, and (c) θ_{ad}. The default values of the parameters are: $\alpha_E = 0.01$, $\alpha_A = 1.0$, $\beta_A = 0.1$, $\theta_f = 0.25$, $t'_r = 80$; (a) $\theta_{ad} = 0.072$, $\gamma = 0.0044$, (b) $\phi_{EA} = 0.1$, $\theta_{ad} = 0.072$, and (c) $\phi_{EA} = 0.1$, $\gamma = 0.0044$.

cure cycle and interphase formation parameters. Similarly, other composite properties such as transverse shear modulus and stress concentration factors may be obtained for a more comprehensive analysis. The approach presented in this article establishes the processing-interphase-property relationship without any assumed interphase properties. The study focused on the effect of the cure temperature cycle on

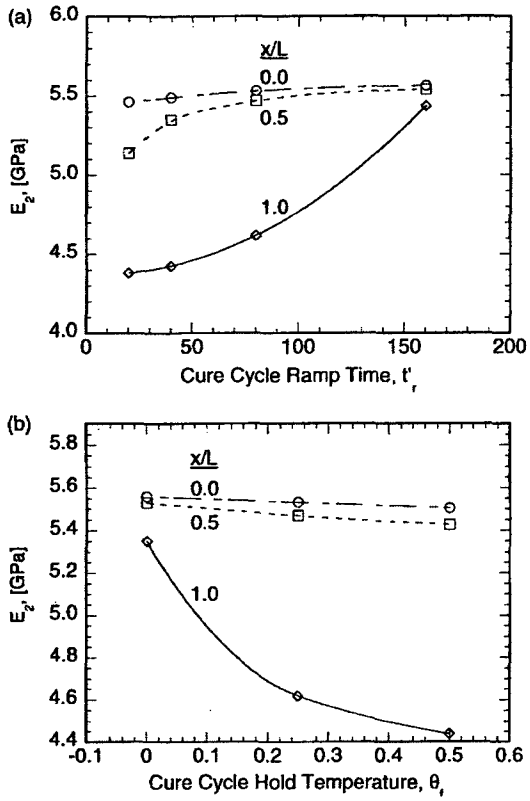

FIG. 11. Composite transverse modulus as a function of (a) t'_r, and (b) θ_f. The default values of the parameters are: $\alpha_E = 0.01$, $\alpha_A = 1.0$, $\beta_A = 0.1$, $\phi_{EA} = 0.1$, $\theta_{ad} = 0.072$, $\gamma = 0.0044$; (a) $\theta_f = 0.25$, and (b) $t'_r = 80$.

the interphase formation. Additionally, the cure pressure cycle may also influence the interphase evolution through its effect on the kinetic parameters as well as by changing the fiber volume fraction during consolidation. These effects will be considered in a future study.

CONCLUSIONS

A microscale kinetics model of interphase formation is coupled with the macroscale energy equation to predict the interphase formation at various locations in fiber reinforced epoxy/amine composites. The cure cycle parameters, i.e., θ_f and t'_r, and the interphase formation parameters are linked for the first time to the interphase and composite properties. Parametric studies on DGEBA/PACM20 thermosetting composites reveal that the interphase thickness and modulus, δ_i and E_i, and the overall composite modulus, E_2, exhibit spatial variation across the thickness of the composites, and are strongly dependent on the values of the interphase formation and the cure cycle parameters. For the parameter combinations in this study, the composite modulus, E_2, decreases with increasing cure cycle temperature or decreasing cure cycle ramp time, owing to softer interphases associated with resulting higher PACM20 concentration in these cases. Nonmonotonic trends of the interphase and composite properties are observed with respect to the interphase formation parameters. Due to the twin-peak characteristic of the interphase concentration-modulus mapping, the change of E_i or E_2 with respect to interphase formation parameters may show maximum (e.g., in Fig. 8). The study provides for the linking of the processing parameters directly to the composite properties, and in turn, for designing the processing parameters to obtain tailored interphase and composite properties.

ACKNOWLEDGMENTS

The work reported in this paper was carried out as part of the MEANS program funded by the Air Force Office of Scientific Research (Grant No. F496200110521). We are grateful for their support.

APPENDIX

Rate Equations of the Microscale Kinetics Model

The mass balance for the species in the "adsorbed" state in any (i)th molecular layer:

$$\underbrace{\frac{dN_{E,i}}{dt}}_{storage} = \underbrace{R_{a,E}(i-1,i) + R_{a,E}(i,i) + R_{a,E}(i+1,i)}_{adsorption,\ \Re_{a,E}(i)} - \underbrace{R_{d,E}(i-1,i) - R_{d,E}(i,i) - R_{d,E}(i+1,i)}_{desorption,\ \Re_{d,E}(i)} - \underbrace{\Re_{r,E}(i)}_{depletion\ (reaction)}$$

$$\underbrace{\frac{dN_{A,i}}{dt}}_{storage} = \underbrace{R_{a,A}(i-1,i) + R_{a,A}(i,i) + R_{a,A}(i+1,i)}_{adsorption,\ \Re_{a,A}(i)} - \underbrace{R_{d,A}(i-1,i) - R_{d,A}(i,i) - R_{d,A}(i+1,i)}_{desorption,\ \Re_{d,A}(i)} - \underbrace{\Re_{r,A}(i)}_{depletion\ (reaction)}$$

$$\frac{dN_{P,i}}{dt} = k_r N_{E,i}.$$

The mass balance for the species in the "bulk" state in any (i)th molecular layer:

$$\frac{dN_{E\infty,i}}{dt} = \frac{D_{EA}}{\Delta L^2}\left(N_{E\infty,i+1}\frac{N_0 - N(i)}{N_0} - N_{E\infty,i}\frac{N_0 - N(i+1)}{N_0}\right) + \frac{D_{EA}}{\Delta L^2}\left(N_{E\infty,i-1}\frac{N_0 - N(i)}{N_0} - N_{E\infty,i}\frac{N_0 - N(i-1)}{N_0}\right) + R_{d,E}(i,\ i$$

$$- 1) + R_{d,E}(i, i) + R_{d,E}(i, i+1) - R_{a,E}(i, i-1) - R_{a,E}(i, i) - R_{a,E}(i, i+1) - n_1 k_r N_{E\infty,i} + \sum_{j=i-1,i+1} \left[\frac{N_{E\infty,j}}{N_{\infty,j}} (R_{d,E}(j, i) + R_{d,A}(j, i) + R_{a,E}(i, j) + R_{a,A}(i, j)) \right] - \frac{N_{E\infty,i}}{N_{\infty,i}} \sum_{j=i-1,i+1} [R_{a,E}(j, i) + R_{a,A}(j, i) + R_{d,E}(i, j) + R_{d,A}(i, j)]$$

$$\frac{dN_{A\infty,i}}{dt} = \frac{D_{EA}}{\Delta L^2} \left(N_{A\infty,i+1} \frac{N_0 - N(i)}{N_0} - N_{A\infty,i} \frac{N_0 - N(i+1)}{N_0} \right) + \frac{D_{EA}}{\Delta L^2} \left(N_{A\infty,i-1} \frac{N_0 - N(i)}{N_0} - N_{A\infty,i} \frac{N_0 - N(i-1)}{N_0} \right) + R_{d,A}(i, i-1) + R_{d,A}(i, i) + R_{d,A}(i, i+1) - R_{a,A}(i, i-1) - R_{a,A}(i, i) - R_{a,A}(i, i+1) - n_2 k_r N_{E\infty,i} + \sum_{j=i-1,i+1} \left[\frac{N_{A\infty,j}}{N_{\infty,j}} (R_{d,E}(j, i) + R_{d,A}(j, i) + R_{a,E}(i, j) + R_{a,A}(i, j)) \right] - \frac{N_{A\infty,i}}{N_{\infty,i}} \sum_{j=i-1,i+1} [R_{a,E}(j, i) + R_{a,A}(j, i) + R_{d,E}(i, j) + R_{d,A}(i, j)]$$

$$\frac{dN_{P\infty,i}}{dt} = k_r N_{E\infty,i}.$$

REFERENCES

1. G.R. Palmese, "Technical Report Number 92-95," University of Delaware Center for Composite Materials (1992).
2. S. Subramanian, J.J. Lesko, K.L. Reifsnider, and W.W. Stinchcomb, *J.Compos. Mater.*, **30**, 309 (1996).
3. R.W. Rydin, P.C. Varelidis, C.D. Papaspyrides, and V.M. Karbhari, *J.Compos. Mater.*, **31**, 182 (1997).
4. L.T. Drzal, *Adv. Polym. Sci.*, **75**, 1 (1986).
5. A. Garton, W.T.K. Stevenson, and S. Wang, *British Polym. J.*, **19**, 459 (1987).
6. C. Sellitti, J.L. Koenig, and H. Ishida, *Mater. Sci. Eng.*, **A126**, 235 (1990).
7. M.S. Madhukar and L.T. Drzal, *J.Compos. Mater.*, **25**, 958 (1991).
8. H.C. Tsai, A.M. Arocho, and L.W. Gause, *Mater. Sci. Eng.*, **A126**, 295 (1990).
9. Y.J. Liu, N. Xu, and J.F. Luo, *J.Appl. Mechanics*, **67**, 41 (2000).
10. C.P. Tsui, C.Y. Tang, and T.C. Lee, *J. Mater. Processing Tech.*, **117**, 105 (2001).
11. J. Hrivnak, "Technical Report Number 92-105," University of Delaware Center for Composite Materials (1997).
12. F. Yang and R. Pitchumani, *J.Appl. Polym. Sci.*, **89**, 3220 (2003).
13. F. Yang, "Investigations on Interface and Interphase Development in Polymer-Matrix Composite Materials," Ph.D. Dissertation, University of Connecticut, Storrs, CT (2002).
14. F. Yang and R. Pitchumani, *Proc. 12th Int. Heat Transfer Conf.*, September, **3**, 153–158 (2002).
15. F. Yang and R. Pitchumani, "Paper Number 078," *Proc. (CD-ROM) of 16th Technical Conference of the American Society for Composites*, Blacksburg, VA, September (2001).
16. F. Yang and R. Pitchumani, *Compos. Sci. Tech.* **64**, 1437 (2004).
17. A. Mawardi and R. Pitchumani, *ASME J.Heat Transfer*, **125**, 126 (2003).
18. N. Rai and R. Pitchumani, *Polym. Compos.*, **18**, 566 (1997).
19. L. Zhu and R. Pitchumani, *Compos. Sci. Tech.*, **60**, 2699 (2000).
20. M.R. VanLandingham, R.F. Eduljee, and J.W. Gillespie, Jr., *J.Appl. Polym. Sci.*, **71**, 699 (1999).
21. F. Yang and R. Pitchumani, *Proc. SAMPE 2004*, Long Beach, CA, May 16–20 (2004).
22. N.K. Anifantis, *Compos. Sci. Tech.*, **60**, 1241 (2000).

Studies on Fiber/Matrix Interphase Development in Thermosetting-Matrix Composites

F. Yang and R. Pitchumani
Composites Processing Laboratory
Department of Mechanical Engineering
University of Connecticut
Storrs, Connecticut 06269-3139

Abstract

During thermosetting polymer composites processing, the presence of the reinforcing fibers significantly alters the cure characteristics via several microscale processes, forming a fiber/matrix interphase region with different chemical and physical properties from the bulk resin. The interphase composition is an important parameter that determines the microstructure and properties of the composite. The mechanisms contributing to the interphase development during processing include mass transport processes of adsorption, desorption, and diffusion near the fiber surface, which are accompanied by simultaneous cure reaction between the resin components. A model is developed in this paper to describe the coupled mass transfer and reaction processes leading to interphase formation, and to predict the evolution of the interphase concentration with time.

1. Introduction

Fabrication of thermosetting-matrix composites is based on a critical step of *cure*, which involves applying predefined temperature cycle to a fiber-resin mixture. The elevated temperatures initiate a crosslinking reaction, called the cure reaction, among the species in the matrix. The presence of fibers has been found to significantly influence the cure reaction, resulting in the formation of a third phase known as the interphase which possesses properties distinct from those of the bulk fiber and the matrix. The structure and properties of the interphase are the dominant factors governing the overall composite properties and performance (Palmese, 1992).

The studies in the literature on interphases have focused primarily on the experimental determination of the influence of interphase on the mechanical behavior of the composite materials (Subramanian *et al.*, 1996; Rydin *et al.*, 1997; Drzal, 1986; Madhukar and Drzal, 1991). Fiber surface modifications such as high temperature treatment and sizing, are commonly implemented to tailor the structure of the interphase regions and to investigate their effects on the mechanical and other properties of the composite materials. Due to complexities of the molecular level mechanisms that occur in the vicinity of the fibers, prediction of the interphase evolution as a function of processing parameters has been the subject of little attention. A handful of interphase mechanisms have been proposed by Drzal (1986). In this paper, focus is placed on the process of preferential adsorption, which is the principal mechanism of interphase formation for a given surface treatment and sizing layers, etc. A kinetics model is presented to describe the preferential adsorption, desorption, diffusion and reaction processes taking place simultaneously during the cure process. Interphase composition profiles are predicted for a combination of the reaction, adsorption, desorption, and diffusion rates.

2. Interphase Formation Model

Cure of thermosetting resin systems is characterized by the reaction between prepolymer (or monomer) molecules and a curing agent to form a crosslinked network that can not flow upon vitrification. The reinforcing fibers alter the cure characteristic by selective adsorption of resin components, which changes the concentration of the reacting species in the vicinity of the fiber surfaces. The goal of the present study is to predict the concentration profiles of the constituent species near the fiber surface by considering the processes that occur in the cure reaction. A graphite fiber/epoxy-amine thermosetting system is considered in the following discussion; however, the model development and results are applicable to a general two-component thermosetting system.

The geometry considered is the inter-fiber space in a composite having a typical staggered fiber arrangement [Figure 1(a)]. The domain in the model development is idealized as the region between two identical infinite

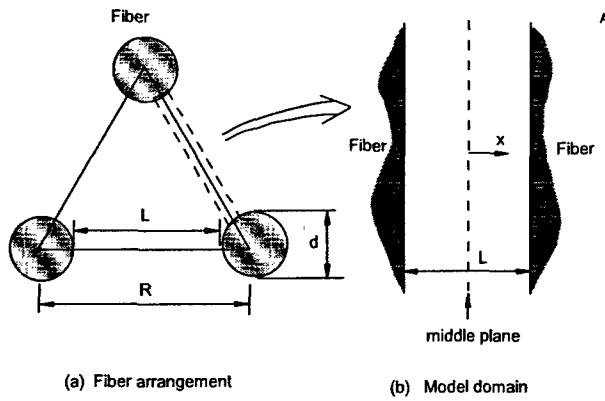

Figure 1: (*a*) A REPRESENTATIVE FIBER ARRANGEMENT IN THE COMPOSITE, AND (*b*) SCHEMATIC OF THE DOMAIN BETWEEN TWO FIBER SURFACES CONSIDERED IN THE MODELING.

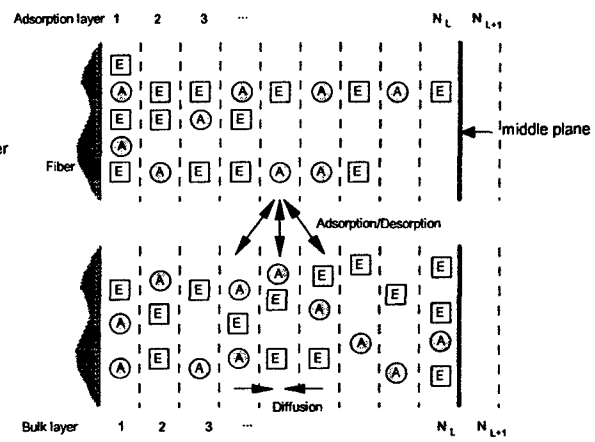

Figure 2: SCHEMATIC OF THE ADSORPTION, DESORPTION, AND DIFFUSION PROCESSES IN AN EPOXY-AMINE SYSTEM

planes representing the fiber surfaces [Figure 1(b)], which may be justified by the fact that the interphase thickness (typically a few hundred nanometers) is often small in comparison to the fiber diameter (typically around 6 microns). The fibers are considered to have an epoxy sizing layer applied to their surfaces. The sized fibers are exposed to an epoxy-amine resin matrix, and the epoxy and amine species begin reacting with each other at $t = 0^+$. Accompanying the chemical reaction, epoxy molecules diffuse away from the sizing layer adjacent to the wall. In a reverse movement, the amine molecules diffuse into the sizing layer due to the relatively higher amine concentration in the bulk resin region. In addition, the "force field" of the fiber surfaces causes the epoxy and amine molecules to migrate in the direction towards the surfaces, a process referred to as adsorption. Also the adsorbed molecules may be desorbed to the bulk resin in a desorption process. All the processes mentioned above take place simultaneously, resulting in a continuously evolving concentration profile that is "frozen" in space upon gelation of the thermosetting system.

The adsorption phenomenon at an equilibrium state near solid surfaces has been described by Brunauer, Emmett and Teller, referred to as BET theory (Hill, 1946; Ponec *et al.*, 1974). The BET model considers a balance between the adsorption and desorption rates at thermodynamic equilibrium without chemical reactions. According to this theory, the solid surface can adsorb molecules from the bulk into an ``adsorbed" state, which may be regarded as a distinct phase with respect to the bulk. The adsorbed molecules can also be desorbed into the bulk as a reverse process. These two processes balance each other at equilibrium, and the concentration of the molecules near the solid surface can be obtained. In the present study, the equilibrium formulation is extended to include the time-dependent (transient) mass migration, and the simultaneous reaction among the species as encountered in thermosetting composite material processing, with the objective of determining the time evolution of the concentration profiles.

The domain between the two fiber surfaces is divided into molecular layers where one molecule of epoxy or amine can occupy only one of these layers, and N_L is the total number of molecular layers in the half domain (Figure 2). The solid surface can adsorb molecules from a "bulk" state into an "adsorbed" state, and conversely, molecules in the "adsorbed" state may be desorbed into the "bulk" state. Molecules in the "adsorbed" state are treated to be fixed in the space and are not permitted to diffuse, while molecules in the "bulk" state may diffuse within the resin mixture.

Chemical reaction between epoxy and amine happens simultaneously during the adsorption, desorption and diffusion processes. The reaction equation may be written as:

$$n_1 E + n_2 A \rightarrow P \tag{1}$$

where P denotes the product, n_1 and n_2 are the mole numbers of the reactants needed to produce one mole product.

The mass balance analysis for the epoxy molecule in any (i)th adsorption layer in Figure 2 yields

$$\underbrace{\frac{dN_{E,i}}{dt}}_{storage} = \underbrace{\sum_{j=i-1}^{i+1} R_{a,E}(j,i)}_{adsorption,\, R_{a,E}(i)} - \underbrace{\sum_{j=i-1}^{i+1} R_{d,E}(j,i)}_{desorption,\, R_{d,E}(i)} - \underbrace{R_{r,E}(i)}_{depletion\,(reaction)} \tag{2}$$

In Eqn. (2), $\frac{dN_{E,i}}{dt}$ is the rate of change of total number of epoxy molecules in the (i)th adsorption layer, and the subscripts E and i denote epoxy and (i)th layer, respectively. Epoxy molecules in the "bulk" state in the (i-1)th, (i)th, and (i+1)th layers may be adsorbed into the (i)th molecular layer, denoting by the rate terms $R_{a,E}(j,i)$, $j=i-1, i, i+1$, respectively; in a reverse process, the adsorbed epoxy molecules in the (i)th layer can also be desorbed into the bulk in the (i-1)th, (i)th, and (i+1)th layers through the rate terms $R_{d,E}(j,i)$, $j=i-1, i, i+1$; further, the depletion of epoxy in the (i)th adsorption layer through chemical reaction is determined by the rate term $R_{r,E}(i)$.

The terms denoting rates of adsorption, desorption, and reaction are determined in the following discussion. First, the adsorption of epoxy molecules from (j)th layer to (i)th layer is given as:

$$R_{a,E}(j,i) = k_{a,E}(N_{i-1} - N_i)\exp\left(-\frac{E_{a,E}}{RT}\right)\frac{N_{E\infty,j}}{N_{\infty,i-1} + N_{\infty,i} + N_{\infty,i+1}} \tag{3a}$$

The parameter $k_{a,E}$ in the above equation is defined as the adsorption rate of epoxy molecules, and N_i is the total number of epoxy and amine molecules adsorbed in the (i)th layer, i.e., $N_i = N_{E,i} + N_{A,i}$. Because a molecule adsorbed into the (i)th layer must adjoin an adsorbed epoxy or amine molecule in the (i-1)th layer, the term $N_{i-1} - N_i$ gives the number of available sites in the (i-1)th layer which are open for adsorption. The exponential term $e^{-E_{a,E}/RT}$ includes the activation energy of adsorption $E_{a,E}$ for the epoxy molecules, which defined the energy barrier for an epoxy molecule to be adsorbed. The parameters $N_{E\infty,i}$ and $N_{A\infty,i}$ are the number of epoxy and amine molecules in the bulk state in the (i)th molecular layer, and $N_{\infty,i} = N_{E\infty,i} + N_{A\infty,i}$. Since the epoxy molecules adsorbed into the (i)th layer come from the (i-1)th, (i)th, and (i+1)th layers, the fraction $N_{E\infty,j}/(N_{\infty,i-1} + N_{\infty,i} + N_{\infty,i+1})$ [$j=i-1, i, i+1$] in the above equation denotes the probability that a site can capture an epoxy molecule from the (j)th layer.

Other rate terms can be defined in a similar way, and are summarized below.

$$R_{d,E}(j,i) = \frac{1}{3}k_{d,E}(N_i - N_{i+1})\exp\left(-\frac{E_{d,E}}{RT}\right)\frac{N_{E,i}}{N_i} \tag{3b}$$

$$R_{r,E}(i) = n_1 k_r \frac{N_{E,i}}{N_i + N_{\infty,i} + N_{P,i} + N_{P\infty,i}} \tag{3c}$$

The fraction $1/3$ in the desorption term arises from the assumption that the probabilities of desorption from the (i)th layer to each of the three neighborhood layers are identical; while the fraction $N_{E,i}/N_i$ comes from the fact that among all the molecules desorbed from the (i)th layer, the probability of finding an epoxy molecule is its mole fraction in the adsorption layer. The "depletion" term, $R_{r,E}(i)$, is determined by the crosslinking chemical reaction between epoxy and amine, where k_r is the reaction rate and $N_{E,i}/(N_i + N_{\infty,i} + N_{P,i} + N_{P\infty,i})$ is the mole fraction of epoxy in the (i)th layer. The parameter $N_{P,i}$ is the number of product molecules in the (i)th layer which results from the chemical reaction in the adsorbed state, while $N_{P\infty,i}$ originates form the reaction in the bulk.

A similar mass conservation analysis may be applied to the amine molecules in the "adsorbed" state and to the product molecules, yielding the following equations for these species:

$$\underbrace{\frac{dN_{A,i}}{dt}}_{storage} = \underbrace{\sum_{j=i-1}^{i+1} R_{a,A}(j,i)}_{adsorption,\, R_{a,A}(i)} - \underbrace{\sum_{j=i-1}^{i+1} R_{d,A}(j,i)}_{desorption,\, R_{d,A}(i)} - \underbrace{R_{r,A}(i)}_{depletion\,(reaction)} \tag{4}$$

$$\underbrace{\frac{dN_{P,i}}{dt}}_{storage} = \underbrace{R_P(i)}_{generation,(reaction)} \tag{5}$$

where the rate terms are defined similarly to those in Eqn. (3) by changing the subscript E to A. Note that the right hand side of Eqn. (5) has only the reaction term since the product molecules are assumed to have no mobility, and will stay in their space of formation.

Equations (2, 4, 5) pertain to the mass transfer rates of the molecules in the "adsorbed" state. The adsorbed materials exchange mass with the bulk resin that undergoes the diffusion process, therefore, the rate equations for species in the "bulk" state must be solved simultaneously with those corresponding to the "adsorbed" state. Consider the rate of change of the number of epoxy molecules in the "bulk" state in the (i)th layer, i.e., $dN_{\infty,i}/dt$, the following four types of contributions are identified: (1) diffusion of epoxy molecules in the "bulk" state from ($i+1$)th and ($i-1$)th layers to (i)th layer, which increases $N_{E\infty,i}$, (2) epoxy molecules in the "bulk" state in the (i)th layer being adsorbed to the ($i-1$)th, (i)th, and ($i+1$)th layers of the "adsorbed" state, which reduces $N_{E\infty,i}$,(3) desorption of epoxy molecules in the "adsorbed" state in the ($i-1$)th, (i)th, and ($i+1$)th layers to the (i)th layer of the "bulk" state, which increases $N_{E\infty,i}$, and (4) chemical reaction in the bulk in (i)th layer. We thus obtain

$$\frac{dN_{E\infty,i}}{dt} = D\left(N_{E\infty,i-1} - 2N_{E\infty,i} + N_{E\infty,i+1}\right) - \sum_{j=i-1}^{i+1} R_{a,E}(i,j) + \sum_{j=i-1}^{i+1} R_{d,E}(i,j) - R_{r,E\infty}(i) \tag{6}$$

where D is the diffusion coefficient of epoxy molecules. Note that all the rate terms can be defined as before. Similarly, we may get the rate equations for $N_{A\infty,i}$ and $N_{P\infty,i}$ as

$$\frac{dN_{A\infty,i}}{dt} = D\left(N_{A\infty,i-1} - 2N_{A\infty,i} + N_{A\infty,i+1}\right) - R_{r,A\infty}(i) - \sum_{j=i-1}^{i+1} R_{a,A}(i,j) + \sum_{j=i-1}^{i+1} R_{d,A}(i,j) \tag{7}$$

$$\frac{dN_{P\infty,i}}{dt} = k_r \frac{N_{E\infty,i}}{N_i + N_{\infty,i} + N_{P,i} + N_{P\infty,i}} \tag{8}$$

It must be pointed out that the reaction rate k_r and the diffusivity D are functions of extent of cure. The diffusivity is described by free volume theory as (Sanford, 1987)

$$D = D_0 \exp\left[-b_D / \left(f_g + \alpha_f \left(T - T_g(\xi)\right)\right)\right] \exp\left(-E_D / RT\right) \tag{9}$$

where $\xi = N_E(t)/N_{E0}$ is a dimensionless epoxy concentration, defined by the ratio of the total concentration of epoxy at a time instant to that at time zero. The parameters D_0, b_D, f_g, α_f, E_D in the model depend on the type of thermosetting system, and can be determined by the approach described by Sanford (1987). The glass transition temperature $T_g(\xi)$ is given by the DiBenedetto equation with three additional constants T_g^0, E_x/E_m, and F_x/F_m, which can be obtained through experimental data of T_g versus extent of reaction (Sanford, 1987)

$$\frac{T_g(\xi) - T_g^0}{T_g^0} = \frac{\left(E_x/E_m - F_x/F_m\right)(1-\xi)}{1 - \left(1 - F_x/F_m\right)(1-\xi)} \tag{10}$$

The reaction rate k_r is controlled by the retarded diffusion process at later stages of polymer cure and is given as

$$k_r = \frac{k_{r0} \exp\left(-E_a / RT\right)}{1 + \delta / D \exp\left(-E_a / RT\right)} \tag{11}$$

where k_{r0}, δ, and E_a are empirically determined parameters (Sanford, 1987).

The unknowns in Eqns. (2–8) are $N_{E,i}$, $N_{A,i}$, $N_{P,i}$, $N_{E\infty,i}$, $N_{A\infty,i}$, and $N_{P\infty,i}$. Additionally, the number of molecules at the (N_L+1)th layer—N_{E,N_L+1}, N_{A,N_L+1}, N_{P,N_L+1}, $N_{E\infty,N_L+1}$, $N_{A\infty,N_L+1}$, and $N_{P\infty,N_L+1}$—are unknowns corresponding to the domain boundaries. Therefore, when i goes from 1 to N_L, we have six more unknown variables than equations. The symmetry conditions at the middle plane provide six additional equations as

$$N_{E,N_L} = N_{E,N_L+1}; N_{A,N_L} = N_{A,N_L+1}; N_{P,N_L} = N_{P,N_L+1}$$
$$N_{E\infty,N_L} = N_{E\infty,N_L+1}; N_{A\infty,N_L} = N_{A\infty,N_L+1}; N_{P\infty,N_L} = N_{P\infty,N_L+1} \quad (12)$$

Equations (2, 4–8) (where $i = 1, 2, \Lambda\ N_L$) and the symmetry conditions [Eqn. (12)] constitute a complete ordinary differential equation (ODE) system for the $6N_L$ unknowns. For a thermosetting system with fiber sizing thickness of N_S molecular layers, the initial conditions of the ODE system may be written as

$$N_{E,i} = N_{A,i} = N_{P,i} = N_{P\infty,i} = 0;\ \ (i = 1, 2, \Lambda\ , N_L)$$
$$N_{E\infty,i} = N_{E,1};\ N_{A\infty,i} = 0;\ \ (i = 1, 2, \Lambda\ , N_S) \quad (13)$$
$$N_{E\infty,i} = N_{E,0};\ N_{A\infty,i} = N_{A,0};\ \ (i = N_S + 1, \Lambda\ , N_L)$$

3. Results and Discussion

The kinetics model developed in the preceding section is implemented numerically to predict the interphase evolution under isothermal conditions, $T = T_0$. A nondimensional form of the governing equations and initial conditions is obtained by introducing a dimensionless time $t' = k_{a,E} e^{-E_{a,E}/RT_0} t$, and dividing all the number of molecules (e.g., $N_{E,i}$, $N_{A,i}$, N_0) by the initial number of epoxy molecules in the layer next to the middle plane $N_{E,0}$ (e.g., $N'_{E,i} = N_{E,i} / N_{E,0}$). Figure 3 shows the distributions of number of epoxy and amine molecules (calculated as the total number of molecules both in "adsorbed" and "bulk" states in each layer) from the fiber surface (Layer 1) to the middle plane (Layer 100 chosen in this case) at different times during the process. The result corresponds to the parameter combination of the following groups: $k_{r0}/k_{a,E}\, e^{(E_{a,E}-E_a)/RT_0} =$ 50, $k_{d,E}/k_{a,E}\, e^{-(E_{d,E}-E_{a,E})/RT_0} = 1.5$, $k_{a,A}/k_{a,E}\, e^{-(E_{a,A}-E_{a,E})/RT_0} = 0.4$, $k_{d,A}/k_{a,E}\, e^{-(E_{d,A}-E_{a,E})/RT_0} = 1.3$, $N'_{E,0} = N'_{A,0} = 1$, $N'_{E,1} = 2$, $N'_0 = 1$, $D_0/k_{a,E}\, e^{E_{a,E}/RT_0} = 50$, $\delta/D_0\, e^{-E_a/RT_0}$ =0.5 , E_x/E_m=0.337, F_x/F_m=0.194, f_g=0.025, T_g^0=254 k, α_f=5.0e-4 1/k ($N'_0 = N_0/N_{E,0}$, where N_0 is the number of adsorption sites at the fiber surface). The mass transfer through the adsorption, desorption, and diffusion processes is stopped when the reacting resin system reaches the gelation point.

The initially large concentration of epoxy and zero concentration of amine (at t'_1) near the fiber surface correspond to the epoxy sizing layer applied on the fiber. At time t'_2, the epoxy profile has two distinctive regions: a large gradient region near the fiber surface, followed by a small gradient region. An examination of the concentration profiles of the epoxy species in the "adsorbed" and "bulk" states separately (omitted here in the interest of brevity) reveals that the large gradient region comes from the molecules in the "adsorbed" state while the small gradient region is determined by the diffusion process in the "bulk" state. These are shown in

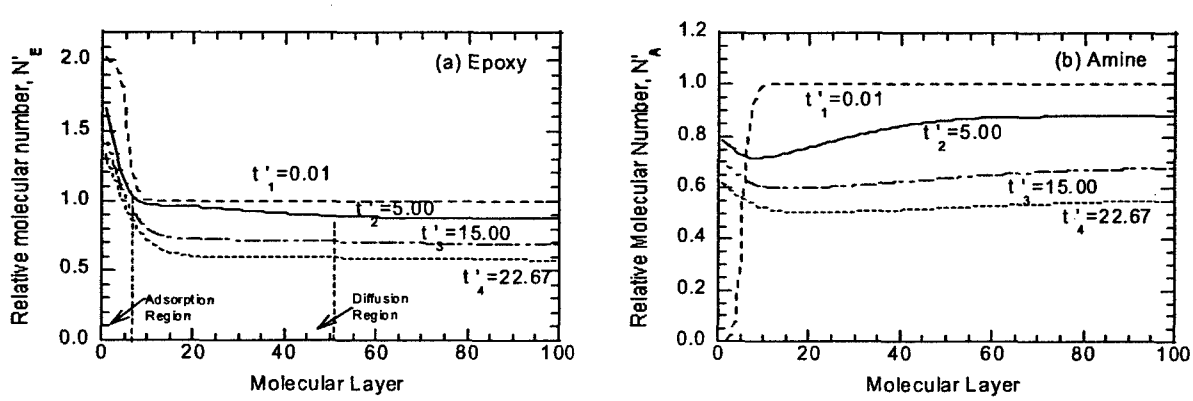

FIGURE 3: RELATIVE NUMBER DISTRIBUTION OF (*a*) EPOXY AND (*b*) AMINE MOLECULES IN EACH MOLECULAR LAYER AT FOUR DIFFERENT TIMES.

Figure 3(a) as the adsorption region and the diffusion region, respectively, for the particular time instant t'_2. Note that these regions grow away from the fiber with time, with the gradients in the diffusion region approaching zero owing to the tendency of the diffusion to equilibrate the concentration, whereas the gradient in the adsorption region approaching an equilibrium value, corresponding to the net balance of the adsorption and desorption effects. Two minima of the epoxy concentration are observed in Figure 3(a) at t'_3 and t'_4, respectively, which can be explained by the fact that epoxy molecules are adsorbed onto the fiber surface from the neighborhood, resulting in the deficiency of the epoxy species which is not sufficiently replenished through the diffusion process. The time t'_4 is the gelation time when the concentration profiles are "frozen" in space.

Figure 3(b) presents the amine concentration evolution with time. In this scenario, the diffusion and adsorption mass transfer are in the same direction, toward the fiber surface, as opposed to that in Figure 3(a) wherein the adsorption causes epoxy migration towards the fiber and diffusion tends to move the epoxy molecules away from the fiber. The two minima of amine concentration at times t'_3 and t'_4 can be explained as above. The influence of other parameter combinations on the concentration profile can be discussed in similar ways and detailed discussion will not be included in the paper. The predicted interphase concentration profiles are important input data to the models which calculate the overall composite material properties (Palmese, 1992). In the present study, the temperature is taken as a given constant, while the real temperature field needs to be solved by coupling to the energy equation written for the whole composite domain. The coupled interphase formation and heat transfer model can be used to select the cure cycles for desired interphase structure.

4. Conclusions

An adsorption-desorption-diffusion-reaction model was developed to predict evolution of the interphase concentration profiles during thermosetting composite processing. The concentration gradient caused by the adsorption-desorption process is seen to approach an equilibrium value, while that caused by the diffusion tends to approach zero. It was also shown that the concentration profiles might have minima instead of following a simple monotonical trend.

5. Acknowledgements

The authors would like to acknowledge the Air Force Office of Scientific Research (AFOSR) for funding this research through Grant No. F496200110521.

References

L. T. Drzal, The Interphase in Epoxy Composites, Advances in Polymer Sciences, vol. 75, pp. 1–32, 1986.

T. L. Hill, Theory of Multimolecular Adsorption from a Mixture of Gases, Journal of Chemical Physics, vol. 14, pp. 268–275, 1946.

M. S. Madhukar and L. T. Drzal. Fiber-Matrix Adhesion and Its Effect on Composite Mechanical Properties: II Longitudinal (0°) and Transverse (90°) Tensile and Flexure Behavior of Graphite/Epoxy Composites, Journal of Composite Materials, vol. 25, pp. 958–991, 1991.

G. R. Palmese, Origin and Influence of Interphase Material Property Gradients in Thermosetting Composites, University of Delaware Center for Composite Materials, Technical Report Number 92-25. 1992.

V. Ponec, Z. Knor, and S. Cerny Adsorption on Solids, Butterworth Co., London. 1974

W. M. Sanford, Cure Behavior of Thermosetting Resin Composites, Ph. D. thesis, University of Connecticut, Newark, Delaware, 1987.

R. W. Rydin, *et al.*, Glass Fabric Vinyl-Ester Composites: Tailoring the Fiber Bundle/Matrix Interphase with Nylon Coating to Modify Energy Absorption Behavior, Journal of Composite Materials, vol. 31, pp. 182–209, 1997.

S. Subramanian, *et al.*, Characterization of the Fiber-Matrix Interphase and Its Influence on Mechanical Properties of Unidirectional Composites, Journal of Composites Material s, vol. 30, pp. 309–332, 1996.

PROCESSING-INTERPHASE RELATIONSHIPS FOR THE CURING OF THERMOSETTING-MATRIX COMPOSITES

F. Yang and R. Pitchumani*
Composites Processing Laboratory
Department of Mechanical Engineering
University of Connecticut
Storrs, Connecticut 06269-3139
*Corresponding Author

ABSTRACT

Fabrication of thermosetting-matrix composites is based on a critical step of cure, which involves applying predefined temperature cycle to a fiber-resin mixture. Several mass transport processes occur in the vicinity of the reinforcement fiber, leading to the formation of an interphase region with different chemical and physical properties from the bulk resin. The cure cycle applied on the macroscopic boundaries of the composite govern the microscopic cure kinetics near the fiber surface, which, in turn, determines the interphase evolution with time, and the life and properties of the composite. Current studies in the literature mostly focus on the macroscopic thermochemical processes, and the linkage between the cure cycles and the interphase structure evolution has not been rigorously studied. A multiscale thermochemical model is presented in this paper to provide the critical link of relating the process parameters to the interphase formation, which is essential for optimizing cure cycles to obtain tailored interphase in composite materials.

KEY WORDS: Polymer Matrix Composites, Process Modeling, Interphase Kinetics, Curing of Polymers

1. INTRODUCITON

During the cure of thermosetting polymer composites, the presence of reinforcing fibers significantly alters the resin composition in the vicinity of the fiber surface via several microscale processes, forming an interphase region with different chemical and physical properties from the bulk resin. The interphase resides in a region between the original constituents of the composite with a size of one to a few thousand nanometers (1–4). The performance of the composite is determined by the ability of the matrix to transfer load to the reinforcing fiber, and is thus controlled by the interphase region. The structure and properties of the interphase are the dominant factors governing the overall composite properties and performance.

The studies in the literature on interphase have focused primarily on the experimental determination of the influence of interphase on the mechanical behavior of the composite

materials (2–5, for example). Fiber surface modifications such as high temperature treatment and sizing, are commonly implemented to tailor the structure of the interphase regions and to investigate their effects on the mechanical and other properties of the composite materials. Due to complexities of the molecular level mechanisms that occur in the vicinity of the fibers during the process, prediction of the interphase evolution as function of processing parameters has been the subject of little attention.

Palmese (1) presented a model for predicting the interphase composition profile under thermodynamic equilibrium conditions of a non-reacting epoxy-amine resin system. The principle of minimum free energy was invoked to set up the equilibrium state, accounting for enthalpy interaction between fiber surface and resin components, and the calculation of Gibbs free energy was based on a Flory-Huggins type lattice structure. Hrivnak (6) extended Palmese's model to a reacting system by using renewal theory models to the construction of the assembly Gibbs free energy and the associated chemical potential. In an alternative approach, a kinetics-based description of the governing phenomena was developed by the authors to predict the interphase development during thermosetting composite processing (7–10). In this method, mass conservation principle was employed to describe the transport processes of multilayer adsorption, desorption and diffusion near a fiber surface, which are accompanied by simultaneous cure reaction between the resin components. The time evolution of interphase concentration profile gradients before the gelation of the thermosetting system was predicted as function of material and process parameters.

The models of interphase formation consider a microscale domain near a fiber surface, and the temperature is assumed to be known. In a simulation of the cure of thermosetting composites, however, the temperature filed must be computed from the energy equation to predict the temperature history at different locations in the material. The solution of the energy equation needs the information of interphase cure kinetics, consequently, the energy equation and the cure kinetics equations are coupled. No study has been reported in the literature to directly link the cure cycles to the interphase kinetics, and this paper is aimed to fill the critical void. A multiscale thermochemical model is developed in the next section, which couples the macroscale energy equation with the microscale interphase cure kinetics equations. The evolution of interphase concentration profiles is presented at various locations of the composite for two selected cure cycles.

2. MULTISCALE THERMOCHEMICAL MODEL

In this study, the geometry of the composite is considered to be cylindrical, which corresponds to a die of circular cross section, in a pultrusion process (11–13). However, the model development and relevant results are readily extended to the other geometries involved in the manufacturing techniques such as autoclave molding and liquid molding. In a pultrusion process, the resin-fiber mixture is pulled through a long heated die with prescribed temperature variation. The elevated temperatures initiate an exothermic crosslinking cure reaction among the species in the resin, which transform the soft initial mixture entering the die to a hard product at the die exit. The dominant physical and chemical phenomena are: (a) the heat transfer associated with the heating of the composite, and (b) the chemical reaction leading the cure process (11–13).

The heat transfer inside the pultrusion die is considered to be one dimensional radially, at steady-state, and with a source term reflecting the reaction heat of the cure process. The Lagrangian form of the heat equation for a composite cross-section may be written as (11):

$$\frac{\partial(\rho c_p T)}{\partial t} = \frac{1}{r}\frac{\partial}{\partial r}\left(kr\frac{\partial T}{\partial r}\right) + C_{E0}\Delta H_r\left(1-v_f\right)\frac{\partial \varepsilon}{\partial t} \tag{1}$$

where the variables t and r are the Lagrangian time and radial coordinate, respectively, ΔH_r is the heat of the cure reaction, C_{E0} is the initial concentration of the epoxy resin at the die entrance, v_f is the fiber volume fraction, and T is the local temperature of the mixture. The three material properties, namely, the thermal conductivity, k, the density, ρ, and the specific heat, c_p, are evaluated based on the weight fraction of the fiber-resin mixture (11). The term $\partial\varepsilon/\partial t$ is the local reaction rate, and its determination is the focus of the remaining discussion in this section.

The cure reaction rate is commonly modeled by empirical correlations, which are obtained by using data from the bulk reactions with uniform mixing of the reacting species in the absence of the reinforcing fibers (11). The presence of fibers, however, has been found to cause concentration gradients in the vicinity of the fiber surfaces through the preferential adsorption mechanism (7–10). Consequently, the reaction kinetics is significantly changed by the spacial variation of the stoichiometric ratio, i.e., the non-uniform mixing of the reacting species. A model of the microscale cure kinetics near the fiber surfaces has been developed by the authors (7–10), and is adopted in this paper to determine the cure reaction rate, $\partial\varepsilon/\partial t$.

The geometry considered in the cure kinetics model is the inter-fiber space in a composite having a typical staggered fiber arrangement [Figure 1(a)]. The domain in the model development is idealized as the region between two identical infinite planes representing the fiber surfaces [Figure 1(b)], which may be justified by the fact that the interphase thickness is often small in comparison to the fiber diameter. A graphite fiber/epoxy-amine thermosetting system is considered in the model development; however, all the derivations and results are applicable to a general two-component thermosetting system. The domain between the two fiber surfaces is

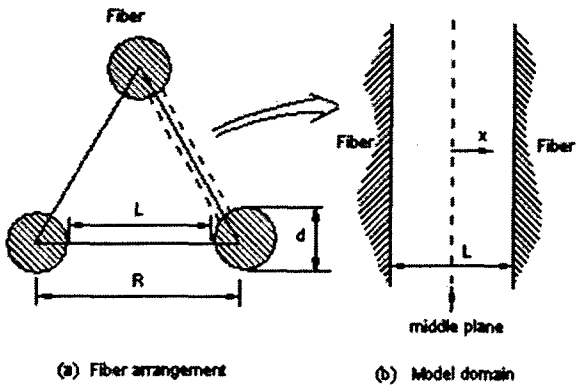

Figure 1: (a) A representative fiber arrangement in the composite, and (b) schematic of the domain between two fiber surfaces considered in the modeling.

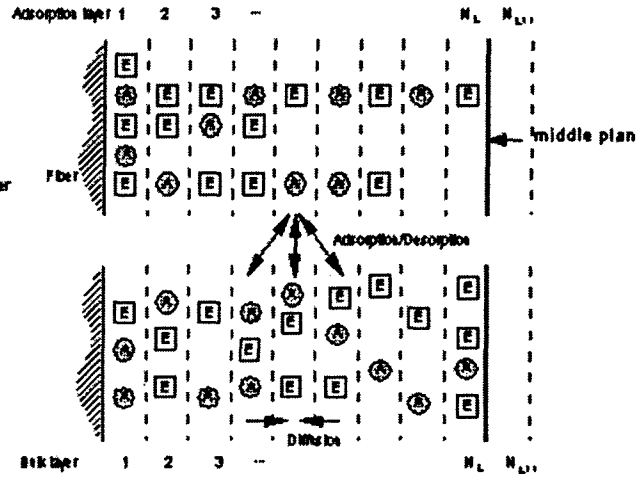

Figure 2: Schematic of the adsorption, desorption, and diffusion processes in an epoxy-amine system.

further divided into molecular layers where one molecule of epoxy or amine can occupy only one of these layers, and N_L is the total number of molecular layers in the half domain (Figure 2).

Due to the interaction between resin molecules and the fiber surface, as well as those among resin molecules themselves, epoxy and amine molecules can move from layer to layer. The solid surface can adsorb molecules from a "bulk" state into an "adsorbed" state, and conversely, molecules in the "adsorbed" state may be desorbed into the "bulk" state. Molecules in the "adsorbed" state are treated to be fixed in the space and are not permitted to diffuse, while molecules in the "bulk" state may diffuse within the resin mixture. Figure 2 shows the molecular layers in the model domain, where the adsorption layers contain molecules in the "adsorbed" state, while the bulk layers hold molecules in the "bulk" state. Although the adsorption and bulk layers are drawn separately to illustrate the mass exchange between the "adsorbed" and "bulk" states, the corresponding layers essentially occupy the same space, i.e., the (i)th adsorption layer and the (i)th bulk layer are overlapped. Chemical reaction between epoxy and amine happens simultaneously during the adsorption, desorption and diffusion processes, resulting in a continuously evolving concentration profile that is "frozen" in space upon gelation of the thermosetting system.

The mass balance analysis for the epoxy molecule in any (i)th adsorption layer in Figure 2 yields

$$\underbrace{\frac{dN_{E,i}}{dt}}_{\text{storage}} = \underbrace{R_{a,E}(i-1,i) + R_{a,E}(i,i) + R_{a,E}(i+1,i)}_{\text{adsorption, } R_{a,E}(i)} - \underbrace{R_{d,E}(i-1,i) - R_{d,E}(i,i) - R_{d,E}(i+1,i)}_{\text{desorption, } R_{d,E}(i)} - \underbrace{R_{r,E}(i)}_{\text{depletion (reaction)}} \tag{2}$$

In Eq. (2), $dN_{E,i}/dt$ is the rate of change of total number of epoxy molecules in the (i)th adsorption layer, and the subscripts E and i denote epoxy and (i)th layer, respectively. Epoxy molecules in the "bulk" state in the (i-1)th, (i)th, and (i+1)th layers may be adsorbed into the (i)th molecular layer, denoting by the rate terms $R_{a,E}(i\text{-}1,i)$, $R_{a,E}(i,i)$, and $R_{a,E}(i+1,i)$ respectively; in a reverse process, the adsorbed epoxy molecules in the (i)th layer can also be desorbed into the bulk in the (i-1)th, (i)th, and (i+1)th layers through the rate terms $R_{d,E}(i\text{-}1,i)$, $R_{d,E}(i,i)$, and $R_{d,E}(i+1,i)$; further, the depletion of epoxy in the (i)th adsorption layer through chemical reaction is determined by the rate term $R_{r,E}(i)$.

Considering the rate of change of the number of epoxy molecules in the "bulk" state in the (i)th layer, i.e., $dN_{E\infty,i}/dt$, we may obtain

$$\frac{dN_{Eq,i}}{dt} = D_{EA}\frac{N_{Eq,i-1} + N_{Eq,i+1} - 2N_{Eq,i}}{\Delta L^2} - R_{a,E}(i,i-1) - R_{a,E}(i,i) - R_{a,E}(i,i+1)$$
$$+R_{d,E}(i,i-1) + R_{d,E}(i,i) + R_{d,E}(i,i+1) - n_1 k_r N_{Eq,i} \tag{3}$$

where D_{EA} is the mutual diffusivity in the binary epoxy-amine mixture, ΔL corresponds to the physical size of a molecular layer, n_1 is the number of moles of epoxy needed to produce one mole product, and k_r is the reaction rate determined by the empirical correlations mentioned above.

The rate terms of adsorption, desorption, and reaction depend on the number of epoxy, amine and product molecules in the adsorption and bulk layers. Similar mass conservation analyses may be applied to the amine and product molecules in the "adsorbed" and "bulk" states, yielding the rate of change equations for the corresponding species. The review of the kinetics model so far paves the way for the development of the thermochemical model in this section, and the readers are referred to refs. (7–10) for details.

The degree of cure, ε, is defined as:

$$\varepsilon = \frac{N_{E0} - N_E}{N_{E0}} \tag{4}$$

where N_{E0} is the initial number of epoxy molecules in the model domain between two fiber surfaces (Fig. 2), and N_E is the instantaneous number of epoxy molecule in the model domain:

$$N_E = \sum_{i=1}^{N_L} \left(N_{E,i} + N_{E\infty,i} \right) \tag{5}$$

Differentiating Eqns. (2) and (3) with respective to time yields:

$$\frac{\partial \varepsilon}{\partial t} = -\frac{1}{N_{E0}} \frac{\partial N_E}{\partial t} = -\frac{1}{N_{E0}} \sum_{i=1}^{N_L} \left(\frac{dN_{E,i}}{dt} + \frac{dN_{E\infty,i}}{dt} \right) \tag{6}$$

where the rates of change, $dN_{E,i}/dt$ and $dN_{E\infty,i}/dt$, are given by Eqns. (2) and (3), respectively. The heat equation, Eq. (1), for the macroscale composite domain and the reaction rate equation, Eq. (6), for the microscale model domain in Fig. 2 consist of a multiscale thermochemical model. Note that Eqns. (1) and (6) are coupled through the temperature dependence of the rate terms in Eqns. (2) and (3).

Two boundary conditions and an initial condition are invoked for Eq. (1): (I) the temperature at the outer radius of the composite material corresponds to the temperature of the die wall (or the prescribed cure cycle), $T_c(t)$, (II) symmetric conditions exist at the centerline of the die, and (III) the initial temperature at the die entrance is specified to be T_i. The initial conditions for Eqns. (2), (3), (6) and the rate equations for the other species are: (IV) the number of molecules of each species in the "adsorbed" state is zero, and (V) the number of product molecules is zero, and all the resin molecules are in the "bulk" state (7–10). The above five conditions may be expressed mathematically as:

$$\begin{aligned} &(I)\ T(R_0,t) = T_c(t);\ (II)\ \partial T/\partial r(0,t) = 0;\ (III)\ T(r,0) = T_i \\ &(IV)\ N_{E,i} = N_{A,i} = N_{P,i} = 0;\ \ (i = 1, 2, \cdots N_L) \\ &(V)\ N_{P\infty,i} = 0; N_{E\infty,i} = N_{E,0};\ N_{A\infty,i} = N_{A,0}; (i = 1, 2, \cdots N_L) \end{aligned} \tag{7}$$

The governing equations, Eqns. (1) and (6), along with the boundary and initial conditions, Eq. (7), were solved numerically using an implicit finite-difference scheme with a control volume formulation (9). The mesh for the macroscopic composite domain contained 64 numerical grids along the radius direction, and the time step Δt was determined such that the mesh Fourier number $k\,\Delta t\ /\ \rho c_p \Delta r^2$ is less than unity. Depending on the fiber volume fraction, each computational grid may consist of a large number of representative volume elements (RVE) shown in Figure 2. All the RVEs in a grid experience the same temperature history, and hence, the same concentration profile evolution history. Within each time step, the temperature field

obtained from Eq. (1) is used to calculate the cure reaction rate $d\varepsilon/dt$ in Eq. (6), which, in turn, is substituted into Eq. (1) to update the temperature field; and the procedure is performed until the temperature filed is converged. The ordinary differential equations [e.g., Eqns. (2) and (3)] were solved by a fourth order Runge-Kutta method (7–10). The stopping criterion for the numerical simulation is that all the sections of the composite reach the gelation point, which corresponds to $\varepsilon = 0.6$.

3. RESULTS AND DISCUSSION

The thermochemical model developed in the previous section is used to calculate the molar concentration of the resin component as a function of the molecular layers at different locations in the composite for various cure cycles. A nondimensional form of the heat equation, Eq. (1), and its boundary and initial conditions is obtained by introducing the dimensionless temperature, location, and time in the radius direction as: $\theta=(T-T_0)/T_0$, $r'=r/R_0$, $t'=k_{a,E}\exp(-E_{a,E}/RT_0)t$, where T_0 is the reference temperature; while the dimensionless form of the reaction rate equation, Eq. (6) , and its initial conditions is derived by introducing a dimensionless time t' and dividing all the number of molecules (e.g., $N_{E,i}$, $N_{A,i}$) by the initial number of epoxy molecules in the layer next to the middle plane $N_{E,0}$ (e.g., $N'_{E,i} = N_{E,i}/N_{E,0}$).

The principal dimensionless groups that govern the interphase concentration evolution at various locations in a composite are identified as follows: (1) the adiabatic reaction temperature $\theta_{ad} = \Delta H_r C_{E0}(1-v_f)/\rho c_p T_0$, (2) dimensionless epoxy adsorption energy, $E^*_{a,E} = E_{a,E}/RT_0$, (3) dimensionless epoxy desorption energy, $E^*_{d,E} = E_{d,E}/RT_0$, (4) epoxy desorption ratio $\beta_E = \{k_{d,E}\, e^{-(E_{d,E}-E_{a,E})/RT_0}\} / k_{a,E}$, (5) epoxy diffusion ratio $\phi_{EA} = \{D_{EA} e^{E_{a,E}/RT_0}\}/\Delta L^2 k_{a,E}$, (6) dimensionless amine adsorption energy, $E^*_{a,A} = E_{a,A}/RT_0$, (7) dimensionless amine desorption energy, $E^*_{d,A} = E_{d,A}/RT_0$, (8) amine desorption ratio $\beta_E = \{k_{d,A}\, e^{-(E_{d,A}-E_{a,E})/RT_0}\} / k_{a,E}$, (9) amine adsorption ratio $\alpha_A = \{k_{a,A}\, e^{-(E_{a,A}-E_{a,E})/RT_0}\} / k_{a,E}$, and (10) adsorption Damköhler number $\gamma = \{k_r e^{E_{a,E}/RT_0}\}/k_{a,E}$, In this study, the number of molecular layers in the model domain is keep fixed at $N_L = 100$, the reference temperature is kept at $T_0 = 80°C$, and the outer radius of the composite $R = 0.00635$m. Furthermore, the cure cycles begin with a linear ramp from $\theta_i = -0.33$ to $\theta_f = 0.50$ within ramp time $\Delta t'_{ramp}$, followed by a hold stage with a constant temperature θ_f.

Figures 3(a)–(f) present the distributions of the number of epoxy and amine molecules within a microscopic representative volume element (shown in Figure 2) at different nondimensional times during the process. The results correspond to a cure ramp time $\Delta t'_{ramp} = 80$, and the location of the RVE is at the centerline of the composite, i.e., r/R=0.0. Although the total concentrations are the most relevant to the composite material properties, the results of the adsorbed and bulk fractions are presented as well to better elucidate the trends in the total concentration development. Figures 3(a) and 3(b) present the concentration profiles for the molecules in the adsorbed state; Figures 3(c) and 3(d) correspond to bulk state concentration profiles; and Figures 3(e) and 3(f) show the total concentrations of epoxy and amine, $N'_{E,tot}$ and $N'_{A,tot}$.; The following parameter combination is employed: $\theta_{ad} = 0.072$, $E^*_{a,E} = E^*_{a,E} = 3.4$, $E^*_{d,E} = E^*_{d,E} = 6.8$, $\gamma = 0.01$, $\beta_E = 0.75$, $\alpha_A = 1.5$, $\beta_A = 0.75$, $N'_{E,0} = N'_{A,0} = 1$, $N'_0 = 1$, ($N'_0 = N_0/N_{E,0}$, where N_0 is the number of adsorption sites at the fiber surface) and $\phi_{EA} = 6.0$. The desorption ratios β_E

and β_A are chosen to be relatively small which indicates that the resin molecules are easily adsorbed onto the fiber surface.

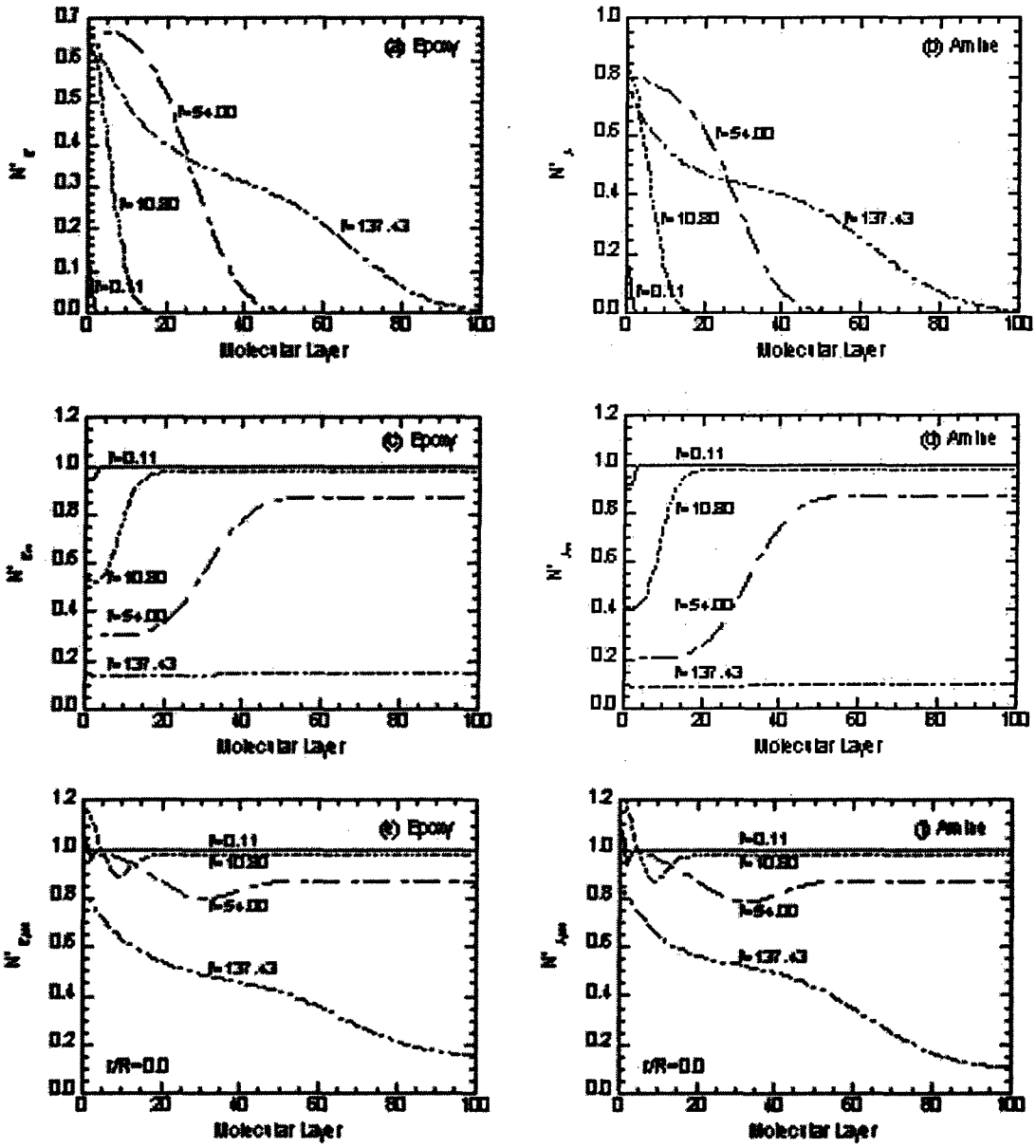

Figure 3: Interphase concentration profiles at the centerline, in terms of relative number of (a) epoxy molecules and (b) amine molecules in the adsorbed state; (c) epoxy molecules and (d) amine molecules in the bulk state; (e) total epoxy molecules and (f) total amine molecules in both states, as a function of the molecular layer at four different times during the cure process.

In the adsorbed state profiles, Figures 3(a) and 3(b), the number of molecules for both of the species increase monotonically from $t' = 0.11$ to $t' = 54.00$ due to adsorption onto the surface, resulting in a high concentration region near the fiber surface; at the gelation time $t' = 137.43$, however, the reactant concentrations in the vicinity of the fiber surface decrease due to chemical reaction. The concentration profiles are seen to propagate from a small region near the fiber

surface at $t' = 0.11$ to the far region at the gelation time, which is identified as a strong adsorption effect. The number of epoxy molecules near the fiber surface is smaller than that of the amine molecules owing to the larger amine adsorption rate (α_A = 1.5). The adsorption/desorption processes cause the deficit of species in the bulk state near the fiber surface, as shown in Figures 3(c) and 3(d) from $t' = 0.11$ to $t' = 54.00$. However, the diffusion process compensates for the deficit at the gelation time, t' = 102.0, when the concentration gradients in the bulk state approach zero. The total concentration profiles of each species [Figures 3(e) and 3(f)] show minima at $t' = 0.11$, $t' = 10.80$ and $t' = 54.00$, which can be explained by the coupled influence of the adsorption/desorption and the diffusion processes as discussed above.

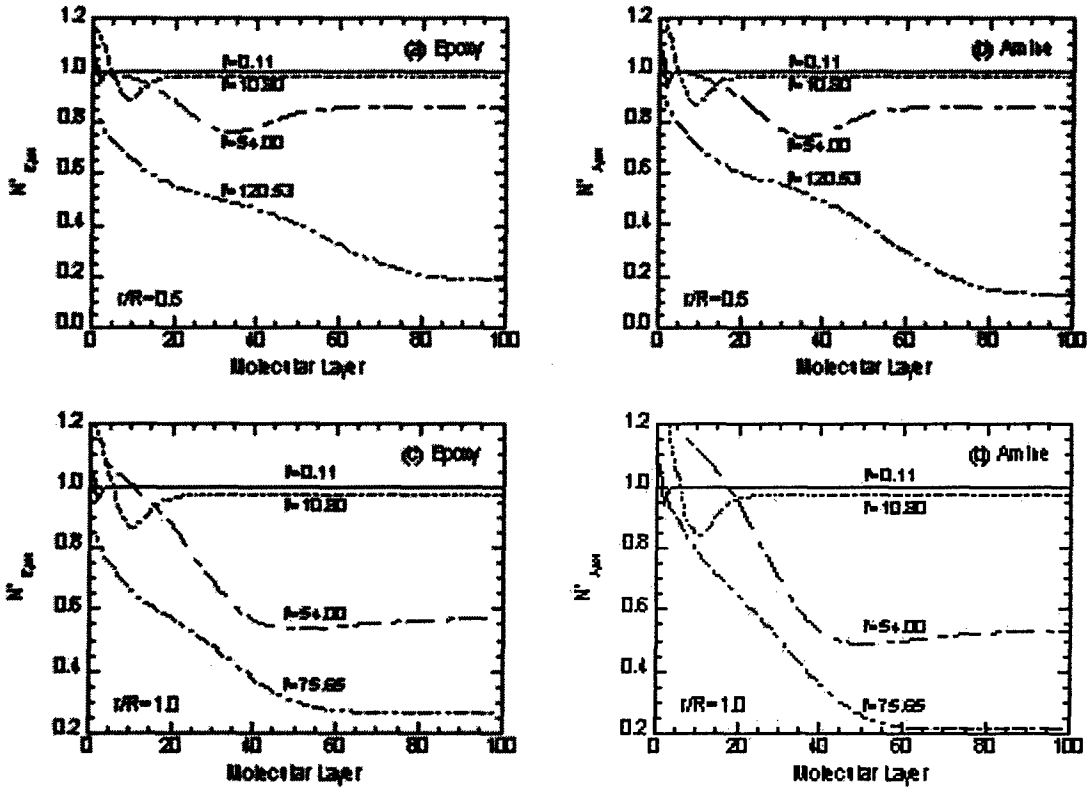

Figure 4: Total interphase concentration profiles for (a) epoxy and (b) amine molecules near the middle point; (c) epoxy and (d) amine molecules near the outer radius. The results correspond to cure ramp time $\Delta t'_{ramp} = 80$, and a strong adsorption effect.

Figures 4(a)–(d) present the total concentration evolution at two other locations in the composite, i.e., the middle point, r/R = 0.5, and the outer radius r/R = 1.0; the cure ramp time and other parameters retain the values as in Figure 3. Since resin materials at larger radius experience higher temperatures, the gelation time decreases from $t' = 137.43$ at the centerline to $t' = 120.53$ at the middle point [Figures 4(a) and (b)], and $t' = 75.65$ at the outer radius [Figures 4(c) and (d)]. All the concentration profiles show minima before the gelation time, which may be explained by the same arguments in Figure 3. At different locations in the composite, the final concentration profiles show significant deviations from each other. In Figures 4(a) and (b), the concentration gradients at the gelation time become zero between layers 80 and 100, while in Figures 4(c) and (d) the zero gradient region is extended between layers 60 and 100. A smaller zero gradient

region is observed in Figures 3(e) and (f). At larger radius, less time (i.e., the gelation time) is available for the concentration gradient to propagate from the fiber surface to the far region, hence the increase in the zero gradient region.

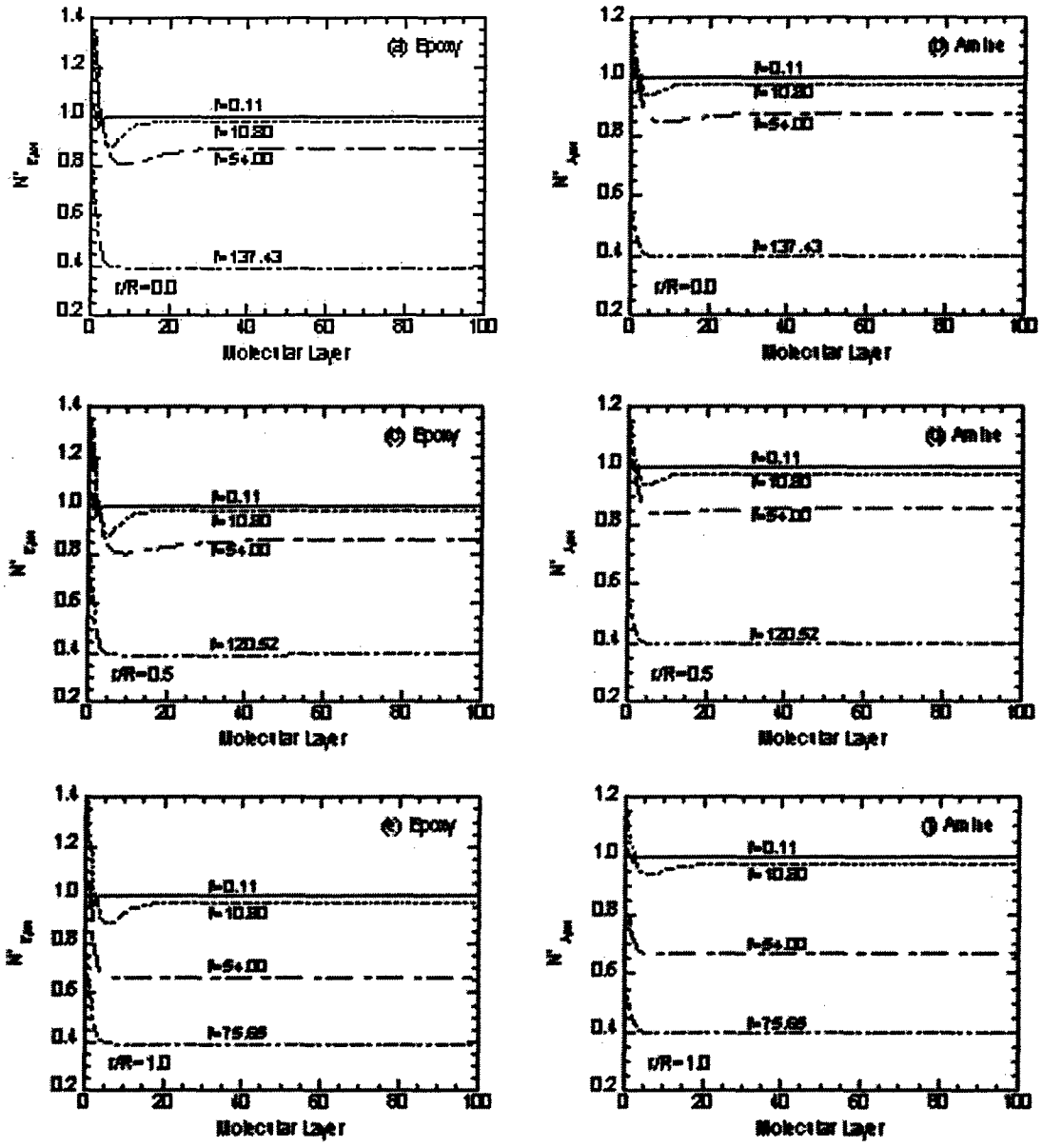

Figure 5: Total interphase concentration profiles for (a) epoxy and (b) amine molecules near the centerline; (c) epoxy and (d) amine molecules near the middle point; (e) epoxy and (f) amine molecules near the outer radius. The results correspond to cure ramp time $\Delta t'_{ramp} = 80$, and a weak adsorption effect.

Figures 5(a)–(f) show the total concentration profiles at three locations in the composites, and the results pertain to the parameter combination of $\beta_E = 1.5$, $\alpha_A = 0.5$, and $\beta_A = 2.0$; the cure ramp time and all other parameters retain the values as in Figure 4. The concentration profiles in the adsorbed state (omitted here for brevity) growth from $t' = 0.11$ to $t' = 10.80$, and remains invariant afterwards. An equilibrium state is thus reached, where the desorption and adsorption

processes balance each other and the influence of the fiber surface only propagate to a few molecular layers. By increasing β_A and β_E, and decreasing α_A, the desorption process is strengthened with respect to adsorption, which corresponds to a relatively weak "force field" by the fiber surface that can only penetrate into a few molecular layers. The gelation times at different locations in Figure 5 are identical to the corresponding values in Figures 3 and 4, which

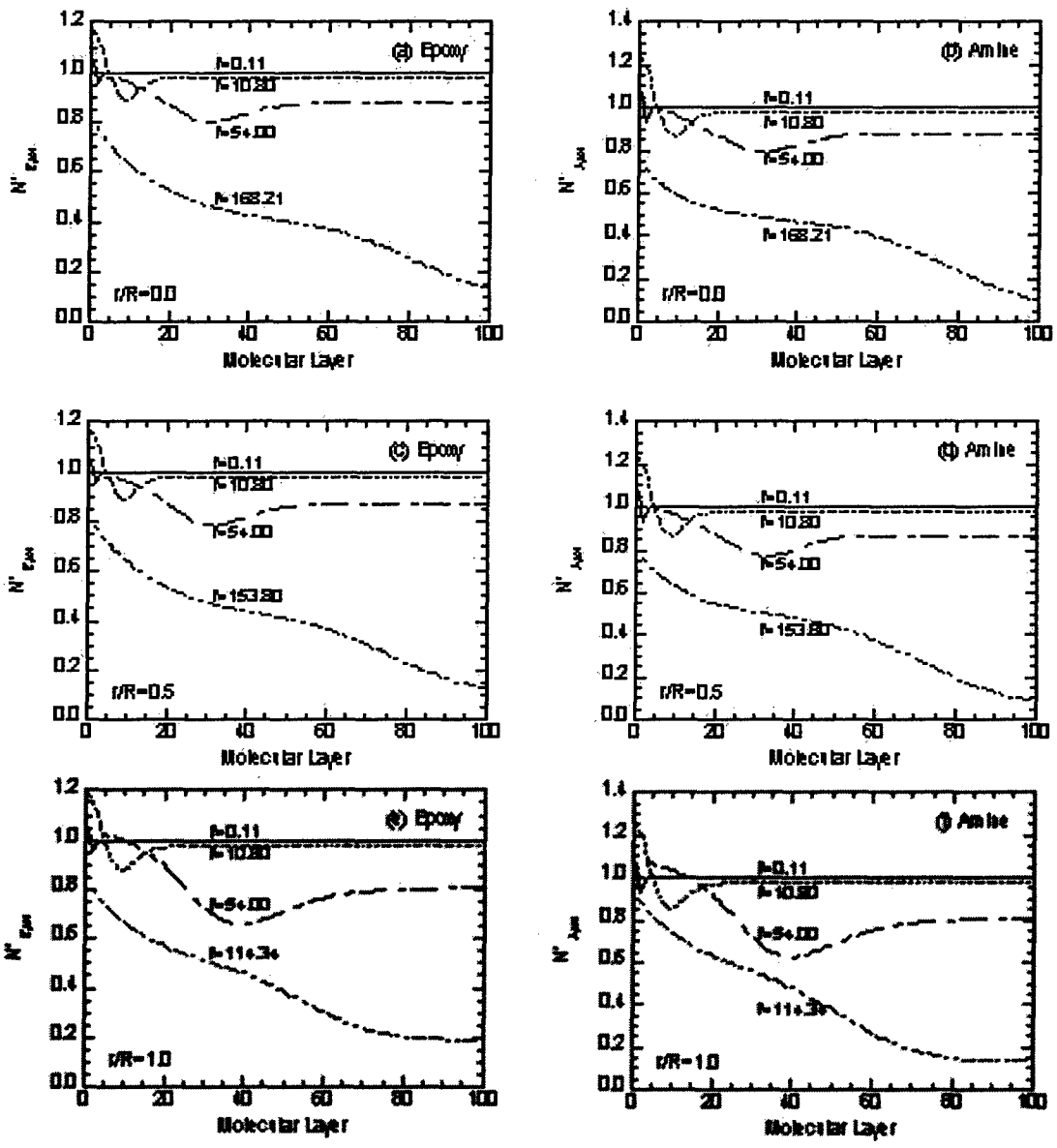

Figure 6: Total interphase concentration profiles for (a) epoxy and (b) amine molecules near the centerline; (c) epoxy and (d) amine molecules near the middle point; (e) epoxy and (f) amine molecules near the outer radius. The results corresponds to cure ramp time $\Delta t'_{ramp} = 160$, and a strong adsorption effect

is caused by the first order cure kinetics adopted in this study. Since only the concentration of the epoxy (instead of the concentrations of both reactants) is considered in the first order kinetics, different concentration profile evolutions in the microscale domains do not influence the overall reaction rate in the composite domain. An improved cure kinetics model will be implemented in

a future work for a more realistic simulation. The equilibrium profiles in the absorbed state were developed at time t' = 10.80, which is before all the gelation times at different location, consequently, the final concentration profiles in Figure 5 are almost identical.

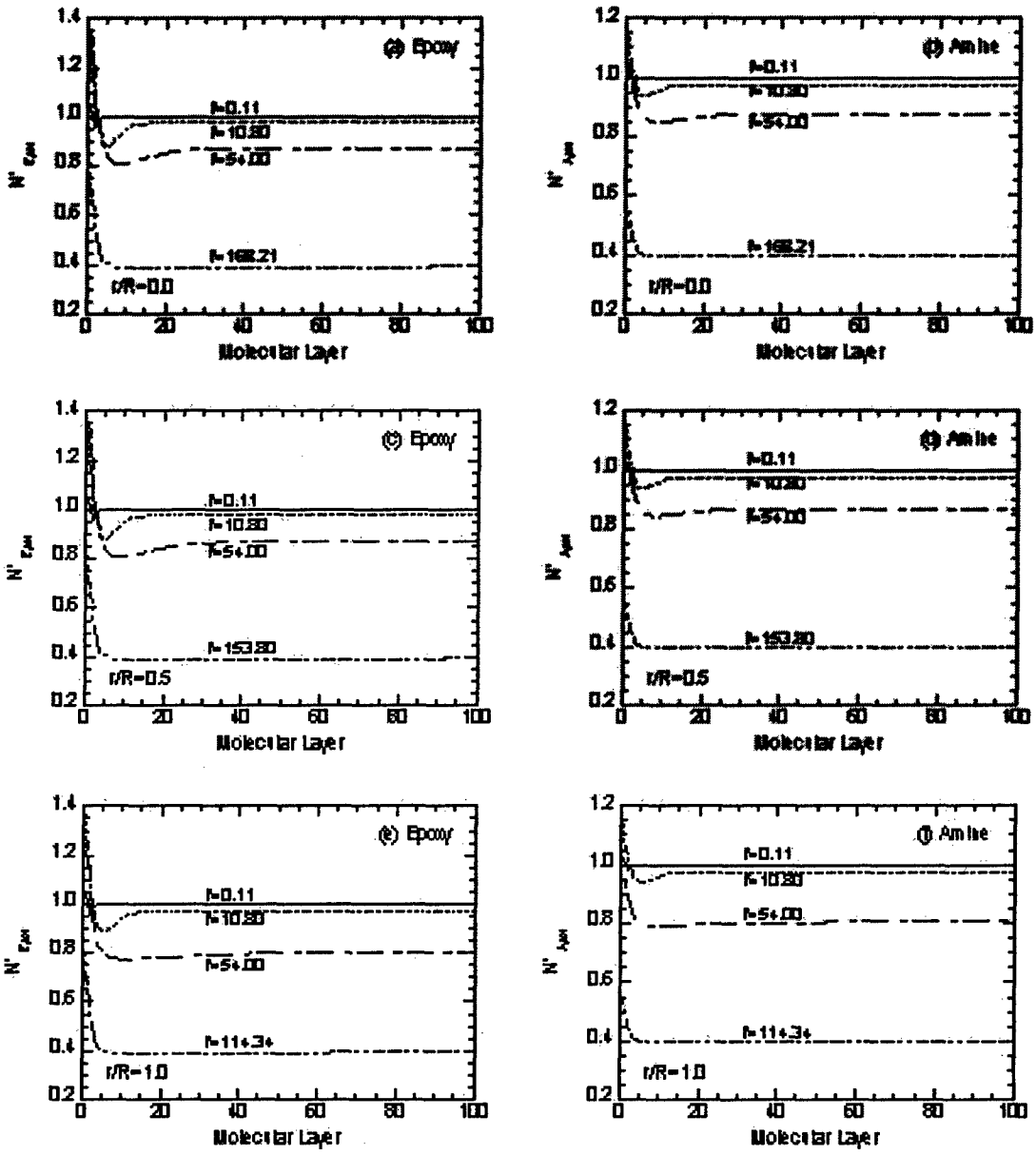

Figure 7: Total interphase concentration profiles for (a) epoxy and (b) amine molecules near the centerline; (c) epoxy and (d) amine molecules near the middle point; (e) epoxy and (f) amine molecules near the outer radius. The results correspond to cure ramp time $\Delta t'_{ramp}$ = 160, and a weak adsorption effect.

The results corresponding to a longer cure ramp time $\Delta t'_{ramp}$ =160 are shown in Figures 6 and 7, which follow the presentation format in Figure 5(a)–(f). Figure 6 retains the parameter combination in Figure 3 (or 4). However, the gelation times in Figure 6 are longer than the corresponding cases in Figures 3 and 4 due to lower cure temperatures, e.g., an increase is found from t' = 137.47 in Figure 3(e) to t' = 168.21 in Figure 6(a). Consequently, the final

concentration profiles are also changed for different cure cycles, and smaller nonzero gradient regions are observed in Figure 6 than the corresponding cases in Figures 3 and 4. Note that the final concentration profiles in Figures 6(a) and 6(c) [or in Figures 6(b) and 6(d)] are identical, which may be explained by the fact that the adsorption/desorption equilibrium states were achieved before the gelation times. Figure 7 has the same parameter combination in Figure 5, and the effect of different cure cycles and locations in the composites are negligible since all the gel times are longer than the adsorption/desorption equilibrium time.

The influence of other parameter combinations and cure cycles on the concentration profile evolution can be discussed in similar ways and detailed discussion will not be included in the paper. The predicted interphase composition profiles at different locations of the composites are important input data to the prediction of overall composite material properties (1, 14). The results presented in this section may be used to select the cure cycles for desired interphase structure.

4. CONCLUSIONS

A microscale kinetics model of interphase formation is coupled with a macroscale energy equation to simulate the cure process of thermosetting composite material. The final concentration gradient caused by the adsorption-desorption process may vary at different locations in the composites, which experience different temperature history. It is shown that the composition profile changes significantly before the adsorption/desorption equilibrium time, but remains constant afterward. Consequently, the effect of cure cycles and locations in the composite may be negligible when gelation times are always longer than the adsorption/desorption equilibrium time in the whole composite domain.

5. ACKNOWLEDGEMENT

The work reported in this paper was carried out as part of the MEANS program funded by the Air Force Office of Scientific Research (Grant No. F496200110521). We are grateful for their support.

6. REFERENCES

1. G. R. Palmese, Univ. of Delaware Center for Composite Materials, Technical Report Number 92-25, (1992).
2. S. Subramanian, *et al.* J. Composites Materials, 30, 309 (1996).
3. R. W. Rydin, *et al.* J. Composite Materials, 31, 182, (1997).
4. L. T. Drzal, Adv. Polym. Sci., 75, 1 (1986).
5. M. S. Madhukar and L. T. Drzal.. J. Composite Materials, 25, 958 (1991).
6. J. Hrivnak, University of Delaware Center for Composite Materials, Technical Report Number 97-05, (1997).
7. F. Yang and R. Pitchumani, Journal of Applied Polymer Science, in press.
8. F. Yang, Ph. D. Dissertation, University of Connecticut, Department of Mechanical Engineering, (2002).
9. F. Yang and R. Pitchumani, Proceedings of the 12th International Heat Transfer Conference, Vol. 3, September 2002, pp. 153-158.
10. F. Yang and R. Pitchumani, Paper Number 078 in Proceedings (CD-ROM) of 16th Technical Conference of the American Society for Composites, Blacksburg, VA, September 2001.
11. A. Mawardi, Ph. D. Dissertation, University of Connecticut, Department of Mechanical Engineering, (2002).
12. N. Rai and R. Pitchumani, Polymer Composites, 18 (4), 566 (1997).
13. L. Zhu and R. Pitchumani, Composites Science and Technology, 60 (14), 2699 (2000).
14. F. Yang and R. Pitchumani, Composites Science and Technology, submitted.

INFLUENCE OF INTERPHASE MATERIAL PROPERTY GRADIENTS ON THE MICROMECHANICS OF FIBROUS THERMOSETTING-MATRIX COMPOSITES

F. Yang and R. Pitchumani

Composites Processing Laboratory

Department of Mechanical Engineering

University of Connecticut

Storrs, Connecticut 06269-3139

ABSTRACT: Both experimental and theoretical studies in the literature have shown that a fiber surface perturbs its surrounding polymer to create a three-dimensional interphase zone with concentration gradients. The interphase region serves as a buffer between the bulk matrix and fiber, and its properties are critical to the overall composite performance. The concentration gradients in the interphase reflect different local stoichiometric ratios, which may be correlated to material properties (e.g., the modulus) via experimental studies. Micromechanical stress analysis needs the interphase material properties as input information. Since relatively scant information is available on the prediction of interphase concentration gradients as function of processing conditions, the material property profiles in an interphase are not readily determined. Consequently, current micromechanical analyses have resorted to using assumed interphase property profiles. An analysis using the property variation corresponding to an actual interphase composition profile is imperative for a realistic property and performance prediction, and forms the focus of the study. Such an analysis also provides for potentially relating the processing parameters to the composite properties, and in turn, for optimal processing of composites.

KEYWORDS: Interphase formation, Micromechanics, Finite element method, Elastic moduli

INTRODUCTION

Fabrication of thermosetting-matrix composites is based on a critical step of cure, which involves applying predefined temperature cycle to a fiber-resin matrix mixture. The elevated temperatures initiate a crosslinking cure reaction among the species in the matrix. The presence of fibers has been found to significantly influence the cure reaction, resulting in the formation of a third phase known as the interphase which possesses property gradient distinct from those of the bulk fiber and the matrix. The interphase resides in a region between the original constituents of the composite with a size of a few to a few thousand nanometers [1-4]. Although the region has a microscopic scale, it essentially forms a significant portion of the matrix in the composite [1]. Also, the performance of the composite is determined by the ability of the matrix to transfer load to the reinforcing fiber, and is thus controlled by the interphase region. The structure and properties of the interphase are the dominant factors governing the overall composite properties and performance.

Several physical and chemical mechanisms contribute simultaneously to the interphase formation and very few of them have been described rigorously in mathematical models. Garton *et al.* [5] showed that the carbon surfaces influence the cross-linking reaction in an anhydride-epoxy system by adsorbing the tertiary amine catalyst and forming amine rich interphase regions near the carbon surfaces. Similarly, Sellitti *et al.* [6] used Fourier transform IR attenuated total reflection spectroscopy to characterize the

interphase phenomena in an epoxy-anhydride-catalyst system, and showed that the surface species introduced on graphitized carbon fibers can promote or inhibit the cross-linking process by the preferential adsorption of the catalyst. Other possible interphase mechanisms are proposed by Drzal [4].

The effects of interphase property gradients on the overall composite properties are extensively investigated in the literature [7-15, for example]. However, the studies are commonly based on assumed or empirical interphase properties. Tsai *et al.* used an axisymmetricfinite element model to study the interface stress, displacement, and fracture toughness [7]. An elastic shear lag analysis was developed and correlated with the micro-debonding test data to determine the thickness and material properties of the interphase. Boundary element method was adopted by Liu *et al.* to predict transverse moduli of fibrous composites [8]. Tsui *et al.* studied the effects of different interphase properties on Young's modulus, maximum stress concentration factor, and stress distribution in particle-filled polymer composites [9]. Transverse Young's storage/loss moduli and physical aging of a viscoelastic composite with fiber reinforcement were investigated by Fisher and Brinson [10]. All the studies in refs. [8-10] assumed interphase thickness and modulus.

Some empirical relations were proposed to predict the interphase property gradients. By assuming that the rate of change of a property is proportional to the value of the property, the interphase modulus variation with radius, $E_i(r)$, was given as [11,12]:

$$E_i(r) = E_m\left[1+\left(pE_f/E_m-1\right)\frac{1-re^{1-r/r_i}/r_i}{1-r_f e^{1-r_f/r_i}/r}\right] \tag{1}$$

where the subscripts i, m, and f refer to interphase, matrix, and fiber, respectively. The parameter p is called an adhesion factor, which is the ratio between the interphase modulus at $r=r_f$ and the fiber modulus.

$$p = E_i\left(r_f\right)/E_f$$

Similar expressions were applied to other elastic moduli, such as Poisson ratio. Thermal stresses due to the interphase property gradients are predicted by Sottos, *et al.*, where the elastic constants vary *linearly* within the interphase [13]. A power law relation was used by Wacker *et al.* to calculate transverse Young's modulus of composites [14].

$$E_i(r) = \left(\alpha E_f - E_m\right)\left[\frac{r_i - r}{r_i - r_f}\right]^n + E_m \tag{2}$$

where $0 \le \alpha \le 1$\$, and $n = 2,3\cdots$. A review on the empirical interphase models and their feartures was given by Jayaraman *et al.* [15].

Due to complexities of the molecular level mechanisms that occur in the vicinity of the fibers during the process, prediction of the interphase evolution as function of processing parameters from first principles has been the subject of little attention. To the authors' knowledge, the first work on modeling interphase formation in thermosetting materials was presented by Palmese [1]. The model predicted the interphase composition profile under thermodynamic equilibrium conditions of a non-reacting epoxy-amine resin system. Minimum free energy principle was invoked to set up the equilibrium state, accounting enthalpy interaction between fiber surface and resin components, and the calculation of Gibbs free energy was based on a Flory-Huggins type lattice structure. Hrivnak extended Palmese's model to a reacting system by using renewal theory models to the construction of the assembly Gibbs free energy and the associated

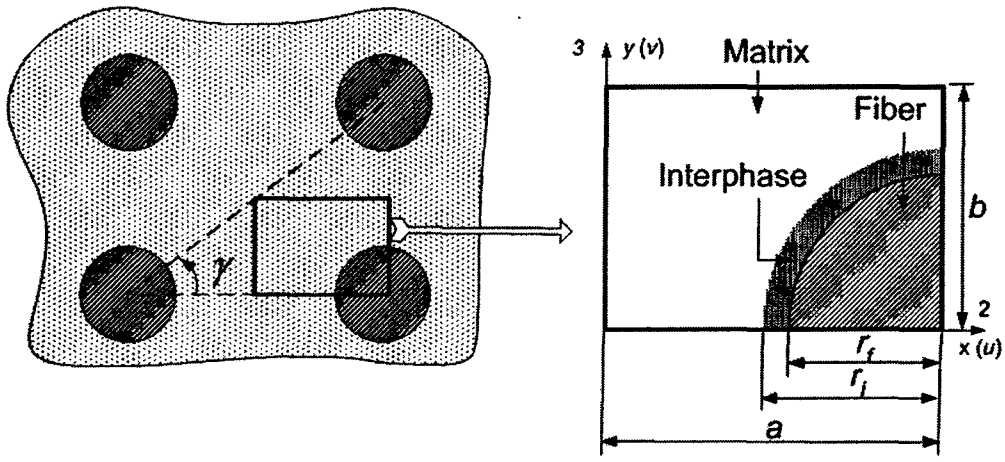

Figure 1 Uint cell considered in the analysis

chemical potential [16]. A kinetics approach is adopted by the authors to predict the interphase development during thermosetting composite processing [17,18]. Mass conservation principle is employed to describe the transport processes of multilayer adsorption, desorption and diffusion near a fiber surface, which are accompanied by simultaneous cure reaction between the resin components. The evolution of interphase concentration profile gradients with time is predicted before the gelation of the thermosetting system.

This paper employs Hrivnak's analytical model to predict the interphase composition profiles, which are subsequently mapped to modulus profiles using an experimental correlation between compositions and moduli. The modulus profiles are used in finite element analyses to calculate the stiffness of fiber reinforced epoxy/amine composites. A commonly used representative volume element (RVE), i.e., the rectangular array in Fig. 1, is adopted in the numerical studies. The effects of several processing parameters on the overall composite modulus are illustrated.

INTERPHASE FORMATION MODEL

To eliminate the need for assumed interphase properties in current micromechanical analyses, the interphase formation model by Hrivnak is adopted to describe the concentration profiles in the interphase region [16]. The model examines the chain/surface and chain/chain interactions of a binary thermosetting resin mixture in the vicinity of a fiber surface. The interaction of a single polymer chain with a surface is described by an analytical molecular partition function, which is incorporated into a sub-lattice model to derive the chain assembly Gibbs free energy. By minimizing the assembly Gibbs free energy, the volume fraction of species *1* at the (*z*)th lattice layer, $v_1(z)$, is obtained as follows.

$$v_1(z) = \kappa v_1(\infty) \underbrace{q(x_1,z)\exp\left[S_1(z)\right]}_{\text{Chain/Surfacne Interaction}} \underbrace{\exp\left[\chi\left(v_2^2(\infty)-v_2^2(z)\right)\right]}_{\text{Chain/Chain Interation}} \underbrace{\exp\left[\frac{\left[v_1(z)-v_1(\infty)\right]}{N_L}(1-x_1/x_2)\right]}_{\text{Excess Mixing}} \tag{3}$$

where

$$q(x_1,z)=1-\sqrt{2/\pi x_1}\left(1-e^{\omega_1/kT}\right)\mathrm{erfc}\left(z/\sigma_1\right) \tag{4}$$

$$S_1(z)=\frac{\omega_1}{kT}\exp\left(\frac{\omega_1}{kT}\right)\sqrt{\frac{2}{\pi x_1}}\mathrm{erfc}\left(\frac{z}{\sigma_1}\right) \tag{5}$$

$$\sigma_1^2=c\frac{x_1 l^2}{3} \tag{6}$$

Similar expressions for species *2* may be obtained by switching the subscripts *1* and *2* in the above equations. The parameter κ is introduced as a normalization constant to ensure that volume fractions $v_1(z)$ and $v_2(z)$ sum to unity, and $v_1(\infty)$ is the volume fraction of species *1* in the far region. Eqs. (4) and (5) show that chain/surface interaction depends on the *surface potential*, ω_1, chain length, x_1, distance of the lattice layer from the surface, z, and the temperature, T. Positive, negative, and zero values of ω_1 correspond to attractive, repulsive, and neutral surfaces to the species *1*, respectively. The second exponential term in Eq. (3) accounts for the chain/chain interaction between the two species in the binary resin mixture, where χ is the *interaction parameter*. For $\chi > 0$, the two species are repulsive to each other. If the surface prefers to adsorb species *1*, positive chain/chain interaction pushes the species *2* further away from the surface, leading to enhanced preferential adsorption on species *1*. The last exponential term in Eq. (3) represents the effect of *excess mixing* causing by different chain lengths (x_1 and x_2) of the species. The quantity N_L is the number of lattice layers of thickness l^0 contained within a sub-lattice, and may be treated as a weighting factor of the *excess mixing*. Note that large values of N_L reduce the effect of *excess mixing*.

Fig. 2 presents a few sample concentration profiles predicted by the above model. The thermosetting mixture consists of an aliphatic bis(p-aminocyclohexyl) methane (PACM20) curing agent and an aromatic diglycidyl ether of bisphenol-A (DGEBA) epoxy resin. Note that the volume fraction of PACM20 is converted to a parts per hundred (i.e., *pph*) concentration, defined as the weight percentage of PACM20 to DGEBA.

$$pph=100\frac{\rho_A v_A}{\rho_E\left(1-v_A\right)} \tag{7}$$

where v_A is the volume fraction of PACM20, and ρ_A and ρ_E are density of PACM20 and DGEBA,

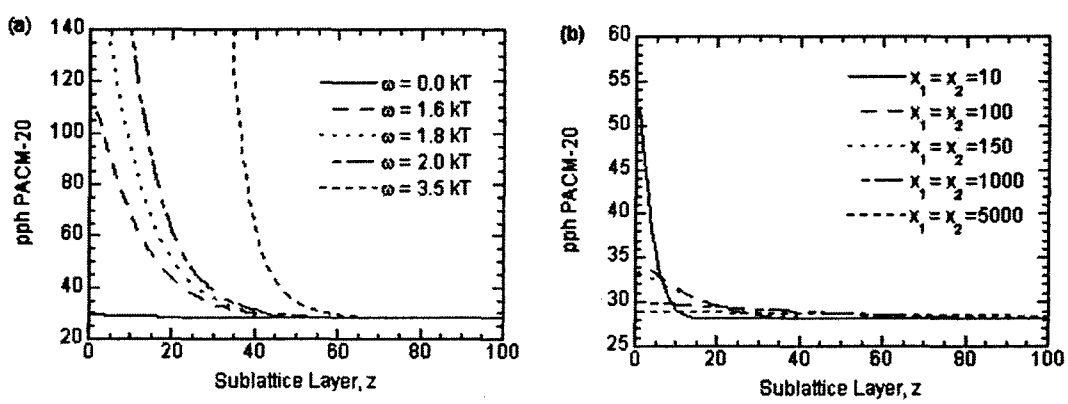

Figure 2 Interphase concentration profile predicted form the model by Hrivnak for different (a) surface potentials, and (b) chain lengths.

respectively. Fig. 2(a) shows the distribution of pph PACM20 from the fiber surface (Layer 0) to the far region (Layer 100) at different surface potentials ω_A. The results correspond to the parameter combination of $\omega_E = -0.28\ kT$, $x_E = x_A = 150$, $\chi = 1.0$, $N_L = 2.5$, as determined by Hrivnak for the DGEBA/PACM20 system [16]. For a neutral surface, the pph PACM20 values near the fiber surface are close to the bulk value of 28. The surface concentrations increase as the surface becomes more attractive to PACM20, and sharp increases are observed for $\omega_A > 1.6\ kT$. As the distance increases, the pph PACM20 decreases asymptotically to the bulk value (28) for all the values of ω_A. Fig. 2(b) presents the effect of chain lengths, following the presentation format of Fig. 2(a), for the parameter combination of $\omega_A = 0.43\ kT$; all other parameters retain the value as in Fig. 2(a). Fig. 2(b) shows that the surface may easily adsorb shorter chains, and the pph concentration at the surface is almost doubled as compared to the bulk value for the case of $x_E = x_A = 10$. However, the magnitudes of the surface concentration increases are not as significant as those in Fig. 2(a). It is also observed that the region perturbed by the surface becomes smaller as the chain length decreases. The discussion on the interphase formation model so far only provides the necessary information for the development of the micromechanical analysis in this paper, the readers are referred to Hrivnak for details [16].

INTERPHASE MODULUS PROFILES

Since matrix modulus is determined by the resin component compositions, the concentration profiles in Fig. 2 may be mapped to modulus profiles. Fig. 3 presents several experimental data on matrix modulus as function of the parameter $X = pph\text{-}1/pph$ for the DGEBA/PACM20 system at 30° [19]. Two peaks of maximal modulus are observed: one around 18 pph PACM20 with a value of 3.2 GPa, and the other between 48 and 56 pph PACM20 having a value of 2.4 GPa. For concentrations between 18 pph and 56 pph, the value of modulus varies about 60%. The modulus drops sharply on both ends of the concentration axis due to the fact that the matrix is in extreme deficit of either resin component and can not be cured sufficiently. Based on these observations, a twin peak function is used to fit the data as follows:

$$E = \frac{1}{(X-19.57)^2/214.42+0.42} + \frac{1}{(X-50.59)^2/803.09+0.47} \tag{8}$$

Eq. (8) has the asymptotic value of 0 as pph approaches 0 and infinity, and it is used in this study to map the concentration profiles, $v_1(z)$ or $v_2(z)$, to modulus profile, $E(r)$. Note that the radius distance from a fiber center, r, may be obtained from the fiber radius, r_f, and the lattice layer, z, as $r = r_f + z\,l^0$.

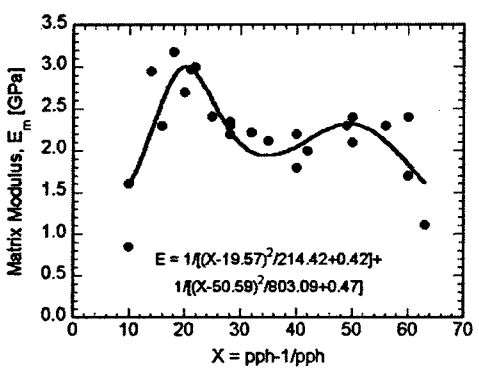

Figure 3 The Young's modulus as a function of stoichiometry for the system DGEBA/PACM20 at 30°C.

The interphase region is typically thin, consequently, most micromechanical models consider only a single uniform interphase layer with thickness δ_i and effective modulus E_i [7-15]. An "interphase thickness" may be defined in a similar way as the boundary layer thickness in fluid mechanics, such as the PACM20 concentration is within 1% of the PACM20 concentration in the far region layers [17,18]. The modulus profile, $E(r)$, may be used to determine the effective interphase modulus as follows [14].

$$E_i = \frac{r_i - r_f}{\int_{r_f}^{r_i} \frac{dr}{E(r)}} \tag{9}$$

The derivation of Eq. (9) is based on a series connection of infinite springs.

FEM ANALYSIS OF LAMINAE TRANSVERSE MODULI

The moduli of an apparent heterogeneous composite lamina (represented by a RVE) are defined as those of an ideal equivalent macroscopic homogeneous medium. The equivalent material is generally anisotropic, and exhibits the same volume and deformation strain energy as the RVE [14,20].

$$V^{eq} = V; \;\; U^{eq} = U \tag{10}$$

where V and U are the volume and strain energy of the RVE, and V^{eq} and U^{eq} are the same quantities for the equivalent material, respectively.

The RVE considered in the present study is shown in Fig. 1, where the cross-sections in the x-y plane are rectangular with length a and height b. To calculate composite moduli, appropriate boundary conditions are essential to model different loading situations [20]. The following boundary conditions are considered to determine transverse longitudinal moduli [14,20].

$$\begin{aligned} u(0,y) = 0; \;\; u(a,y) = \text{constant} = \delta_2 \\ v(x,0) = 0; \;\; v(x,b) = \text{constant} = \delta_3 \end{aligned} \tag{11}$$

where u and v denote displacement in the x and y directions, respectively.

The strain energy of the *equivalent material* subject to the loading conditions in Eq. (11) is as follows

$$U^{eq} = \frac{1}{2}\int_v C_{ij}\Phi_i\Phi_j dV = \frac{1}{2}C_{ij}\Phi_i\Phi_j V$$

where C_{ij} are the components of stiffness matrix of the *equivalent material*, and Φ_i and Φ_j are macrostrains in the contracted notations. Note that the macrostrains are constants within the homogeneous *equivalent material*. Similarly, the strain energy of the RVE may be written as:

$$U = \frac{1}{2}\int_v c_{ij}\varepsilon_i\varepsilon_j dV$$

where the stiffnesses, c_{ij}, and the microstrains ε_i and ε_j are functions of locations in the RVE. The RVE strain energy U is computed using ABAQUS V6.3, a commercial finite element package. Substituting the above two expressions into Eq. (10) yields

$$\frac{1}{2}C_{ij}\Phi_i\Phi_j V = \frac{1}{2}\int_v c_{ij}\varepsilon_i\varepsilon_j dV \tag{12}$$

By introducing sufficient number of admissible deformation states of the RVE, Eq. (12) may be used repetitively to form a set of linear algebraic equations which, in turn, can be used to determine all the stiffnesses of the *equivalent* (or composite) material.

Three deformation states are configured by specifying the following requirements for the boundary conditions in Eq. (11).

$$\begin{aligned} &\text{state I}: \quad \delta_2 \neq 0, \quad \delta_3 = 0 \\ &\text{state II}: \quad \delta_2 \neq 0, \quad \delta_3 \neq 0 \\ &\text{state III}: \quad \delta_2 = 0, \quad \delta_3 \neq 0 \end{aligned} \tag{13}$$

The macrostrains in the *equivalent material* corresponding to the deformation states are

$$\begin{aligned} &\text{state I}: \quad \Phi_2^I = \frac{\delta_2}{a}, \quad \Phi_3^I = 0, \quad \Phi_{23}^I = 0 \\ &\text{state II}: \quad \Phi_2^{II} = \frac{\delta_2}{a}, \quad \Phi_3^{II} = \frac{\delta_3}{b}, \quad \Phi_{23}^{II} = 0 \\ &\text{state III}: \quad \Phi_2^{III} = 0, \quad \Phi_3^{III} = \frac{\delta_3}{b}, \quad \Phi_{23}^{III} = 0 \end{aligned} \tag{14}$$

where the subscripts *2* and *3* correspond to the directions x and y, respectively, as shown in Fig. 1. Combining Eqs. (12) and (14) yields

$$\begin{aligned} &\text{state I}: \quad \frac{1}{2} C_{22} \left(\Phi_2^I\right)^2 V = U_I \\ &\text{state II}: \quad \frac{1}{2}\left[C_{22}\left(\Phi_2^{II}\right)^2 + C_{23}\Phi_2^{II}\Phi_3^{II} + C_{33}\left(\Phi_3^{II}\right)^2\right] V = U_{II} \\ &\text{state III}: \quad \frac{1}{2} C_{33} \left(\Phi_3^{III}\right)^2 V = U_{III} \end{aligned} \tag{15}$$

where U_I, U_{II}, U_{III} are the strain energies of the RVE (obtained from FEM analysis) for deformation states *I*, *II* and *III* respectively. Eq. (15) may be used to solve the stiffnesses C_{22}, C_{23}, and C_{33}, which, in turn, are used to determine transverse longitudinal moduli of composite laminae.

In this study, a lamina is consider to be an orthotropic material, and has two independent transverse longitudinal moduli, E_2 and E_3 (Fig. 1). Under plain stress conditions, the relationships between the stiffnesses and the elastic constants are [21,22]:

$$C_{22} = \frac{E_2}{1 - \nu_{23}^2 E_3 / E_2}; \; C_{22} = \frac{\nu_{23} E_3}{1 - \nu_{23}^2 E_3 / E_2}; \; C_{33} = \frac{E_3}{1 - \nu_{23}^2 E_3 / E_2} \tag{16}$$

where ν_{23} is Poisson's ratio. The solutions of the elastic constants in Eq. (16) are

$$E_2 = C_{22}\left[1-\frac{C_{23}^2}{C_{22}C_{33}}\right];\ E_3 = C_{33}\left[1-\frac{C_{23}^2}{C_{22}C_{33}}\right];\ \nu_{23} = C_{22}/C_{33} \tag{17}$$

RESULTS

The finite element predictions of the composite elastic moduli based on Eqs. (15) and (17) are compared with calculations by Wacker *et al.* [14] at different interphase moduli, as shown in Table 1. It must be pointed out that the assumption of transverse isotropic is used in ref. (14), which is a special case of orthotropic medium considered in this study. By setting the array angle γ to 45°, the orthotropic solutions are reduced to the corresponding transverse isotropic solutions (E_2 = E_3). The RVE used in the comparison study is a rectangular array (γ= 45°) with 50% fiber volume fraction. The properties and the geometries of the constituent materials, Epoxy/E-glass, are:

$$E_f = 84\text{GPa}; \nu_f = 0.22; r_f = 8.5\mu m$$
$$E_m = 4\text{GPa}; \nu_m = \nu_i = 0.34; r_i = 9.5\mu m$$

Current finite element analysis uses eight-noded quadratic plane stress elements, and mesh convergence studies are conducted to ensure correct modulus values. Good agreement between the FEM predictions and the literature results is observed for all the values of the interphase modulus studied.

Table 1 Interphase effect on the transverse elastic modulus of an epoxy/E-glass composite lamina

E_i GPa	Present FEM	Wacker *et al.* [14]
4	12.15	12.25
6	13.70	13.71
8	14.66	14.68
12	15.79	15.91

With the validated FEM formulation as basis, effects of the processing parameters on the composite modulus are described in the following discussion. An examination of the interphase formation model shows that the following processing parameters are of primary interests: (1) surface potentials for chain/surface interaction, ω_A and ω_E, (2) interaction parameter for chain/chain interaction, χ, (3) lattice layer thickness, l^o, (4) number of lattice layer within a sub-lattice, N_L, and (5) chain lengths, x_E and x_A. The DGEBA/PACM20 thermosetting system is considered in the parametric studies, however, all the analyses are readily extended to a general two-component thermosetting system. At the stoichiometric point (28 pph PACM20), the modulus of the DGEBA/PACM20 system, E_m, has a value of 2.3 GPa. The interphase modulus profiles are obtained by combining Eqs. (3) and (8), and effective interphase modulus, E_i, is calculated from Eq. (9). Relevant numerical results are presented for the first time where composite stiffness is directly linked to the processing parameters without assumed structures or properties of the interphase. The results provides guidlines for selecting material components and processing temperatures to achieve desired overall composite properties.

Fig. 4(a) shows the dimensionless composite transverse Young's modulus, E_2/E_m, as a function of fiber modulus ratio, E_f/E_m at different surface potentials ω_A. The results correspond to a parameter combination of v_f= 0.5, γ= 45°; all other parameters retain the value as in Fig. 2(a). For the case of ω_A = 0, the fiber surface is neutral to PACM20, and its concentration near the surface is almost identical to that of the far region [see Fig. 2(a)]. Consequently, the composite material is similar to a two components (fiber and matrix) system without distinct interphase regions. When E_f/E_m = 1, the curve starts at E_2/E_m= 1 since the

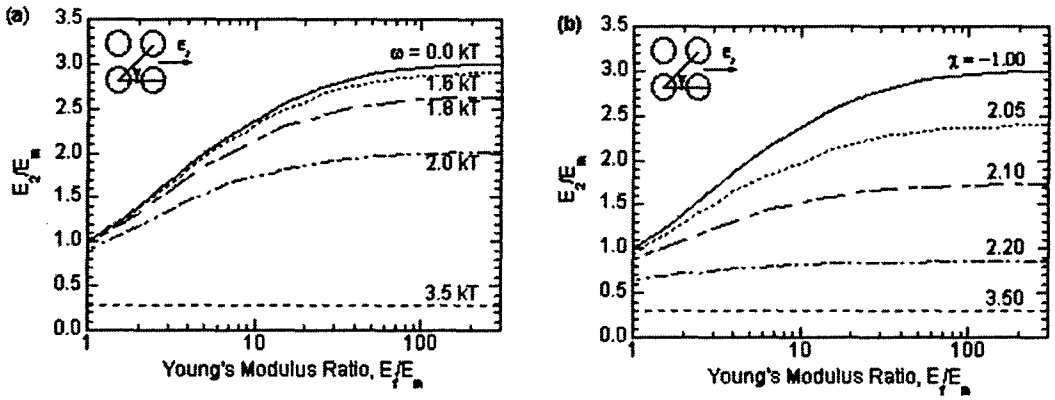

Figure 4 Transverse Young's modulus of composite as a function of the ratio Ef/Em for different (a) surface potentials, and (b) chain/chain interactions.

material is essentially homogeneous. The composite modulus is seen to increase with increasing fiber modulus, as physically expected. However, the increase rate of E_2 slows down at larger E_f values; as $E_f \rightarrow \infty$, E_2 approaches an asymptotic value, which is obtained from an ideal rigid body reinforcement.

Interphases richer in PACM20 are developed as ω_A increases. When ω_A increases from 0 to 1.6 kT, the pph PACM20 at the fiber surface increases from 28 to 115, while the interphase modulus E_i decreases 38 percent from 2.30 GPa to 1.43 GPa. Since the interphase thickness is thin (about 0.12 microns), the composite modulus has only slight decrease. Further increases of surface potential to 1.8 kT and 2.0 kT yield sharp decreases of E_i to 0.67 GPa and 0.24 GPa, respectively, and significant decreases of the E_2 are observed. As ω_A = 3.5 kT, the interphase almost consists of pure PACM20, which corresponds to a near zero value of E_i. In this case, the composite modulus is close to that of a matrix with holes, and the influence of the fiber is negligible. In Fig. 4(b), the influence of the chain/chain interaction, χ, on the composite modulus is demonstrated. The result corresponds to ω_A = 0.43 kT, with all the other parameters retain their values in Fig. 4(a). Recall that positive chain/chain interaction enhances the preferential adsorption on PACM20, therefore, the influence of χ is similar to that of surface potential ω_A. Discussions on Fig. 4(b) follow those in Fig. 4(a), and are omitted here for brevity.

The influence of other parameters on the overall composite properties can be discussed in similar ways and detailed discussion will be presented in a future publication. In this paper, the interphase formation is predicted by a thermodynamic approach, where the temperature is taken as a given constant. For nonisothermal cure processes, the real temperature field needs to be solved by considering the energy equation written for the whole composite domain, and the kinetics model is to be coupled with the energy equation to predict the interphase evolution and the final composite properties.

CONCLUSION

An interphase formation model obtained from first principles is adopted to predict the stiffness of a fibrous composite, eliminating the need for assumed interphase properties. Processing parameters such as the surface potentials and chain/chain interaction are directly linked for the first time to the overall composite properties. Parametric studies on DGEBA/PACM20 thermosetting composites reveal that transverse stiffness of the composites strongly depends on the chain/surface and chain/chain interactions. The transverse Young's modulus shows a monotonic decrease as surface potential ω_A or interaction parameter χ increase, due to softer interphases with higher PACM20 concentration.

ACKNOWLEDGMENTS

The work reported in this paper was funded in part by the National Science Foundation (Grant No. CTS-9912093) and the Air Force Office of Scientific Research (Grant No. F496200110521). We are grateful to Prof. P. Zhang and Mr. W. Xie of University of Connecticut for their suggestions on finite element modeling.

REFERENCES

1. Palmese GR. Origin and influence of interphase material property gradients in thermosetting composites.University of Delaware Center for Composite Materials, Technical Report Number 92-25, 1992.
2. Subramanian S, Lesko JJ, Reifsnider KL, Stinchcomb WW. Characterization of the fiber-matrix interphase and its influence on mechanical properties of unidirectional composites. *Journal of Composites Materials* 1996;30:309--32.
3. Rydin RW, Varelidis PC, Papaspyrides CD, Karbhari VM. Glass fabric vinyl-ester Composites: tailoring the fiber bundle/matrix interphase with nylon coating to modify energy absorption behavior. *Journal of Composite Materials* 1997;31:182--209.
4. Drzal LT. The interphase in epoxy composites. *Advances in Polymer Sciences* 1986;75:1--32.
5. Garton A, Stevenson WTK, Wang S. Interfacial reactions in carbon-epoxy composites. *British Polymer Journal* 1987;19:459--67.
6. Sellitti C, Koenig JL, Ishida H. Surface characterization of carbon fibers and interphase phenomena in epoxy-reinforced composites. *Materials Science and Engineering* 1990;A126:235--44.
7. Tsai HC, Arocho AM, Gause LW.Prediction of fiber-matrix interphase properties and their influence on interface stress, displacement and fracture toughness of composite material. *Materials Science and Engineering* 1990;A126:295--304.
8. Liu YJ, Xu N, Luo JF. Modeling of interphases in fiber-reinforced composites under transverse loading using the boundary element method. *Journal of Applied Mechanics* 2000;67:41--9.
9. Tsui CP, Tang CY, Lee TC. Finite element analysis of polymer composites filled by interphase coated particles. *Journal of Materials Processing Technology* 2001;117:105--10.
10 Fisher FT, Brinson LC. Viscoelastic interphases in polymer-matrix composites: theoretical models and finite-element analysis. *Composites Science and Technology* 2001;61:731--48.
11. Papanocolaou GC, Michalopoulou MV, Anifantis NK. Thermal stresses in fibrous composites incorporating hybrid interphase regions. *Composites Science and Technology* 2002;62:1881--194.
12. Anifantis NK. Micromechanical stress analysis of closely packed fibrous composites. *Composites Science and Technology* 2000;60:1241--48.
13. Sottos NR, McCullough RL, Guceri SI. Thermal Stresses due to property gradients at the fiber/matrix interface.in Mechanics of Composites Materials and Structures, Reddy JN, Teply JL eds., *American Society of Mechanical Engineers*, 1989;11--20.
14. Wacker G, Bledzki AK, Chate A. Effect of interphase on the transverse Young's modulus of glass/epoxy composites. *Composites Part A* 1998;29A:619--26.
15. Jayaraman K, Reifsnider KL, Swain RE. Elastic and thermal effects in the interphase: part II. comments on modeling studies. *Journal of Composites Technology & Research* 1993;15:14--22.
16. Hrivnak J. Interphase formation in reacting systems. University of Delaware Center for Composite Materials, Technical Report Number 97-05, 1997.
17. Yang F, Pitchumani R. A kinetics model for interphase formation in thermosetting-matrix composites. *Journal of Applied Polymer Science* in press.
18. Yang F. Investigations on interface and interphase development in polymer-matrix composite materials. Ph. D. Dissertation, University of Connecticut, Department of Mechanical Engineering, 2002.
19. VanLandingham MR, Eduljee RF, Gillespie JW Jr. Relationships between stoichiometry, microstructure, and properties for amine-cured epoxies. *Journal of Applied Polymer Science* 1999;71:699--712.
20. Sun CT, Vaidya RS. Prediction of composite properties from a representative volume element. *Composites Science and Technology* 1996;56:171--9.
21. Yu YY. Vibrations of elastic plates: linear and nonlinear dynamical modeling of sandwiches, laminated composites, and piezoelectric layers. Springer-Verlag New York, Inc. 1996.
22. Jones RM. Mechanics of composite materials. Taylor & Francis, Inc. 1999.

CHARACTERIZATION OF THE INTERPHASE FORMATION KINETICS IN THERMOSETTING-MATRIX COMPOSITES

F. Yang and R. Pitchumani*
Composites Processing Laboratory
Department of Mechanical Engineering
University of Connecticut
Storrs, Connecticut 06269-3139
*Corresponding Author

ABSTRACT

The cure kinetics of thermosetting resins is affected by the presence of the reinforcement, which leads to the formation of an interphase region in the vicinity of the fiber. The structure and the properties of the interphase are critical factors to the overall composite performance. A kinetics model for interphase formation has been developed by the authors to determine the concentration and properties profiles near the fiber surface. In this paper, two approaches are presented for the estimation of the model parameters: one based on direct measurements of the nanoscale interphase composition and the other based on measured property variations near a fiber surface using micro-interferometry and nano-indentation tests. Characterization of the kinetics parameters provides the critical information for establishing processing-property relationships, which, in turn, provide for optimizing cure cycles to obtain tailored interphase in the composite materials. The estimated parameter values are reported for AS4, copper, graphite, and aluminum fibers in epoxy/amine curing agent systems.

KEY WORDS: Polymer Matrix Composites, Process Modeling, Interphase Kinetics, Curing of Polymers

1. INTRODUCTION

During the cure of thermosetting polymer composites, the presence of reinforcing fibers significantly alters the resin composition in the vicinity of the fiber surface via several microscale processes, forming an interphase region with different chemical and physical properties from the bulk resin. The interphase resides in a region between the original constituents of the composite with a size of one to a few thousand nanometers (1–5). The performance of the composite is determined by the ability of the matrix to transfer load to the reinforcing fiber, and is thus controlled by the interphase region. The structure and properties of the interphase are the dominant factors governing the overall composite properties and performance.

Due to complexities of the molecular level mechanisms that occur in the vicinity of the fibers during the processing, prediction of the interphase evolution as function of processing parameters has been the subject of little attention. Palmese (1) presented a model for predicting the interphase composition profile under thermodynamic equilibrium conditions of a non-reacting epoxy-amine resin system. The principle of minimum free energy was invoked to set up the equilibrium state, accounting for enthalpy interaction between fiber surface and resin components, and the calculation of Gibbs free energy was based on a Flory-Huggins type lattice structure. Hrivnak (6) extended Palmese's model to a reacting system by using renewal theory models to the construction of the assembly Gibbs free energy and the associated chemical potential. In an alternative approach, a kinetics-based description of the governing phenomena was developed by the authors to predict the interphase development during thermosetting composite processing (7–10). In this method, mass conservation principle was employed to describe the transport processes of multilayer adsorption, desorption and diffusion near a fiber surface, which are accompanied by simultaneous cure reaction between the resin components. The time evolution of interphase concentration profile gradients before the gelation of the thermosetting system was predicted as function of material and process parameters.

The goal of this work is to systematically determine the parameters in the kinetics model of the interphase formation for typical thermosetting composite systems, which provide critical information to establish the complete processing-interphase-properties relationship. To this end, two approaches are explored based on the type of available experimental data. In one approach, the amine concentration profile measured near a fiber surface by electron energy loss spectroscopy (11) is used to correlate to the model, and thereby determine the model parameters. In a second approach, two experimental data that implicitly contain the interphase concentration information are investigated. First, the modulus variations near a fiber surface obtained through nano-indentation tests (12) are used to determine the effective interphase thickness δ_i and modulus E_i via numerical simulations of indentation tests on equivalent fiber-interphase-matrix composite systems. In an alternative approach, values of δ_i and E_i may be obtained via interferometry tests (13). The values of δ_i and E_i obtained using either of the two methods are, in turn, used together with an empirical interphase concentration-modulus mapping to determine the kinetics parameters. The model is briefly reviewed in the next section to identify the critical microscale phenomena and parameters during the interphase formation process. The details of the experimental data and the correlation results for several composite systems are discussed in Section 3.

2. INTERPHASE FORMATION MODEL

Cure of thermosetting resin systems is characterized by the reaction between prepolymer (or monomer) molecules and a curing agent to form a crosslinked network that can not flow upon vitrification. The reinforcing fibers alter the cure characteristic by selective adsorption of resin components, which changes the concentration of the reacting species in the vicinity of the fiber surfaces. The goal of the present study is to predict the concentration profiles of the constituent species near the fiber surface by considering the processes that occur in the cure reaction. An inorganic fiber/epoxy-amine thermosetting system is considered in the following discussion; however, all the derivations and results are applicable to a general two-component thermosetting system.

The geometry considered in the cure kinetics model is the inter-fiber space in a composite having a typical staggered fiber arrangement (7–10). The domain in the model development is idealized as the region between two identical infinite planes representing the fiber surfaces (7–10), which may be justified by the fact that the interphase thickness is often small in comparison to the fiber diameter. The domain between the two fiber surfaces is divided into molecular layers such that there are N_L layers in the half domain, Each layer is further discretized along the fiber direction, and molecule of epoxy or amine can occupy only one of these discretized cells (7–10).

Due to the interaction between resin molecules and the fiber surface, as well as those among resin molecules themselves, epoxy and amine molecules can move from layer to layer. The solid surface can adsorb molecules from a "bulk" state into an "adsorbed" state, and conversely, molecules in the "adsorbed" state may be desorbed into the "bulk" state. Molecules in the "adsorbed" state are treated to be fixed in the space and are not permitted to diffuse, while molecules in the "bulk" state may diffuse within the resin mixture. Chemical reaction between epoxy (E) and amine (A) happens simultaneously during the adsorption, desorption and diffusion processes, resulting in a continuously evolving concentration profile that is "frozen" in space upon gelation of the thermosetting system. The reaction equation may be written as

$$n_1 E + n_2 A \rightarrow P \tag{1}$$

where P denotes the product and n_1 and n_2 are the molar numbers of the reactants needed to produce 1 mol of product.

The mass balance for the epoxy molecules in the "adsorbed" state in any (i)th molecular layer yields (7–10):

$$\underbrace{\frac{dN_{E,i}}{dt}}_{storage} = \underbrace{R_{a,E}(i-1,i) + R_{a,E}(i,i) + R_{a,E}(i+1,i)}_{adsorption,\ R_{a,E}(i)} - \underbrace{R_{d,E}(i-1,i) - R_{d,E}(i,i) - R_{d,E}(i+1,i)}_{desorption,\ R_{d,E}(i)} \underbrace{- R_{r,E}(i)}_{depletion\ (reaction)} \tag{2}$$

In Eq. (2), $dN_{E,i}/dt$ is the rate of change of total number of epoxy molecules in the (i)th adsorption layer, and the subscripts E and i denote epoxy and (i)th layer, respectively. Epoxy molecules in the "bulk" state in the (i-1)th, (i)th, and (i+1)th layers may be adsorbed into the (i)th molecular layer, denoting by the rate terms $R_{a,E}(i-1,i)$, $R_{a,E}(i,i)$, and $R_{a,E}(i+1,i)$ respectively; in a reverse process, the adsorbed epoxy molecules in the (i)th layer can also be desorbed into the bulk in the (i-1)th, (i)th, and (i+1)th layers through the rate terms $R_{d,E}(i-1,i)$, $R_{d,E}(i,i)$, and $R_{d,E}(i+1,i)$; further, the depletion of epoxy in the (i)th adsorption layer through chemical reaction is determined by the rate term $R_{r,E}(i)$. The expressions of the rate terms and the mass conservation analysis to the amine and product in the adsorbed state (i.e., $N_{A,i}$ and $N_{P,i}$) may be discussed in a similar way, and the readers are referred to refs. (7–10) for details.

The adsorbed state exchanges mass with the bulk state, in which the molecules undergo diffusion in addition to the adsorption, desorption, and reaction processes. The mass balance for the epoxy molecules in the bulk state in any (i)th molecular layer yields (7–10):

$$
\begin{aligned}
\frac{dN_{E\infty,i}}{dt} = & \frac{D_{EA}}{\Delta L^2}\left(N_{E\infty,i+1}\frac{N_0-N(i)}{N_0}-N_{E\infty,i}\frac{N_0-N(i+1)}{N_0}\right)+\frac{D_{EA}}{\Delta L^2}\left(N_{E\infty,i-1}\frac{N_0-N(i)}{N_0}-N_{E\infty,i}\frac{N_0-N(i-1)}{N_0}\right) \\
& +R_{d,E}(i,i-1)+R_{d,E}(i,i)+R_{d,E}(i,i+1)-R_{a,E}(i,i-1)-R_{a,E}(i,i)-R_{a,E}(i,i+1)-n_1k_rN_{E\infty,i} \\
& +\sum_{j=i-1,i+1}\left[\frac{N_{E\infty,j}}{N_{\infty,j}}\left(R_{d,E}(j,i)+R_{d,A}(j,i)+R_{a,E}(i,j)+R_{a,A}(i,j)\right)\right] \\
& -\frac{N_{E\infty,i}}{N_{\infty,i}}\sum_{j=i-1,i+1}\left[\left(R_{a,E}(j,i)+R_{a,A}(j,i)+R_{d,E}(i,j)+R_{d,A}(i,j)\right)\right]
\end{aligned}
\tag{3}
$$

where the mutual diffusion coefficient D_{EA} in the binary epoxy-amine mixture is a function of temperature T and cure extent ξ (7–10), ΔL corresponds to the physical size of a molecular layer, and k_r is the reaction rate. The terms in the last two lines of Eq. (3) account for the constant number density assumption, and the diffusion terms are derived to consider the blockage effect of the adsorbed molecules (8).

The subscripts E and A in Eq. (3) may be switched to obtain the rate equation for $N_{E\infty,i}$, and the equation for $N_{P\infty,i}$ follows that in ref. (7). The symmetry of the geometry between two identical fiber surfaces suggests the following conditions:

$$
\begin{aligned}
&[\text{adsorbed state}]\ N_{E,N_L}=N_{E,N_L+1};N_{A,N_L}=N_{A,N_L+1};N_{P,N_L}=N_{P,N_L+1} \\
&[\text{bulk state}]\ N_{E\infty,N_L}=N_{E\infty,N_L+1};N_{A\infty,N_L}=N_{A\infty,N_L+1};N_{P\infty,N_L}=N_{P\infty,N_L+1}
\end{aligned}
\tag{4}
$$

For a thermosetting system with fiber sizing thickness of N_S molecular layers, the initial conditions of the species rate equations are: (1) the numbers of molecules for each species in the adsorbed state and the number of product in the bulk state are zero, (2) within the epoxy sizing layer, the number of epoxy is a constant, $N_{E,1}$, while the number of amine is zero, and (3) beyond the sizing layer, the numbers of epoxy and amine species are constants, $N_{E,0}$ and $N_{A,0}$, respectively. The mathematical expressions for the initial conditions may be written as:

$$
\begin{aligned}
& N_{E,i}=N_{A,i}=N_{P,i}=N_{P,\infty};\ \left(i=1,2,\cdots,N_L\right) \\
& N_{E\infty,i}=N_{E,1};N_{A\infty,i}=0;\ \left(i=1,2,\cdots,N_S\right) \\
& N_{E\infty,i}=N_{E,0};N_{A\infty,i}=N_{A,0};\ \left(i=N_S+1,\cdots,N_L\right)
\end{aligned}
\tag{5}
$$

For a given temperature history, the microscale cure kinetics model [Eqs. (2)–(5)] may be used to predict the concentration profiles [e.g., $N_{E,i}$, $N_{A,i}$] evolution with time near a fiber surface.

The concentration profiles predicted by the kinetics model may be further mapped to modulus profiles using a correlation of matrix modulus as a function of concentration (14). Since the interphase region is typically thin (around 10-500 nm), most experimental or theoretical analyses consider only a single uniform interphase layer with effective thickness δ_i and modulus E_i. An "interphase thickness" may be defined as that distance from the fiber surface where the amine concentration is within 1% of the amine concentration in the far region layers. The modulus profiles within the interphase thickness are averaged to determine the effective interphase modulus E_i (14). The relationship between concentration profile and the effective interphase thickness and modulus forms the basis for extracting the kinetics parameters for given values of δ_i and modulus E_i.

3. RESULTS AND DISCUSSION

The model reviewed in the previous section is used to calculate the molar concentration profiles (or modulus profiles and effective interphase thickness and modulus for given composition-modulus mapping) under isothermal conditions, $T = T_0$, where T_0 is the isothermal temperature at which the cure process takes place. It must be pointed out that all the composite systems discussed in this paper are cured with an isothermal temperature $T_0 = 80°C$. The kinetics model is correlated to experimental data on the interphase concentration profiles or moduli to determine the parameters of the model. A thermosetting resin system consisting of an aliphatic bis(p-aminocyclohexyl) methane (PACM20) curing agent and an aromatic diglycidyl ether of bisphenol-A (DGEBA) epoxy resin is considered in this study. The properties of the resin components and experimental data on matrix modulus as a function of the component concentration are reported in the literature (1, 14). In this section, the two approaches introduced in section 1 are adopted respectively to determine the parameters of the kinetics model for several composite systems.

In the first approach, the involved experimental data is the interphase concentration profile of an Aluminum/DGEBA/PACM20 system measured by Arayasantiparb et al. (11) using spatially resolved electron energy-loss spectroscopy (EELS) in a scanning transmission electron microscope (STEM). An optimization program implementing the simulated annealing method (7) was used to minimize the objective function that defines the sum of the squares of the difference between the model prediction of the composition profile and the experimental data from Arayasantiparb *et al.* (11). The objective functions are governed by six independent variables, namely, the diffusivity scaled by ΔL^2 at temperature $T = 80°C$ and cure extent $\xi = 0$, $D_{EA,ref}/\Delta L^2$; the reaction parameter, $k_{r0}\exp(-E_a/RT)$; and the adsorption and desorption rate parameters, $k_{a,E}\exp(-E_{a,E}/RT)$, $k_{d,E}\exp(-E_{d,E}/RT)$, $k_{a,A}\exp(-E_{a,A}/RT)$, and $k_{d,A}\exp(-E_{d,A}/RT)$, where $k_{a,A}$ is the adsorption rate of amine molecules, $E_{a,A}$ is the adsorption activation energy of amine molecules, $k_{d,A}$ is the desorption rate of amine molecules, $E_{d,A}$ is the desorption activation energy of amine molecules. The interested readers are referred to the literature for details on the optimization technique (7).

Figure 1 shows the correlation results in terms of the PACM20 volume fraction at the gelation time as a function of distance from the aluminum wire surface. The dashed line denotes the experimental data from Arayasantiparb *et al.* (11), while the solid line corresponds to model prediction. Recall that the mass transfer through the adsorption, desorption, and diffusion processes is dramatically slowed when the reacting resin system reaches the gelation point, and the final concentration profiles can be approximated by the profiles at the gelation point. It is seen that the prediction follows closely to the data over the entire range. The concentration of PACM20 in terms of a percentage volume, is seen to be a large value of 80% at the aluminum surface, indicating a preferential adsorption on the species, and decreases sharply away from the fiber surface. In the region beyond 100 *nm*, experimental measurements were not reported, and Arayasantiparb *et al.* (11) state that the concentration is a constant bulk value of 25%. It is noted from Figure 1 that the model predicts a decrease in the concentration to 22% before the recovery of the bulk concentration at 25%. The model prediction points to the fact that the mass aggregation in the region 0–100 *nm* must be compensated by the mass deficit beyond the region. However, the deficit may be too small to be discerned in the experimental technique.

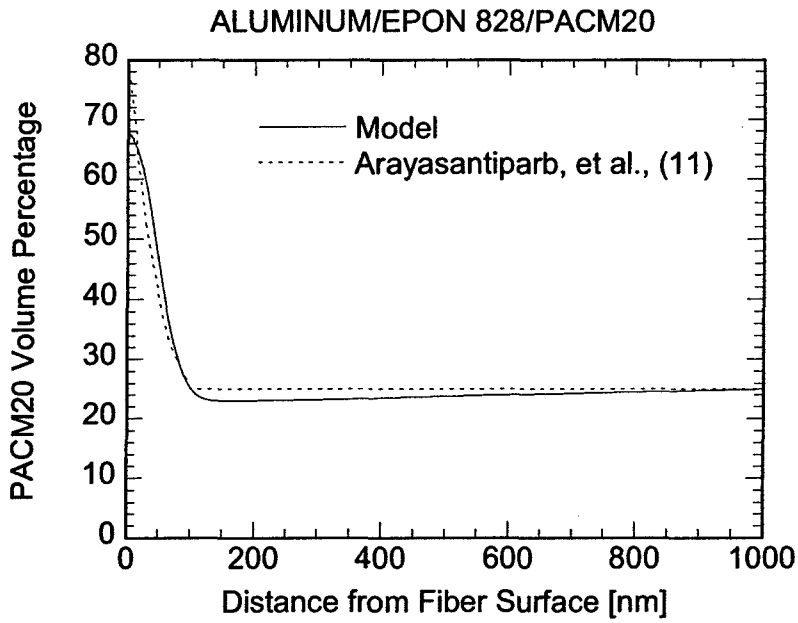

Figure 1 Comparison of the interphase composition profile predicted by the kinetics model and available experimental data for an Aluminum/EPON 828/PACM20 system. The parameters of the kinetics model are obtained from a correlation of the model to the data.

The values of the kinetics parameters obtained from the correlation study in Fig. 1 are presented as the 2nd column in Table 1. The following observations are obtained for the values of the parameters: (a) the adsorption rate of DGEBA, $k_{aE}\exp(-E_{aE})/RT$, is two orders of magnitude smaller than its desorption rate, $k_{dE}\exp(-E_{dE})/RT$, indicating that the aluminum surface does not have affinity with the DGEBA molecules, (b) the adsorption rate of PACM20, $k_{aA}\exp(-E_{aA})/RT$, is about two orders of magnitude larger than its desorption rate, $k_{dA}\exp(-E_{dA})/RT$, denoting a preferential adsorption on the PACM20 species as reported by Arayasantiparb *et al.*, (c) the value of reaction rate, $k_{r0}\exp(-E_a)/RT$, is similar to that reported by Sanford (15), and (d) the value of diffusivity determined by the parameters $D_{EA,ref}$ is roughly an order of magnitude larger than that reported by Sanford (15). It is seen that in most cases the fitting results are consistent with the data in the literature.

Table 1 Kinetics parameters determined from the correlation studies.

Parameter [s^{-1}] \ Fiber	Aluminum	Graphite	Sized Copper	Sized AS4	Unsized AS4
$k_{aE}\exp(-E_{aE}/RT)$	5.00×10^{-3}	3.80×10^{-3}	4.30×10^{-3}	3.25×10^{-3}	2.90×10^{-3}
$k_{aA}\exp(-E_{aA}/RT)$	0.49	0.37	0.14	0.07	0.08
$K_{dE}\exp(-E_{dE}/RT)$	0.23	0.12	0.27	0.17	0.18
$K_{dA}\exp(-E_{dA}/RT)$	0.01	0.03	0.90×10^{-3}	0.93×10^{-3}	0.70×10^{-3}
$D_{EA,ref}/\Delta L^2$	6.00×10^{4}	6.00×10^{4}	5.00×10^{3}	2.10×10^{4}	6.00×10^{4}
$K_{r0}\exp(-E_a/RT)$	1.00×10^{-4}	1.00×10^{-4}	0.90×10^{-4}	0.93×10^{-4}	1.00×10^{-4}

For the experimental data that do not explicitly contain concentration profiles, the second approach is adopted to conduct the correlation studies in two steps. First, the data are used to derive the effective interphase thickness and modulus via analytical or numerical methods. Next, the objective function used in the optimization program is modified to be the sum of the squares of the difference between the model prediction of the effective interphase thickness and modulus as function of the kinetics parameters and the derived E_i and δ_i values from experiments. The kinetics parameters are determined so as to minimize the error in a least square sense. In the present study, the experimental data from Sottos et al. (13) and VanLandingham *et al.* (12) are used to determine the kinetics parameters for four fiber/resin/sizing combinations.

Sottos *et al.* (13) reported a nondestructive interferometric method to measure the thermal displacement of a Graphite/DGEBA/PACM20 system near the graphite fiber surface. An elasticity solution was also introduced for a three phase cylindrical composite consisting of concentric fiber, interphase and bulk matrix region. The analytical elasticity solutions were compared with the experimental displacement data, and the effective interphase modulus and thickness were found to be 0.045 *GPa* and 0.87 *nm*, respectively (13). In another experimental investigation, the indenting capability of the atomic force microscope (AFM) was untilized by VanLandingham *et al.* (12) to measure the apparent modulus profiles in the vicinity of several inorganic fiber surfaces. Since the indent deformation near a fiber is significantly restricted by the presence of the much stiffer fiber, the measured modulus (i.e., apparent modulus) is consistently larger than the intrinsic modulus of the material. The effective interphase modulus and thickness are determined from the apparent modulus profiles using a finite element analysis as presented below.

For the contact problem between a rigid indenter and an elastic half-space, contact mechanics yields the relationship between the indentation load, P, and the indentation depth, z, as (16):

$$P = \frac{2rzE}{m\left(1-\nu^2\right)} \tag{6}$$

where m is a constant depending on the indenter geometry, r is the contact radius, and E and ν are the apparent elastic modulus and Poissons ratio, respectively. Using Eq. (6) at two different locations on a single sample, the ratio of local apparent modulus values, E and E_{ref}, is related to the ratios of the contact loads, radii and displacements as:

$$\frac{E}{E_{ref}} = \frac{P}{P_{ref}} \bullet \frac{r_{ref} z_{ref}}{rz} \tag{7}$$

where the subscript *ref* denotes a reference location. In this study, the contact between a rigid indenter and a fiber/interphase/matrix system is simulated using ABAQUS, with E_i and δ_i as input information. At given indenter displacement, z, the finite element analysis yields the contact load P and radius r. To avoid the stiffening effect of the fiber, the reference location is chosen to be a location at the bulk matrix region, where the apparent modulus is equal to the bulk matrix modulus. The indenter is then moved to locations in the interphase region to obtain the apparent modulus profiles using Eq. (7).

Figure 2(a) shows the apparent modulus as a function of the distance from the fiber, where the symbols are experiment data from VanLandingham *et al.* (12), and the solid line represents the numerical results from a two-dimensional axisymmetric finite element indentation model. The

results correspond to an unsized AS4 carbon fiber/EPON 828/PACM20 system with fiber modulus $E_{AS4} = 223\ GPa$ and matrix modulus $E_{828} = 2.23\ GPa$. It is observed that the apparent modulus increases sharply as the distance decreases, owing to the stiffening effect of the carbon fiber; and the matrix modulus is asymptotically approached as the distance increases. The width and height of the fiber and matrix regions are chosen to be large enough to eliminate the boundary effects on the prediction of the apparent modulus profile. An interphase thickness value of $\delta_i = 100\ nm$ is approximated from the data, and an interphase modulus value of $E_i = 1.49\ GPa$ is found to yield a best fitting between the finite element indentation model and the experimental data.

The effective interphase thickness and modulus for two other composite systems are determined using the apparent modulus data from VanLandingham *et al.* (12), and the results are shown in Figs. 2(b) and 2(c), following the same presentation format as that in Fig. 1(a). Figure 2(b) pertains to a sized Copper/EPON 828/PACM20 system, where EPON 1001F resin is applied as a sizing layer on the copper fiber surface. The modulus ratio between a fully cured EPON 1001F and EPON 828 (i.e., DGEBA) is $E_{1001f}/E_{828} = 1.4$, and the interphase thickness is estimated to be 500 *nm* from the modulus data (12). It is found that an interphase modulus of $E_i = 1.90\ GPa$ yields the best fitting to the experimental data. The copper fiber has a modulus of $E_{cu} = 120\ GPa$, therefore, the stiffening effect of the fiber surface is again apparent.

Figure 2(c) presents the results for a sized AS4/EPON 828/PACM20 system, where the sizing material is EPON 1001F and has a thickness of 1 μm. When the distance from fiber is greater

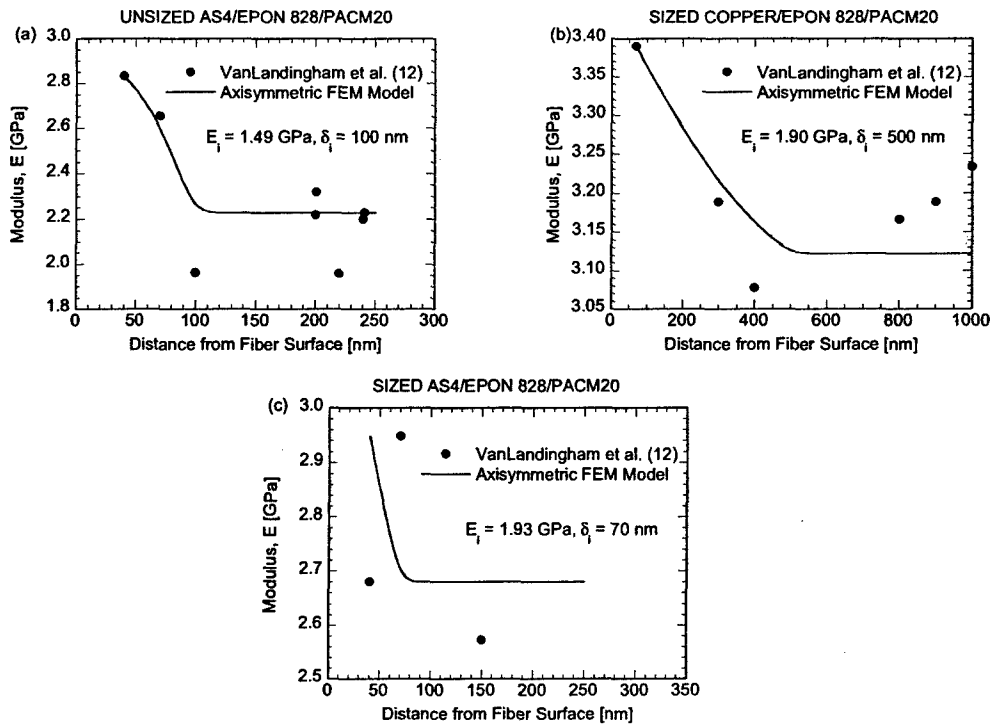

Figure 2. Comparison between predictions of finite element analyses and AFM based indentation data of apparent modulus near (a) unsized AS4, (b) sized Copper, and (c) sized AS4 fiber surfaces.

Table 2 Effective Interphase thickness and Modulus

Fiber	δ_i [nm]	E_i [GPa]	Reference
Graphite	870	0.045	Sottos (13)
Sized Copper	500	1.90	VanLandingham *et al.* (12)
Sized AS4	70	1.93	VanLandingham *et al.* (12)
Unsized AS4	100	1.49	VanLandingham *et al.* (12)

than 70 *nm*, the apparent modulus data becomes constant, which indicates that the EPON 1001F resin is uniformly mixed with EPON 828 to form a hybrid resin beyond an interphase region with thickness $\delta_i = 70$ *nm*. In this study, the modulus of the fully cured hybrid resin is assumed to be the averaged values of the EPON 828 and EPON 1001F, i.e., $E_{hybrid}/E_{828} = 1.2$. Finite element analysis shows that $E_i = 1.53$ *GPa* yields the best fitting with experimental data. Table 2 summarizes the effective interphase thickness and modulus values for the various composites systems mentioned above.

The interphase properties of the various composite systems in Table 2 are used to determine the corresponding kinetics parameters using the second approach mentioned above and the results are listed in the 3rd–6th columns in Table 1. Using the values of parameters in the 3rd column of Table 1 as input for the kinetics model, the final profiles of PACM20 concentration (in term of pph PACM20) and modulus near a graphite surface are obtained in Fig. 3. The modulus profile is mapped from the concentration profiles by using a twin-peak empirical equation reported in ref. (14). Since the parameter combination in this case pertains to a preferential adsorption of amine

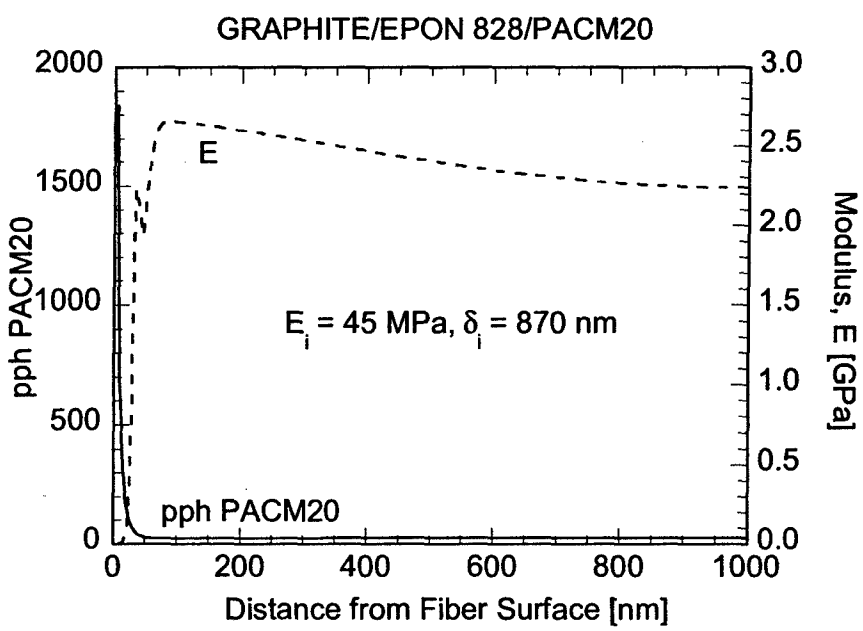

Figure 3 The interphase concentration and modulus profiles that match the effective interphase modulus and thickness reported by Sottos *et al.* (13) for a Graphite/EPON 828/PACM20 system.

molecules, the surface concentration pph = 1800 is well above the bulk value of 28. It is interesting to notice that the modulus profile has two peaks, which is attributed to the twin-peak empirical concentration-modulus correlation (14). The final twin-peak modulus profile predicted by the current model deviates from the monotonic interphase modulus profiles assumed in the literature (17), and may have significant influence on the overall composite properties.

The interphase composition or modulus profiles for the other composite systems in Table 1 are omitted for brevity. An overall trend observed in Table 1 is that all the inorganic fiber surfaces represent preferential adsorption of the PACM20 species, which is consistent with results reported in the literature. From the values of the amine adsorption rate, it is found that the aluminum has the strongest affinity to PACM20, followed by graphite and copper, and AS4 shows the weakest adsorption of amine molecules.

All the composite systems in this study are cured at an isothermal temperature T_0 = 80°C, and consequently, the activation energies (e.g., E_{aA}, E_{dA}) can not be determined. It is necessary to conduct a systematic study on cure temperatures to determine all the parameters in the model. At this stage, direct theoretical or experimental methods to determine the kinetics parameters are not available and may be a subject of future work. The two correlation approaches presented in this article establish the processing-interphase-property relationship without any assumed interphase properties. Since the concentration profiles provide more precise information about the interphase structure than the two values E_i and δ_i, the correlation based on composition profiles may be more reliable than that based on effective interphase property values. The results provide capabilities for tailoring composite properties and interphases via suitable material and processing parameter selection.

4. CONCLUSIONS

A microscale kinetics model of interphase formation is correlated with available experimental data on interphase properties to determine the parameters of the model. Depending on the type of available experimental data, two approaches of the correlation study are presented. The correlation based directly on concentration profiles is preferred since more accurate interphase structure is employed. In particular, all the inorganic fiber surfaces show preferential adsorption of the PACM20 species. The affinity of the fiber surfaces to the amine species may be ordered in a decrease sequence as: Aluminum, Graphite, Copper, and AS4.

5. ACKNOWLEDGEMENT

The work reported in this paper was carried out as part of the MEANS program funded by the Air Force Office of Scientific Research (Grant No. F496200110521). We are grateful for their support.

6. REFERENCES

1. G. R. Palmese, Univ. of Delaware Center for Composite Materials, Technical Report Number 92-25, (1992).
2. S. Subramanian, *et al.* J. Composites Materials, 30, 309 (1996).
3. R. W. Rydin, *et al.* J. Composite Materials, 31, 182, (1997).
4. L. T. Drzal, Adv. Polym. Sci., 75, 1 (1986).
5. M. S. Madhukar and L. T. Drzal.. J. Composite Materials, 25, 958 (1991).
6. J. Hrivnak, University of Delaware Center for Composite Materials, Technical Report Number 97-05, (1997).
7. F. Yang and R. Pitchumani, Journal of Applied Polymer Science, 89, 3220 (2003)
8. F. Yang and R. Pitchumani, Polymer Composites, submitted, (2004)
9. F. Yang, Ph. D. Dissertation, University of Connecticut, Department of Mechanical Engineering, (2002).
10. F. Yang and R. Pitchumani, Proceedings of the 12th International Heat Transfer Conference, Vol. **3**, August 2002, pp. 153-158.
11. D. Arayasantiparb, S. McKnight, and M. Libera, J. Adhesion Sci. Technol., 15, 1463 (2001).
12. M.R. VanLandingham, et al., Composites Part A, 30, 75 (1999).
13. N.R. Sottos, Ph. D. Dissertation, Univ. of Delaware, (1990).
14. F. Yang and R. Pitchumani, Composites Science and Technology, in press, (2004).
15. W.M. Sanford, Ph. D. Dissertation, Univ. of Delaware, (1987).
16. M.R. VanLandingham, et al., J. Adhesion, 64, 31 (1997).
17. N.K. Anifantis, Composites Science and Technology, 60, 1241 (2000).